8-2015

Evaluation of Shiryaev-Roberts Procedure for On-line Environmental Radiation Monitoring

Mara Watson
Clemson University, maramae@umich.edu

Evaluation of Shiryaev-Roberts Procedure for On-line Environmental Radiation Monitoring

---

A Thesis
Presented to
the Graduate School of
Clemson University

In Partial Fulfillment
of the Requirements for the Degree
Master of Science
Environmental Engineering and Earth Sciences

---

by
Mara Mae Watson
August 2015

Accepted by:
Dr. Timothy A. DeVol, Committee Chair
Dr. Calvin L. Williams
Dr. Brian A. Powell

Abstract

An on-line radiation monitoring system that simultaneously concentrates and detects radioactivity is needed to detect an accidental leakage from a nuclear waste disposal facility or clandestine nuclear activity. Previous studies have shown that classical control chart methods can be applied to on-line radiation monitoring data to quickly detect these events as they occur; however, Bayesian control chart methods were not included in these studies. This work will evaluate the performance of a Bayesian control chart method, the Shiryaev-Roberts (SR) procedure, compared to classical control chart methods, Shewhart 3-σ and cumulative sum (CUSUM), for use in on-line radiation monitoring of ^{99}Tc in water using extractive scintillating resin. Measurements were collected by pumping solutions containing 0.1-5 Bq/L of ^{99}Tc, as $^{99}TcO_4^-$, through a flow cell packed with extractive scintillating resin coupled to a Beta-RAM Model 5 HPLC detector. While $^{99}TcO_4^-$ accumulated on the resin, simultaneous measurements were acquired in 10-s intervals and then re-binned to 100-s intervals. The Bayesian statistical method, Shiryaev-Roberts procedure, and classical control chart methods, Shewhart 3-σ and cumulative sum (CUSUM), were applied to the data using statistical algorithms developed in MATLAB®. Two SR control charts were constructed using Poisson distributions and Gaussian distributions to estimate the likelihood ratio, and are referred to as Poisson SR and Gaussian SR to indicate the distribution used to calculate the statistic. The Poisson and Gaussian SR methods

required as little as 28.9 mL less solution at 5 Bq/L and as much as 170 mL less solution at 0.5 Bq/L to exceed the control limit than the Shewhart 3-σ method. The Poisson SR method needed as little as 6.20 mL less solution at 5 Bq/L and up to 125 mL less solution at 0.5 Bq/L to exceed the control limit than the CUSUM method. The Gaussian SR and CUSUM method required comparable solution volumes for test solutions containing at least 1.5 Bq/L of ^{99}Tc. For activity concentrations less than 1.5 Bq/L, the Gaussian SR method required as much as 40.8 mL less solution at 0.5 Bq/L to exceed the control limit than the CUSUM method. Both SR methods were able to consistently detect test solutions containing 0.1 Bq/L, unlike the Shewhart 3-σ and CUSUM methods. Although the Poisson SR method required as much as 178 mL less solution to exceed the control limit than the Gaussian SR method, the Gaussian SR false positive of 0% was much lower than the Poisson SR false positive rate of 1.14%. A lower false positive rate made it easier to differentiate between a false positive and an increase in mean count rate caused by activity accumulating on the resin. The SR procedure is thus the ideal tool for low-level on-line radiation monitoring using extractive scintillating resin, because it needed less volume in most cases to detect an upward shift in the mean count rate than the Shewhart 3-σ and CUSUM methods and consistently detected lower activity concentrations. The desired results for the monitoring scheme, however, need to be considered prior to choosing between the Poisson and Gaussian distribution to estimate the likelihood ratio, because each was advantageous under different circumstances.

Once the control limit was exceeded, activity concentrations were estimated from the SR control chart using the slope of the control chart on a semi-logarithmic plot. Five of nine test solutions for the Poisson SR control chart produced concentration estimates within 30% of the actual value, but the worst case was 263.2% different than the actual value. The estimations for the Gaussian SR control chart were much

more precise, with six of eight solutions producing estimates within 30%. Although the activity concentrations estimations were only mediocre for the Poisson SR control chart and satisfactory for the Gaussian SR control chart, these results demonstrate that a relationship exists between activity concentration and the SR control chart magnitude that can be exploited to determine the activity concentration from the SR control chart. More complex methods should be investigated to improve activity concentration estimations from the SR control charts.

Dedication

To Mom and Rick

Acknowledgments

I would like to express my sincere gratitude to my advisor, Dr. Tim DeVol, for supporting me through my Master's degree the last two years. I am forever grateful for the freedom he gave me to work on my research, but am also grateful for his willingness to help when needed, particularly when equipment did not work. His expertise and guidance were also greatly appreciated when filling out applications for scholarships, fellowships, and doctoral programs. I do not believe that I would have been as successful without his advice and recommendation. I would also like to thank my other committee members, Dr. Calvin Williams and Dr. Brian Powell, and Dr. Lindsay Shuller-Nickels for helping with this research project and providing career advice and suggestions in general.

Thank you as well to Dr. Scott Husson, Dr. Ayman Seliman, Dr. Valery Bliznyuk, Amy Meldrum, Christine Duval, Shelby Thies, and Jonathon Locklair for listening to my saga week after week and providing technical advice to troubleshoot my instrument problems at the DTRA research group meetings. I especially thank Dr. Ayman Seliman for always being willing to assist me in the lab at the drop of a hat. I owe it to him for making me feel comfortable working in a lab with chemicals so that I could complete this work.

I thank my friends for providing the support and friendship that I needed. I could not imagine my time at Clemson University without the friendly pranks and

distractions. Thank you for keeping it real.

A special thanks goes to my parents, Leesa and Rick, for their unceasing love and support. I cannot thank them enough for understanding and accepting my desire to pursue higher (and higher!) education. I really would not be where I am today without them.

This work was supported by the Defense Threat Reduction Agency, Basic Research Award #HDTRA1-12-1-0012, to Clemson University.

Table of Contents

List of Tables

List of Figures

Chapter 1

Introduction

Radioactive contamination in water could be caused by a leak or discharge from nuclear facilities, including waste disposal facilities; incidental contamination as a result of the assemblage of a radionuclide dispersal device (RDD), an improvised nuclear device (IND), or a nuclear weapon (NW); or intentional contamination as an act of terrorism. Conventional methods to detect radionuclides in water are time-consuming and laborious, possibly leading to a detection delay. Many of these methods require a water sample to be collected in the field and brought to a laboratory. Extraction chromatographic resins packed into a column, such as TRU and UTEVA® resins by Eichrom Technologies, LLC, are then employed to preferentially separate the analyte(s) of interest from the matrix, concentrating them in the process. A combination of acids are then used to elute the analyte(s) from the column. The quantity of analyte in the sample is then determined through analytical and radioanalytical techniques. In total, these methods can take several days to run before the results are known. Thus, an on-line detection system that simultaneously concentrates and detects increases in radionuclide concentrations at ultra-trace levels is needed to continuously monitor public water systems so that these events can be

quickly detected. One such method is a flow cell packed with extractive scintillating resin and coupled to a photomultiplier tube to detect radioactivity as it accumulates on the resin.

Previous work has shown that certain statistical control chart methods significantly lower the detection limit in on-line radiation monitoring systems using extractive scintillating resin (Hughes et al. 2008). Although the detection limit was lowered using alternative methods to the common Shewhart 3-σ control chart, the study was limited to classical control chart methods, cumulative sum (CUSUM) and exponentially-weighted moving average (EWMA); it did not consider Bayesian control charts, such as the Shiryaev-Roberts (SR) procedure. The SR procedure has been shown to detect smaller changes than classical control chart methods, thus reducing the volume of water required for detection (Pollak and Siegmund 1985; Pollak and Tartakovsky 2008).

This work will compare the performance of the SR procedure to the Shewhart 3-σ and CUSUM control chart methods for use in on-line radiation monitoring of water. A method to estimate the activity concentration will then be developed to determine the extent of radionuclide contamination in the water so that personnel can implement proper remedial action.

Chapter 2

Background

2.1 Statistics in Radiation Monitoring

An inevitable degree of uncertainty is present in every radiation measurement, because radioactive decay is a random process. Uncertainty from radioactive decay is inversely proportional to the measurement count time: the longer a measurement is collected for, the smaller the uncertainty will be. The uncertainty associated with a measurement can be quantified by applying statistical concepts to radiation counting data.

Uncertainty in low-level radiation measurements can pose a problem when determining if radioactivity is present in a sample, because the detection limit could be contained within the uncertainty. If the measured quantity is taken to be absolute, then radioactivity is present in the sample if the measured value is above a detection limit or not present in the sample if the measured value is below a detection limit. If the uncertainty in the measurement is considered, then radioactivity could be present in the sample even when the signal is below a limit, or it could not be present in the sample when the signal is above the limit. Classical statistics is generally employed

to determine if radioactivity is present in a sample; however, Bayesian statistics has been gaining popularity in health physics applications to determine these answers.

2.2 Bayesian Statistics

Bayesian statistics refers to any statistical inference that applies Bayes' Theorem to estimate a parameter. Bayes' theorem was originally derived for point probabilities; however, it has also been derived for probability distributions, which are more useful for health physics applications. Using probability distributions, Bayes' Theorem is expressed as

$$f(\mu|\text{CR}) = \frac{f(\text{CR}|\mu)f(\mu)}{f(\text{CR})} \tag{2.1}$$

where $f(\mu|\text{CR})$ is the posterior distribution of μ, or the conditional probability of the expected mean, μ, occurring given the count rate data, CR; $f(\text{CR}|\mu)$ is the sampling density–which is proportional to the Likelihood ratio, the probability of an event occurring compared to the probability of the same event not occurring –or the conditional probability of the count rate data occurring given the expected mean; $f(\mu)$ is the prior distribution for the parameter; and $f(\text{CR})$ is the marginal probability of the data (Lynch 2007; Hamada et al. 2008). More generally, Bayes' Theorem is stated as

$$\text{Posterior} \propto \text{Likelihood Ratio} \times \text{Prior}$$

because $f(\text{CR})$ acts as a proportionality constant in the mathematical expression (Lynch 2007).

For a series of independent measurements, the prior distribution is continuously updated after each new measurement is obtained using the posterior distribution. This allows new knowledge to be incorporated into the prior distribution so that

the state of the parameter can be estimated using all available information (Bolstad 2007). In order to accomplish this, the prior probability must be defined before implementing Bayesian statistics to radiation measurements; however, little information is available in the health physics field to appropriately define the prior probability distribution (Miller et al. 2001). The prior distribution is commonly estimated as a "flat" distribution, where all events are equally likely, when there is little information available to construct a prior distribution; however, this approach is conservative and often leads to larger estimated values for the prior distribution relative to more realistic functional forms of the prior distribution (Miller et al. 1993).

2.3 Classical Statistics versus Bayesian Statistics

Classical statistics and Bayesian statistics ultimately have the same goal: perform statistical inference about a parameter; however, the methods used to come to a conclusion are fundamentally different. One of the primary differences is how probability is incorporated to estimate a parameter. In classical statistics, a probability distribution is used only to describe the sampling distribution, which is the distribution of all possible statistic values for representative random samples of the population under consideration. This distribution is then used to perform an inference on the parameter via point estimation, confidence intervals, or hypothesis testing. Since classical statistical inference is dependent on the distribution from many sampling events, it is not directly dependent on the actual data that occurred. In Bayesian statistics, the posterior distribution is updated as more data become available to account for new information. Statistical inference is then performed on the parameter using the newly updated posterior distribution. This process continues as new information becomes available by using the previous posterior distribution as the prior

distribution to calculate a new posterior distribution (Bolstad 2007).

Another key difference between classical and Bayesian statistics is the definition of parameters. Classical statistics assumes the parameter is a fixed, unknown value with no uncertainty associated with it. Uncertainty in classical statistics arises from fluctuations among statistics of random samples used to estimate the parameter; thus, only sampling distributions, not parameters, can have uncertainty associated with them (Lynch 2007). Bayesian statistics, on the other hand, treats parameters as random, unknown variables; so, the parameter is represented as a probability distribution to account for the randomness in the estimation. The parameter is continuously updated as new information becomes available through the posterior distribution (Bolstad 2007).

2.4 Bayesian Statistics in Health Physics

Applying Bayesian statistics to health physics problems has been gaining popularity in the field for the past three decades, because Bayesian statistics allows the parameter to be estimated using the data collected. Classical statistics, on the other hand, uses the parameters to predict the distribution of values the data could have if the measurement was statistically the same as the value of the parameter. Since health physicists want to estimate the parameter (e.g. radiation dose) from the data collected, employing Bayesian statistical methods seems to be the most logical direction for the health physics field (Miller et al. 1993; Strom 2011).

Little (1982) was the first to investigate Bayesian statistics as an alternative method to differentiating between background and a low-level activity source. When employing classical statistics, a negative net count rate can be obtained for a radiation measurement due to natural fluctuations in radioactive decay; however, negative net

count rates were eliminated when Bayesian statistics were employed. This was accomplished by defining a prior probability distribution with zero probability of a net negative count rate occurring. When calculating the net count rate using Bayesian statistics, a Gaussian distribution is sufficient to analyze counting data when the number of observed counts is large; however, a Poisson distribution should be used when the number of observed counts is small (Groer 2002).

A group of researchers at Los Alamos National Lab (LANL)–namely G. Miller, W. C. Inkret, and H. F. Martz–have extensively studied Bayesian statistics for radiation measurements, particularly for internal and external dosimetry. Bayesian statistics was initially investigated as a method to determine if a sample for measured bioassay, dosimetry, or environmental monitoring was "positive" for radioactive contamination or "zero" (Miller et al. 1993). The framework was later developed for Bayesian hypothesis testing to interpret radiation measurements as "detected" or not (Miller et al. 2008b). The success of this work led them to define the prior distribution and likelihood function for different scenarios health physicists frequently encounter in internal dosimetry measurements as well as develop the framework for Bayesian hypothesis testing. They found that the "alpha" distribution, a simplification of the Gamma distribution, should be used as an estimate for the prior distribution when there is little prior information available, and a log-Gaussian distribution should be used when there is substantial prior information available (Miller et al. 2001). Although these distributions were studied in the context of internal dosimetry, Miller et al. (2000) suggests that they have universal use in the health physics field. They also found that approximating the likelihood function as a Gaussian distribution was surprisingly accurate for radioactivity counting data, but noted that differences occur in some cases of small numbers of measured counts (Miller et al. 2002). Analytical approximations were obtained numerically for exact Poisson-logGaussian likelihood

functions using count data (Miller 2008a). The group also applied Bayesian statistics to bioassay measurements using successful techniques applied to internal dosimetry measurements (Miller et al. 2000, 2003).

Bayesian statistics was also used to calculate the concentration of airborne ^{218}Po on filter paper (Groer and Lo 1996). The build-up and decay of ^{218}Po had to be considered during counting, because it is a short-lived radionuclide. By employing Bayesian statistics, they were able to use prior information about the ^{218}Po concentration in the sampling area to estimate the mean and variance of the measurement. This technique was particularly useful for measuring low-level concentrations of airborne short-lived radionuclides, because it accounted for the natural statistical fluctuations of the collection and counting processes.

The prior distribution can also become saturated by background data when monitoring a process using Bayesian statistical methods, causing a delayed alarm to indicate a change in the process. Modified Bayesian analysis methods have been developed to remedy this, such as the enhanced reset method and moving prior method (Luo 2013). The purpose of the enhanced reset method is to compare the posterior distribution to a distribution that is consistent with background after a set number of measurements have been taken. If the posterior distribution is similar to the background distribution, the process will be restarted using the newest measurement with the initial prior distribution; if it is not, then the process will continue as it was without resetting the prior distribution for a set number of measurements. The moving prior method only allows a set number of measurements to be included in the prior distribution. The oldest measurement is no longer included in the measurement once the limit has been reached, and the newest measurement is added first-in, first-out.

Many government agencies have adopted Bayesian techniques to develop standards and design software. The U.S. Environmental Protection Agency (EPA) has

revised and updated its estimates for cancer risk coefficients using Bayesian statistics (Pawel 2013). Los Alamos National Lab (LANL) has used Markov Chain Monte Carlo methods, which are based on Bayesian statistics, for more than a decade (Strom 2011). The decision thresholds and detection limits established by the International Organization for Standardization (ISO) 11929-series standards were determined using Bayesian statistics (Weise 2006). The Integrated Modules for Bioassay (IMBA) software package utilized by the DOE incorporates the Weighted Likelihood Monte Carlo Sampling (WeLMoS) method, which is based on Bayesian statistics. The National Council on Radiation Protection and Measurements (NCRP) will also likely endorse Bayesian methods (Strom 2011). Investigating Bayesian detection methods is worthwhile for use in environmental monitoring, because the health physics field will likely head in this direction based on the actions of many government agencies.

2.5 Statistical Process Control

Statistical process control (SPC) was introduced in 1924 by W. A. Shewhart. He recognized that the manufacturing industry needed a system to differentiate between two sources of variability: common causes and assignable causes (Walpole et al. 2012). Common causes result from natural fluctuations in the process–for example, electronic noise, environmental conditions, and differences among equipment. An assignable cause is a change that is not inherent in the process, such as operator error or a change in process settings (Kenett and Zacks 1998). SPC seeks to minimize variability in the process and identify when an assignable cause occurs. This is achieved by using a graphical tool called a control chart. A control chart monitors a process to determine when it is affected by an assignable causes and requires action to restore it to an in-control state (Kenett and Zacks 1998).

A typical control chart has a centerline, an upper control limit (UCL), and a lower control limit (LCL). The centerline corresponds to the process mean in an in-control state, and the upper and lower control limits represent the allowed range of variability in the process before an out-of-control alarm is sounded (Kenett and Zacks 1998; Montgomery 2009). The data points are expected to randomly walk around the center line while remaining between the upper and lower control limits when process monitoring is in progress; the variability among these measurements stems from common causes. The data point will lay exceed the control limits if the variability stems from assignable causes, indicating an out-of-control process that requires personnel to put the process back on track.

Although a control chart is meant to signal a change in the process, variability in the system can cause an out-of-control alarm to sound despite the process still being in control. This is known as false positive (type I error), and it occurs with probability α. The system can conversely become out of control without any indication from the control chart that the process has changed. This is known as a false negative (type II error), and it occurs with probability β.

An important measure of control chart performance is the average run length (ARL). The ARL is defined as the average number of data points plotted on the control chart before an out-of-control alarm is sounded (Kenett and Zacks 1998). It is expected to be large when variability among the data points is solely the result of common causes to indicate a constant process mean; however, it is expected to be small if an assignable cause occurred to signal a change in the process mean. The ARL is identified as ARL_0 when an out of control alarm is sounded, but the process is still in control. It is calculated using

$$ARL_0 = \frac{1}{\alpha} \tag{2.2}$$

where α is the probability of producing a false positive. This number should be large assuming the probability of a false positive error is small, because the process is in control and thus has a low probability of crossing the alarm threshold. The ARL is identified as ARL_δ when an alarm is sounded as a result of an out of control process. It should be small, because the control chart is designed to quickly signal an out of control process (Montgomery 2009).

Although on-line environmental radiation monitoring is not a process in the sense of a production line, SPC methods can be utilized to detect changes in radioactivity concentrations in a system. Differentiating between variability among background measurements and an increase in the radioactive material is important to indicate contamination or clandestine nuclear activity. By employing SPC methods, water systems can be continuously monitored, and an alarm can sound when a change occurs that result from assignable causes. This project will focus on the Bayesian control chart method, Shiryaev-Roberts (SR) procedure, compared to two classical control chart methods–Shewhart 3-σ and CUSUM.

2.6 Shewhart 3-σ Control Chart

The Shewhart 3-σ control chart method is the most common and simple type of control chart used in SPC. Process monitoring occurs by comparing the statistic of a sample of size n taken every h units of time to the sampling distribution. The sampling distribution is assumed to follow a Gaussian distribution with mean μ and standard deviation σ. An upper control limit (UCL) and lower control limit (LCL) signal a positive or negative change in the process mean, respectively. They are calculated using

$$\text{UCL} = \mu + z_{\alpha/2}\frac{\sigma}{\sqrt{n}} \tag{2.3}$$

$$\text{LC}L = \mu - z_{\alpha/2}\frac{\sigma}{\sqrt{n}} \tag{2.4}$$

where $z_{\alpha/2}$ is the critical level of the standard Gaussian distribution. The critical level is linked to the probability that data will not lie outside a certain number of standard deviations, or the control limits, from the process mean. If the statistic lies outside of the control limits, then an alarm sounds to indicate the process is out of control (Montgomery 2009).

The critical level determines the sensitivity of the control chart, because it determines the probability that a false alarm will occur. This value is found by defining the probability that a false positive will not occur and then looking up the associated critical level on a standard Gaussian distribution table. It is commonly set at 3 to minimize the probability of a false alarm occurring (Kenett and Zacks 1998; Montgomery 2009; Walpole et al. 2012). Thus, a change must be at least 3-σ in this case from the process mean to sound an alarm. This practice is effective when detecting large shifts in the process mean, but it is often insensitive to small changes; so, other SPC methods should be considered to monitor processes that are expected to have smaller shifts in the process mean

2.7 CUSUM Control Chart

The CUSUM control chart method was designed to alert personnel to a change in the process mean more quickly than the Shewhart 3-σ control chart method. Although this method was originally designed for variables, Lucas (1985) also applied the method to attributes, or counting data. In the CUSUM method, the CUSUM statistic, C_i, is the cumulative difference between the most recent observed value, Y_i,

and the reference value, K, such that

$$C_i = \sum_{i=1}^{N} (Y_i - K) \tag{2.5}$$

If the CUSUM statistic remains close to zero, then the process is in control, indicating a small difference between the observed sample and reference value; however, if the difference between the two increases or decreases, then the CUSUM statistic becomes increasingly positive or negative, indicating that the process mean has changed. An alarm will sound when the CUSUM statistic crosses the decision interval value, h, (Lucas 1985; Montgomery 2009).

In on-line radiation monitoring, only an increase in deviation between the observed value and reference value is of interest; thus, a one-sided CUSUM method should be used. The upper-CUSUM statistic is defined as

$$C_i^+ = \max(0, Y_i - K + C_{i-1}^+) \tag{2.6}$$

where the lower limit is set to zero. By doing this, a change in the process mean is detected more quickly, because negative deviations are eliminated (Page 1961).

The observed value is commonly Gaussianized in the CUSUM method so that different CUSUM control charts can be directly compared. The Gaussianized variable, y_i, is found using

$$y_i = \frac{Y_i - \mu_0}{\sigma} \tag{2.7}$$

Using the Gaussianized value, the Gaussianized upper-CUSUM statistic, c_i^+, becomes

$$c_i^+ = \max(0, y_i - k + c_{i-1}^+) \tag{2.8}$$

where k is the Gaussianized reference value and defined as

$$k = \frac{K}{\sigma}. \tag{2.9}$$

Optimal values should be chosen for k and h, because they determine the performance of the CUSUM control chart. The reference value is calculated using

$$k = \frac{\delta}{2} \tag{2.10}$$

where δ is the size of the shift to be detected. The decision interval value is then found in a table using the reference value and desired ARL_0 (Montgomery 2009).

2.8 Shiryaev-Roberts Procedure

Bayesian detection, like classical methods, seeks to alert personnel to a change in the process mean when it occurs; however, the point where this occurs, known as the change-point, τ, is unknown, unlike in classical methods. The change-point location is predicted by a geometric prior probability distribution, $\pi(\tau)$, which assigns weights to possible change-point locations. This distribution is then used in Bayes' Theorem to calculate the posterior probability distribution, π_m, as new information becomes available. A change-point occurs when $\pi_m \geq \pi^*$, where π^* is the stopping threshold, whose value is expected to be close to 1 in (0,1). If the process is in control when process monitoring commences, then π_m can be simplified to

$$\widetilde{\pi}_m = \frac{\sum_{i=1}^{m-1} \prod_{j=i+1}^{m} R_j}{\left(\sum_{i=1}^{m-1} \prod_{j=i+1}^{m} R_j \right) + 1} \tag{2.11}$$

where $\widetilde{\pi}_m$ is the approximated value of π_m, m is the number of sampling events, and R_j is the likelihood ratio (Kenett and Zacks 1998).

To simplify the Bayesian detection framework, the SR procedure defines the SR statistic, W_m, as

$$W_m = \sum_{i=1}^{m-1} \prod_{j=i+1}^{m} R_j \tag{2.12}$$

and the stopping threshold as $W_m \geq \pi^*/(1-\pi^*)$. For the particular case that the data follow a Poisson distribution, the likelihood ratio of the SR statistic becomes

$$W_m = \sum_{i=1}^{m-1} \exp\left[-j\delta\sqrt{(}\mu) + \sum_{j=i+1}^{m} CR_j \log\left(\frac{\mu + \delta\sqrt{(}\mu)}{\mu}\right)\right] \tag{2.13}$$

where CR_j is the j^{th} count rate measurement, μ is the process mean, δ is the size of the shift to be detected, and m is the measurement number. For the particular case that the data follow a Gaussian distribution, the likelihood ratio of the SR statistic becomes

$$W_m = \sum_{i=1}^{m-1} \exp\left[-\frac{n\delta^2(m-i)}{2\sigma^2} + \frac{n\delta}{\sigma^2} \sum_{j=i+1}^{m} (CR_j - \mu)\right] \tag{2.14}$$

where σ is the standard deviation of the process mean. (Kenett and Zacks 1998).

DeVol et al. (2009) previously investigated the SR procedure using a Gaussian distribution to estimate the likelihood ratio, alongside the Shewhart 3-σ method and CUSUM method, to determine the false positive and false negative incidence rates for on-line radiation monitoring of transient signals. Although the false positive rate was small for the SR procedure when detecting a transient signal, the false negative rate was much higher, because the probability of a false positive is inversely related to the probability of a false negative. Since a false negative can have dangerous implications in health physics for human safety, an alarm reset method for the SR procedure was utilized to lower the false negative rate after an alarm sounds to indicate the presence

of activity.

Studies have shown that the SR procedure performance is typically superior to the Shewhart 3-σ method and comparable to the CUSUM method overall; however, the CUSUM method performs slightly better than the SR procedure when a large change is to be detected, and the SR procedure performs better than the CUSUM method when detecting a small change in the distant future (Moustakides et al. 2009; Pollak and Siegmund 1985; Pollak and Tartakovsky 2008). On-line environmental radiation monitoring with extractive scintillating resin typically involves detecting small, gradual changes; thus, the SR procedure should be evaluated for use in this application.

2.9 Extractive Scintillating Resin Flow Cell

Detection of charged-particle-emitting radionuclides in an aqueous solution is often laborious and time-consuming, because the radionuclide must be concentrated to obtain a sufficient signal to detect radionuclides using radiation detection techniques. Flow cell detectors packed with extractive scintillating resin have been used to simultaneously concentrate and detect alpha- and beta-emitting radionuclides under laboratory conditions and in groundwater and freshwater solutions (Ayaz and DeVol 2003; Clapham and Sutherland 2000; DeVol et al. 2000, 2001, 2002; Egorov et al. 1999; Hughes and DeVol 2003; Roane and DeVol 2002, 2005; Seliman et al. 2011, 2013). The extractive scintillating resins are composed of inert macroporous polystyrene co-impregnated with selective extraction material and organic fluors (Roane 2001). The selective extraction material, usually an organic extractant or extractant-diluent mixture, preferentially uptakes specific ions or groups of ions as an aqueous solution passes through the flow cell detector, concentrating them on

the resin (DeVol et al. 2002). When the analyte radioactively decays, the emitted charged particle interacts with the polymer and excites it to a higher energy state. The excess energy in the polymer is then transferred to the fluor molecule contained in the polymer, which de-excites by emitting visible photons. These photons are then absorbed by a secondary fluor that shifts the photon wavelength to the optimal detection wavelength for a photomultiplier tube (PMT). An electronic signal is then produced and recorded in a pulse height analysis (PHA) or time series spectrum to signal the presence of the radionuclide (Roane 2001).

2.10 Activity Concentration Estimation Using the Control Chart

Control charts are powerful tools for detecting an upward shift in the mean count rate in on-line radiation monitoring; however, most do not indicate the state of the mean count rate after an alarm sounds. Hughes et al. (2008) estimated the activity concentration in water using the CUSUM and exponentially weighted moving average (EWMA) control charts using the slope of the statistic after the control limit was exceeded. Pictured in Fig. 2.1 are illustrations of the three methods studied: the three point method (CUSUM only), the single point method, and the least squares fit to the data.

The three point method exploited the quadratic nature of the CUSUM statistic to estimate the activity concentration using three equidistant points on the CUSUM curve–c_i, c_j, and c_k–with distance q between them, as shown in Fig. 2.1a. The first point, c_i was chosen near the stopping threshold, c_k, was approximately equal to c_N=120 for best results, and c_j was midway between c_i and c_k (Hughes et al. 2008).

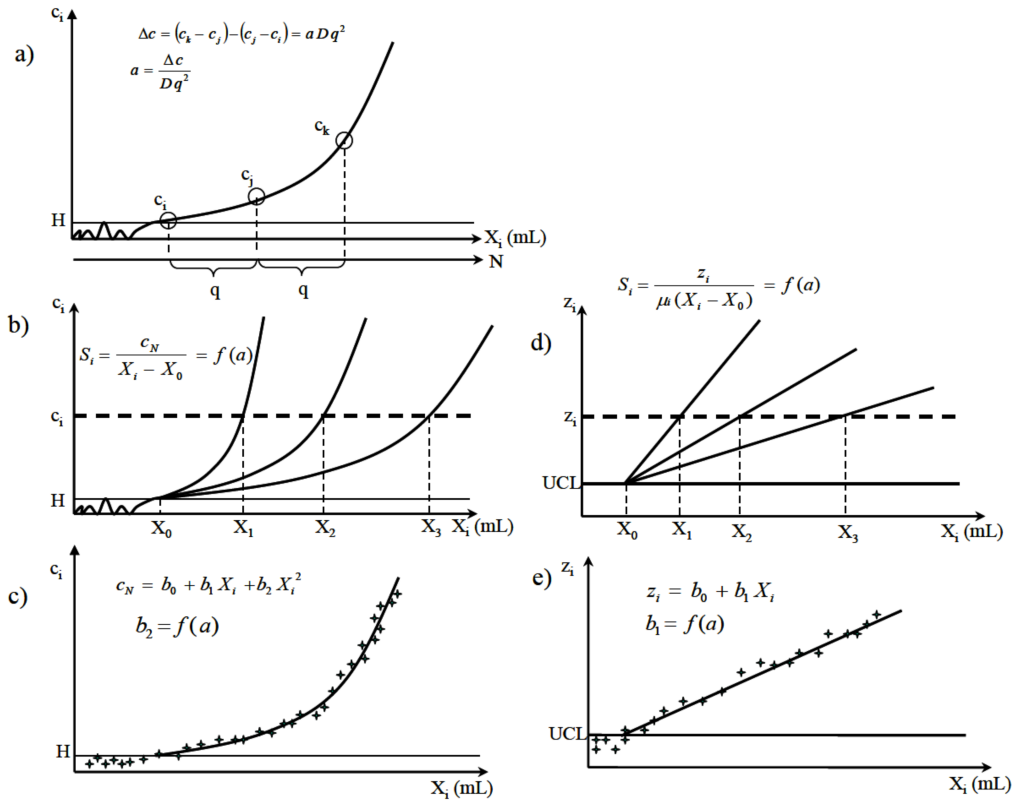

Figure 2.1: Illustrations for the activity concentration estimation methods for the CUSUM control chart, a) the three point method, b) the single point method, and c) the least squares fit to the data; and for the EWMA charts: d) the single point method and e) the least squares fit to the data. A calibration curve is required for methods in figures b)-e) prior to predicting an activity concentration for an unknown sample. From Hughes 2006. Reproduced with permission.

These points were used to estimate the slope of the curve, a, such that

$$a = \frac{\sigma_0}{Dq^2} \left[(c_k - c_j) - (c_j - c_i) \right] \tag{2.15}$$

where σ_0 is the background standard deviation and D is the volume increment in one counting interval. The slope variance is calculated by

$$Var(a) = \frac{2\sigma_0}{D^2 q^3} \tag{2.16}$$

This method produced activity concentration estimates within 30% of the actual value for data collected under laboratory conditions. Estimates for two synthetic groundwater samples were within 37.23% and 177.77% of the actual activity concentrations (Hughes et al. 2008). Overall, this method produced acceptable activity concentration estimates for samples in 0.01 M HNO_3, but did not perform well when using groundwater samples.

The one-point method considered the overall magnitude of the CUSUM and EWMA curves at a particular point. A value, S_i, was defined to estimate the activity concentration. This value is calculated by dividing the value at a particular point on CUSUM, c_i, or EWMA, z_i, curves by the solution volume, X_i, that passed through the flow cell since the detection limit was exceeded, as pictured in Fig. 2.1b and 2.1d. The EWMA value was Gaussianized by their respective background mean, μ_0, for easier comparison. In mathematical terms, S_i is calculated by

$$S_i = \frac{c_i}{X_i} \tag{2.17}$$

for the CUSUM curve, and

$$S_i = \frac{z_i}{\mu_0 X_i} \tag{2.18}$$

for the EWMA curve. A calibration curve is required for this method, because the relationship between S_i and activity concentration is empirical. A quadratic fit was applied to the CUSUM control chart, and a linear fit was applied to the EWMA control chart, as shown in Fig. 2.2. The calibration curves required a value of $c_i = 60$ for CUSUM or $z_i/\mu_0 = 1.18$ for EWMA to obtain acceptable results ($R^2 > 0.9$). The one-point method produced estimates within 7% and 30% of the actual concentration value for the CUSUM and EWMA methods, respectively, for laboratory

and environmental samples (Hughes et al. 2008). The simplicity and accuracy of this method makes it the ideal tool to use for activity concentration estimation in an unknown sample when implementing the CUSUM or EWMA control chart methods to on-line radiation monitoring using extractive scintillating resin.

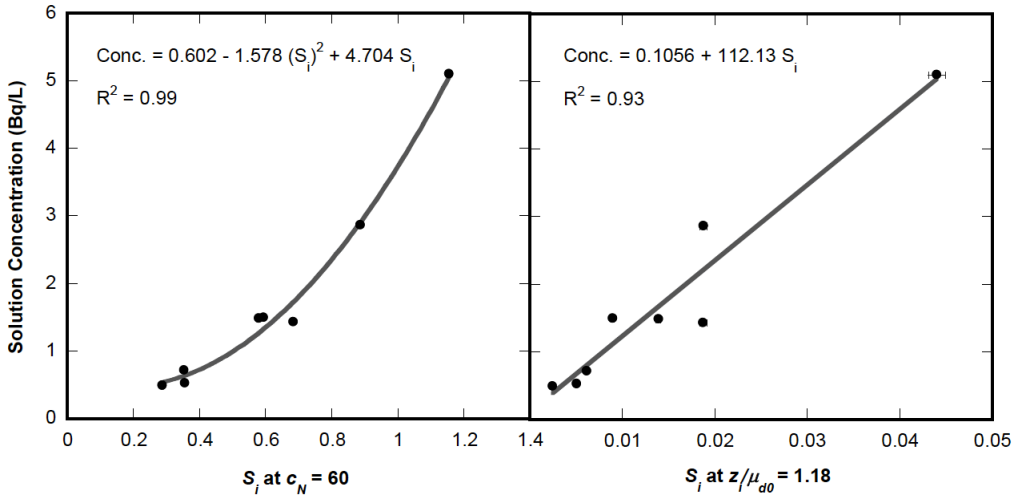

Figure 2.2: One-point method calibration curve for CUSUM (left) and EWMA (right) control chart methods. From Hughes et al. 2008. Reproduced with permission from Springer.

The third method used to estimate the activity concentration fit a least squares regression model to the CUSUM and EWMA curves starting from the point that crossed the control limit, as shown in Fig. 2.1c and 2.1e, respectively. Calibration curves were then created based on the properties of the fit. A quadratic least squares regression model was applied to the CUSUM curve; so, the corresponding calibration curve used the slope of the square of X_i, b_2. A CUSUM value of approximately 100 was necessary to obtain an acceptable fit. The EWMA curve used a linear least squares regression model, and the slope of the line, b_1, was used for the calibration curve. An EWMA value of approximately 1.68 was necessary to obtain an acceptable fit. Calibration curves are pictured in Fig. 2.3 for the CUSUM and EWMA curves.

Even still, both calibration curves had large amounts of variation associated with them, because remediating autocorrelation in the data inflated the error significantly. The resulting estimates from this method ranged from 23.13% to 161.38% different from the actual activity concentration for the CUSUM method and 4.25% to 210.39% for the EWMA method (Hughes 2006). The large error associated with this method does makes it an ideal method to use to estimate the activity concentration from the CUSUM or EWMA curve.

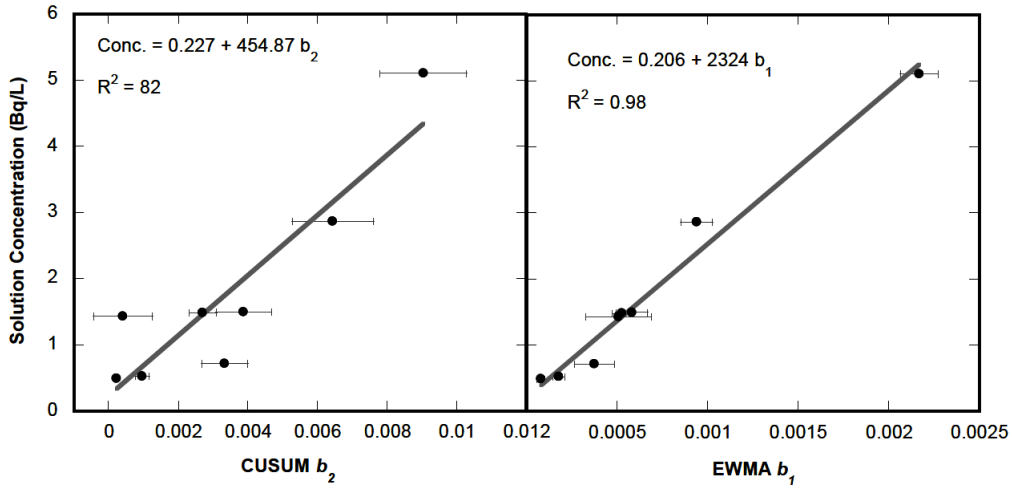

Figure 2.3: Least squares fit calibration curve for CUSUM (left) and EWMA (right) control chart methods. From Hughes 2006. Reproduced with permission.

2.11 Technetium-99 in the Environment

Technetium-99 is a man-made isotope that is produced as a fission product from ^{235}U in nuclear reactors or from a nuclear weapon detonations. It has a long half-life of $2.1 \cdot 10^5$ y and relatively high fission yield of 6.13%, making it one of the principal components of nuclear waste, particularly after the high-activity, short-lived fission products have decayed away. Approximately 1 kg of ^{99}Tc is produced for every

1 ton of uranium fuel in a nuclear power reactor (Chen et al. 2000). The predominant form of ^{99}Tc in the environment and nuclear waste is pertechnetate ($^{99}TcO_4^-$), the stable chemical form Tc in non-reducing conditions (Chen et al. 2000). Pertechnetate is highly mobile in the environment and weakly sorbs to geologic material; so, it readily migrates through soil in the presence of an aqueous environment and into groundwater (Pourbaix 1966). Technetium-99 decays by emitting a low energy beta particle ($E_{\beta,max}$=294 keV). The EPA Radionuclides Rule established a maximum contaminant level of 4 mrem/y for beta/photon emitters in drinking water (US EPA 2000). For ^{99}Tc, this equates to 33 Bq/L allowed in drinking water before remedial action must occur.

Chapter 3

Research Objective

This research evaluates the effectiveness of a Bayesian detection method, Shiryaev-Roberts procedure, applied to on-line radiation monitoring data from flow cells packed with extractive scintillating resin relative to that of the Shewhart 3-σ and CUSUM control chart methods. The evaluation is based on the ability of the SR procedure to differentiate between natural fluctuation in the background count rate from an increase in the count rate caused by activity accumulating on extractive scintillating resin, thus reducing the detection limit. The sample activity concentration is then estimated from the SR control chart to determine the level of contamination in a water sample.

3.1 Experimental Objectives

1. Data acquisition

   (a) Collect on-line radiation monitoring data from flow cells as ^{99}Tc accumulates on extractive scintillating resin

2. Evaluate the Shiryaev-Roberts procedure for the detection of an accumulating low-level signal

   (a) Apply the Shewhart 3-σ, CUSUM, and Shiryaev-Roberts control chart methods to on-line monitoring data from flow cells packed with extractive scintillating resin to identify upward shifts in the mean count rate as activity accumulates on the resin

   (b) Compare the detection limit of the Shiryaev-Roberts procedure to the detection limits of the Shewhart 3-σ and CUSUM control chart methods

   (c) Evaluate the effectiveness of the Shiryaev-Roberts procedure compared to the Shewhart 3-σ and CUSUM control chart methods for on-line radiation monitoring data from a flow cell

3. Activity concentration estimation

   (a) Estimate the ^{99}Tc activity concentration of a solution using the Shiryaev-Roberts procedure control chart

Chapter 4

Materials and Methods

4.1 Detection System

The detection system used for this study, shown in Fig. 4.1, consisted of a flow cell packed with extractive scintillating resin, henceforth referred to as flow cell, coupled to a BetaRAM Model 5 radio-HPLC detector (LabLogic Systems, Inc., Brandon, FL). Each flow cell contained 55.5±3.2 mg of extractive scintillating resin in 170 mm long clear fluorinated ethylene propylene (FEP) tubing (1/16" inner diameter, 1/8" outer diameter). The base of the extractive scintillating resin was synthesized by the copolymerization of an organic fluor (vinyl-NPO) and styrene. The resin was then functionalized with methyl dioctylamine (MDOA), an anion exchange ligand selective for $^{99}TcO_4^-$. Preparation of this resin is described elsewhere (Bliznyuk et al. 2015; Seliman et al. 2015). Small, triangular pieces of Teflon were fitted into each flow cell to prevent resin from escaping while still allowing solution to flow through.

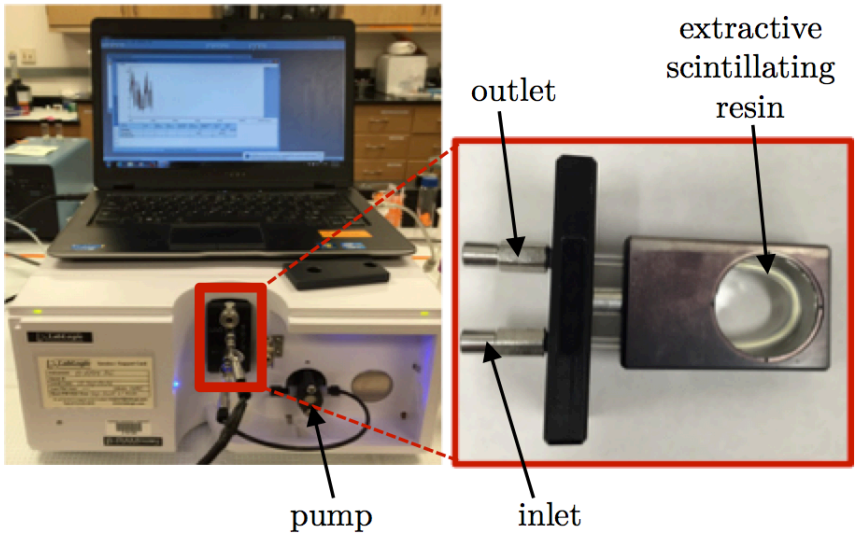

Figure 4.1: LabLogic Beta-RAM dual PMT detection system with flow cell packed with extractive scintillating resin

Pictured in Fig. 4.1 is the flow cell holder with flow cell in place. To install the flow cell in the holder, the tubing was bent into a U-shape, and the ends were fed through holes in the holder. The flow cell holder was then installed into the BetaRAM.

The loading efficiency and detection efficiency of the resin were determined by passing two 5 mL solutions containing 0.01 M HCl and 25.3 Bq or 20.2 Bq of ^{99}Tc through flow cells. The effluent was collected and counted for 30 minutes using a Quantulus Liquid Scintillation Spectrometer (Perkin Elmer, Inc., Waltham, MA) to quantify the amount of radioactivity the resin did not uptake.

Time series data were collected in 10-s intervals using Laura™ software (LabLogic Systems, Inc., Brandon, FL) while solution was pumped through the flow cell at a flow rate of 0.93 mL/min by a pump internal to the BetaRAM. The background count rate for each flow cell was established by pumping at least 100 mL of 0.01 M HCl acid through the flow cell. Once a stable background count rate was observed,

a solution containing 0.01 M HCl and 0.1-5 Bq/L $^{99}TcO_4^-$ was pumped through the flow cell. Measurement continued until all of the solution from the prepared sample was pumped through the flow cell. The test solution was followed by 30 mL of Tc-free 0.01 M HCl solution.

A schematic displaying the data processing steps is pictured in Fig. 4.2. Upon measurement completion, time series data from the Beta-RAM were re-binned into 100-s intervals using an algorithm developed in MATLAB (Appendix A). A longer counting interval was used to be consistent with previous studies of control chart methods applied to on-line radiation monitoring data collected using flow cells. Each data set was then input into statistical algorithms developed for the three control chart methods using MATLAB® (Appendix A). The algorithms calculated the Shewhart 3-σ, CUSUM, and Shiryaev-Roberts statistics using the parameters described below, determined the location the statistic exceeded the control limits, and plotted the statistic versus volume to construct the control charts. Poisson distributions and Gaussian distributions were used to estimate the likelihood ratio for the Shiryaev-Roberts statistic. They are referred to as Poisson SR and Gaussian SR, respectively.

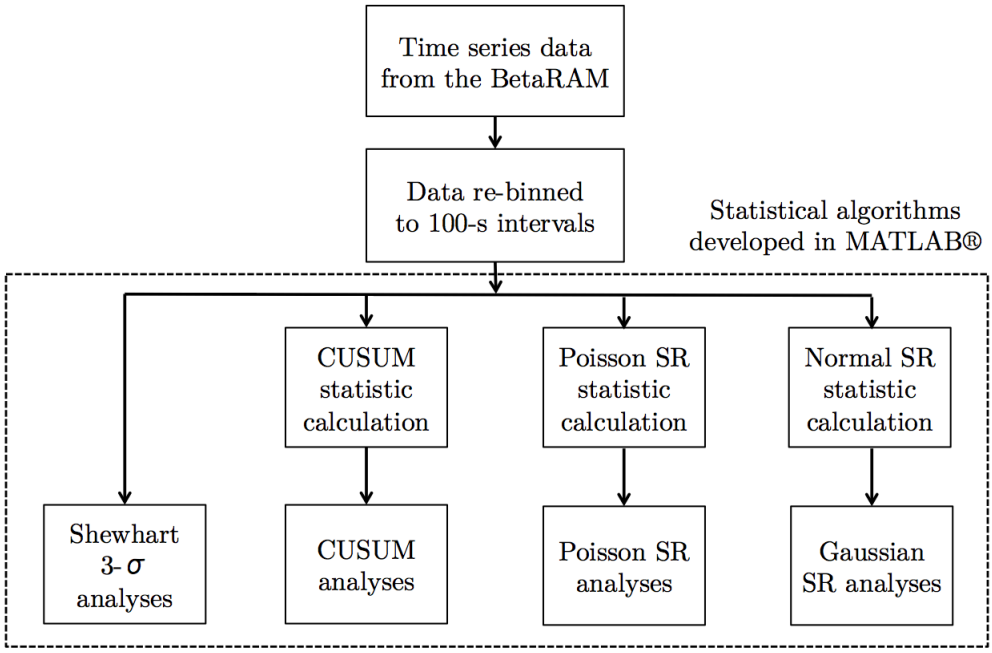

Figure 4.2: Schematic of post-data collection processing

4.2 Control Chart Design

The CUSUM and SR control limits were chosen to have approximately equal ARL_0 values as the Shewhart 3-σ control chart. A small false positive incidence rate and long ARL_0 were desired to ensure that a control limit exceedance was a positive detection and not a false positive detection. A critical level of $z_{\alpha/2} = 3$ was chosen for the Shewhart 3-σ control chart method, because it is the most common value quoted in the literature and fit the control chart sensitivity criteria for this study. The probability of a false positive is 0.00135 using this critical level, which was found using a standard Gaussian probability table. Equation 2.2 was used to calculate $ARL_0 = 741$. An upper CUSUM design was used with parameters $k = 0.5$ and control limit $h = 4.77$ to correspond to the ARL_0 of 741. The SR Likelihood ratio was estimated by both Poisson distributions and Gaussian distributions. The SR control

limit, or stopping threshold, was set using a program written by Kenett and Zacks (1998) that calculated ARL_0 values for Poisson and Gaussian distributions for a given SR stopping threshold. Based on 500 runs of this program, $W_{stop} = 700$ produced an $\text{ARL}_0 = 783.86 \pm 56.74$ for Poisson SR method and $\text{ARL}_0 = 733.86 \pm 56.66$ for Gaussian SR method; so, this value was chosen as the control limit for these methods. The SR parameters were $\delta = 3$ for the Poisson and Gaussian SR methods and $n = 1$ for the Gaussian SR method.

Chapter 5

Results and Discussion

Each time series data set was collected in 10-s intervals while a solution containing ^{99}Tc and 0.01 M HCl was pumped through a flow cell packed with extractive scintillating resin by a pump internal to the BetaRAM. The data were then re-binned to 100-s intervals and then passed through statistical algorithms developed in MATLAB® (Appendix A). The statistical algorithms constructed Shewhart 3-σ, CUSUM, and SR control chart plots and determined the volume required for the control chart to exceed the control limit for each method. Two SR control charts were constructed: the first using the Poisson distribution to estimate the likelihood ratio and the second using the Gaussian distribution, an approximation to the Poisson distribution for counting data, to estimate the likelihood ratio. These are henceforth referred to as the Poisson SR and Gaussian SR, respectively.

The detection efficiency was determined by passing 5 mL 0.01 M HCl and ^{99}Tc standard through flow cells packed with extractive scintillating resin. The first solution had 25.3 Bq ^{99}Tc in solution, and the second solution had 20.2 Bq ^{99}Tc in solution. Each test solution was preceded by 5 mL 0.01 M HCl and followed by 5 mL 0.01 M HCl. On-line time series data were collected while solution was pumped

through the flow cell. The detection efficiency was calculated by dividing the net count rate (cps) by the activity accumulated on the resin. The net count rate was calculated by summing 60-s of counts before the ^{99}Tc solution passed through the flow cell, summing 60-s of counts after all of the ^{99}Tc accumulated on the resin, calculating the difference between the two values, and then dividing the difference by 60-s to obtain count rate units of counts per second. Liquid scintillation counting confirmed that no radioactivity was present in the effluent above the maximum detectable concentration (MDC); thus, a loading efficiency of 100% was used for the detection efficiency calculation. The average ^{99}Tc detection efficiency was calculated to be 81.9% with an average counting error of 3.7% for this system.

5.1 Comparison of Control Chart Methods

Typical Shewhart 3-σ, CUSUM, and Poisson and Gaussian SR control charts are shown in Fig. 5.1 for a background solution (left). Note the semi-logarithmic scale for SR control charts. The average background count rate for all test solutions was 0.96 ± 0.14 cps. The false positive rate are listed in Table 5.1 for all background data ($N = 2602$) for each control chart method. The CUSUM and Poisson SR false positive rates were slightly higher than the theoretical false positive rate of 0.135%, and the Shewhart 3-σ and Gaussian SR were slightly lower than the theoretical false positive rate. ARL_0 values could not be calculated for each control chart method, because not all background data sets produced a false positive result. Thus, an absolute number could not necessarily be obtained for the location of a false positive for each data set, making it problematic to calculate accurate ARL_0 values.

Table 5.1: False positive incidence rates for Shewhart 3-σ, CUSUM, Poisson and Gaussian SR control chart methods based on $N = 2602$ measurements

Control Chart Method	False Positive Rate (%)
Shewhart 3-σ	0.0744
CUSUM	0.298
Poisson SR	1.19
Gaussian SR	0

Figure 5.1 shows typical Shewhart 3-σ, CUSUM, and Poisson and Gaussian SR control charts for a 1.51 Bq/L solution (right). An increasing trend is evident for the 1.51 Bq/L solution on all four control chart plots while no increasing trend is apparent for the background control charts after the control limit is exceeded. A continuous increasing trend was observed for all Gaussian SR control charts and most Poisson SR and CUSUM control charts for solutions containing radioactivity (≥ 0.1 Bq/L), whereas none of the background data sets exhibited a continuous increasing trend. The Shewhart 3-σ control charts showed a continuous increasing trend only for solutions containing more than 1 Bq/L; a trend was not obvious for solutions with lower activity concentrations. Control chart plots for all data sets are in Appendix B.

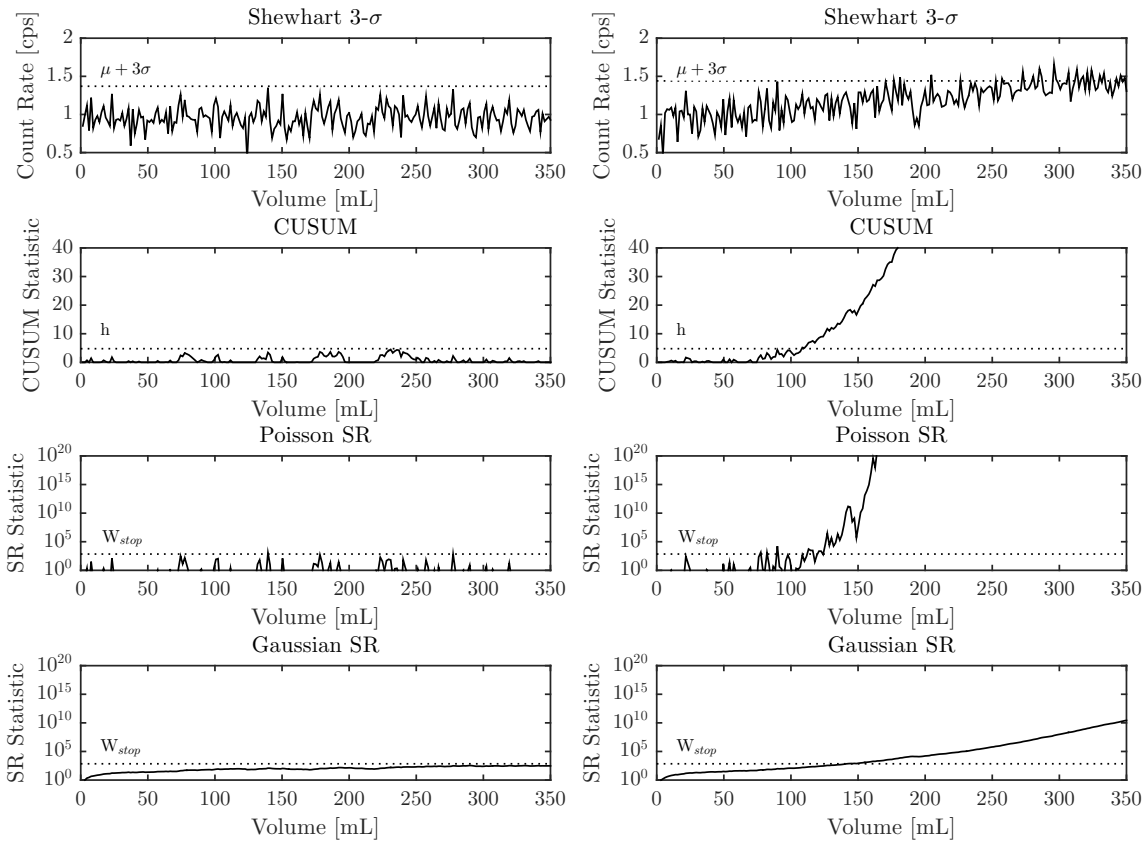

Figure 5.1: Typical Shewhart 3-σ, CUSUM, and Poisson and Gaussian SR control charts for background solution (left) and 1.51 Bq/L solution (right). Note the semi-log scale for the SR procedure control charts.

Control chart performance was measured by the volume of ^{99}Tc solution pumped through the flow cell before the control limit was exceeded, which is analogous to ARL_δ. The volume needed to exceed the control limit was averaged for triplicate test solutions containing approximately 0.1 Bq/L, 0.5 Bq/L, 1 Bq/L, 1.5 Bq/L, 2.5 Bq/L, and 5 Bq/L and plotted versus activity concentration, as shown in Fig. 5.2. Note the absence of vertical bars at 0.1 Bq/L for the Shewhart 3-σ and CUSUM control chart methods, because these methods did not consistently exceed

the control limit at this activity concentration. Control chart performance was not measured using activity accumulated when the control limit was exceeded to establish a detection limit, as was done in a similar study (Hughes et al. 2008). This value was expected to be constant across all activity concentrations; however, a general decreasing trend was observed with decreasing activity concentration for all control chart methods in this study. Activity to control limit exceedance data are displayed in Appendix D.

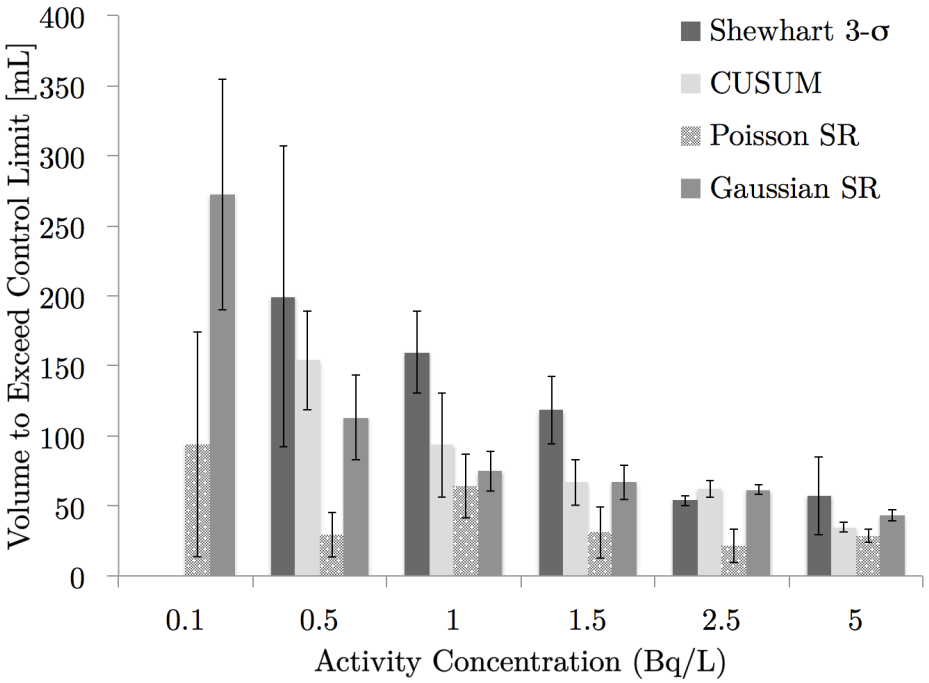

Figure 5.2: Average volume needed to exceed the control limit for the Shewhart 3-σ, CUSUM, Poisson and Gaussian Shiryaev-Roberts procedures. Error bars represent one standard deviation from the average of triplicate test solutions for each activity concentration. Note the absence of vertical bars at 0.1 Bq/L for the Shewhart 3-σ and CUSUM control chart methods, because these methods did not consistently exceed the control limit at this activity concentration.

Overall, the Poisson and Gaussian SR required less solution volume to exceed the control limit than the Shewhart 3-σ method. The Poisson SR method required 28.9 mL less solution at 5 Bq/L and up to 170 mL less solution at 0.5 Bq/L than

the Shewhart 3-σ method. The Gaussian SR method needed less solution than the Shewhart 3-σ method to exceed the control limit for all of the activity concentrations except for 2.5 Bq/L; it required 7.75 mL more solution than the Shewhart 3-σ method at this activity concentration. This likely occurred because the count rate for two of three 2.5 Bq/L test solutions initially exceeded the UCL on the Shewhart 3-σ control chart 50 mL and 100 mL before an increasing trend was apparent, as shown in Fig. 5.3, which significantly reduced the quantity of solution needed to exceed the control limit for this method. The iterative nature of the Gaussian SR method did not cause it to respond to the early spike, because the Gaussian SR statistic was saturated by previous data and needed more than a single spike to exceed the control limit. Additional data collected at approximately 2.5 Bq/L would likely increase the average volume to exceed the control limit for the Shewhart 3-σ. This would possibly lead to the Gaussian SR method needing less volume to exceed the control limit at this activity concentration, thus becoming consistent with the other measured concentrations. The Gaussian SR performed best compared to the Shewhart 3-σ method at 1 Bq/L, where 84.7 mL less solution was needed to exceed the control limit.

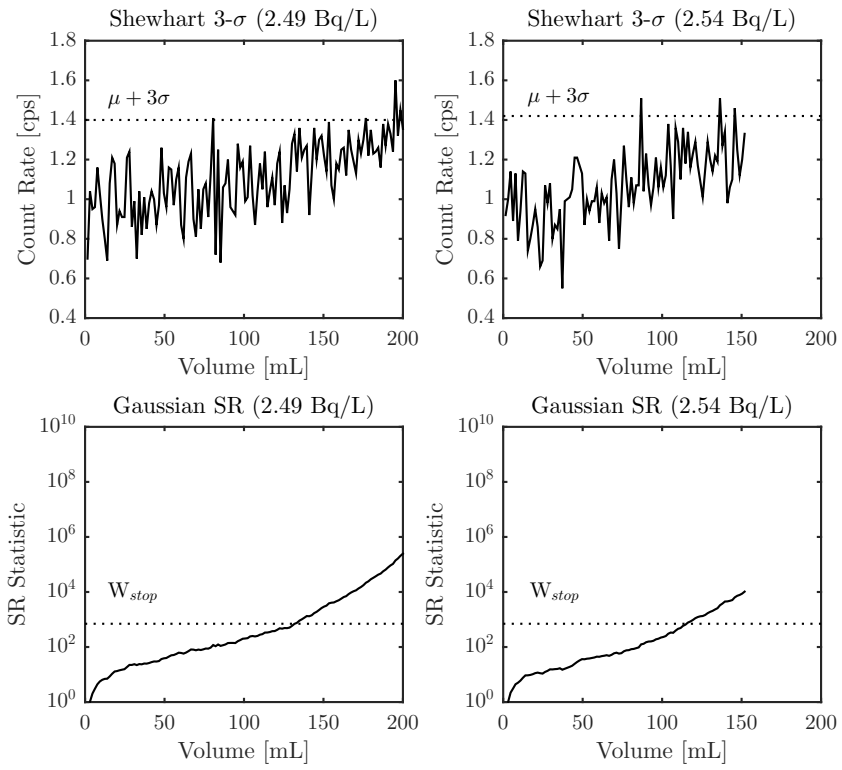

Figure 5.3: Shewhart 3-σ and Gaussian SR control charts for 2.49 Bq/L (left) and 2.54 Bq/L (right) to illustrate that the Shewhart 3-σ control charts had an early spike that caused early detection compared to the Gaussian SR control charts for these test solutions

The Poisson SR also required less solution volume to exceed the control limit than the CUSUM method, but the Gaussian SR method used comparable solution volume to the CUSUM method until the activity concentration was less than 1.5 Bq/L. The Poisson SR method required at least 6.20 mL less solution at 5 Bq/L and up to 125 mL less solution at 0.5 Bq/L than the CUSUM method. The Gaussian SR and CUSUM method, on the other hand, required comparable solution volumes for test solution containing at least 1.5 Bq/L of ^{99}Tc. For activity concentrations less than 1.5 Bq/L, the Gaussian SR method required as much as 40.8 mL less solution to exceed the control limit than the CUSUM method. The Gaussian SR method was expected

to use less volume as the activity concentration decreased, because the Gaussian SR and CUSUM methods perform comparably when large or moderate changes occur in the process mean; however, the Gaussian SR outperforms the CUSUM method when small changes occur in the process mean (Moustakides et al. 2009). Thus, for activity concentrations less than 1.5 Bq/L, the change in the process mean likely became small enough for the Gaussian SR to use less volume than the CUSUM method to exceed the control limit.

Although the Poisson and Gaussian SR mostly required less solution volume to exceed the control limit than the Shewhart 3-σ and CUSUM methods, the Poisson SR required much less solution volume than the Gaussian SR in most cases. The Poisson SR required a comparable quantity of solution volume as the Gaussian SR at 1 Bq/L, requiring only 10.9 mL less solution to exceed the control limit. However, four of the six activity concentrations compared required up to 178 mL less solution at 0.1 Bq/L for the Poisson SR than the Gaussian SR. The delayed response of the Gaussian SR was not surprising, because the false positive rate for this method was much lower than the false positive rate for the Poisson SR. Since a lower false positive rate means that the false negative rate is higher, this translates to a detection delay and longer ARL_δ in statistical process control, which is evident when comparing the volume to exceed the control limit for the Poisson SR and Gaussian SR methods. Ultimately, a choice must be made between a lower false positive rate, resulting in higher ARL_0 and more solution to exceed the control limit, or a lower false negative rate, resulting smaller ARL_δ and less solution to exceed the control limit, when deciding which distribution to implement in the SR method for on-line environmental radiation monitoring.

Comparing the magnitude of the increasing trend for the control charts, the Poisson SR control chart increased most rapidly after crossing the stopping threshold, followed by the Gaussian SR, CUSUM, and Shewhart 3-σ methods, respectively. This

trend is illustrated in Fig. 5.1 for the 1.51 Bq/L solution (right). Evidence of a continuous, steep increasing trend after exceeding the control limit is an important feature for a control chart in on-line environmental radiation monitoring. It indicates to the user that activity is accumulating on the resin and that the control limit exceedance is not the result of a false positive caused by statistical variation in radioactive decay. The steeper the control plot curve, the easier it is for the user to differentiate between activity accumulation and a false positive. Because of this, the rapid increasing trend on the Poisson and Gaussian SR control charts was an excellent advantage over other control charts to indicate that activity is accumulating on the resin.

The difference between the Poisson and Gaussian SR control chart magnitudes lies within the equations used to calculate the respective SR statistics. Plugging the constants $\mu = 96$, $\sigma = 14$, $\delta = 3$, and $n = 1$ into Eqns. 2.13 and 2.14 for the Poisson and Gaussian SR, respectively, the equations became

$$W_m = \sum_{i=1}^{m-1} \exp\left[-29.4i + 0.116 \sum_{j=i+1}^{m} CR_j\right]$$

for the Poisson SR method, and

$$W_m = \sum_{i=1}^{m-1} \exp\left[-0.023(m-i) + 0.015 \sum_{j=i+1}^{m} (CR_j - 96)\right]$$

for the Gaussian SR method, where m is the measurement number. The constant associated with count rate data, CR_j, in the Poisson SR statistic equation was an order of magnitude greater than the constant associated with the Gaussian SR. The expected mean background count rate was also not subtracted from each data point in the Poisson SR method, but was subtracted from each data point in the Gaussian SR method. So, hundreds of counts were summed for CR_j for the Poisson SR statistic

compared to only tens of counts summed for CR_j for the Gaussian SR statistic. Since the count rate data are associated with positive exponential growth, the larger constant and more counts summed for the data causes the Poisson SR statistic caused it to increase much more quickly than the Gaussian SR statistic.

Gaussian SR and CUSUM methods had a distinct continuously increasing trend immediately after crossing the stopping threshold for the 1.51 Bq/L solution in Fig. 5.1, indicating that ^{99}Tc was accumulating on the resin. An increasing trend was not, however, evident on the Poisson SR control chart until 130 mL, 45 mL after the control limit was initially exceeded, or the Shewhart 3-σ control chart until about 200 mL, 55 mL after the control limit was initially exceeded. The delay between the initial control limit exceedance and an increasing trend becoming apparent could cause personnel to misinterpret the initial threshold exceedance as a false positive. This could be detrimental to remediation and nonproliferation efforts by delaying action to stop the contamination. Thus, it is important that the control chart exhibit a continuously increasing trend promptly after exceeding the control chart limit.

The Shewhart 3-σ and CUSUM methods only exceeded the control limit for two of three 0.1 Bq/L test solutions, the lowest activity concentration tested, whereas the Poisson and Gaussian SR methods consistently exceeded the control limit for these test solutions. Only the Gaussian SR method, however, consistently exhibited a continuous increasing trend for all control charts at this activity concentration, as shown in Fig. 5.4. The control limit exceedance for the Shewhart 3-σ, CUSUM, and Poisson SR for the 0.1 Bq/L solutions could be confused as a false positive, because the respective statistic does not continually increase past the control limit. As previously stated, a continuous increasing trend after the control limit exceedance is an important control chart feature to indicate accumulated activity; without it, the signal indicating a change in the mean count rate could be mistaken as a false positive.

Despite this, the ability of both SR methods to consistently detect low-level activity concentrations is an advantage over other control charts for on-line environmental radiation monitoring. Most environmental radiation measurements involve detecting low levels of activity; so, consistent detection at low activity concentrations is an ideal quality for a control chart.

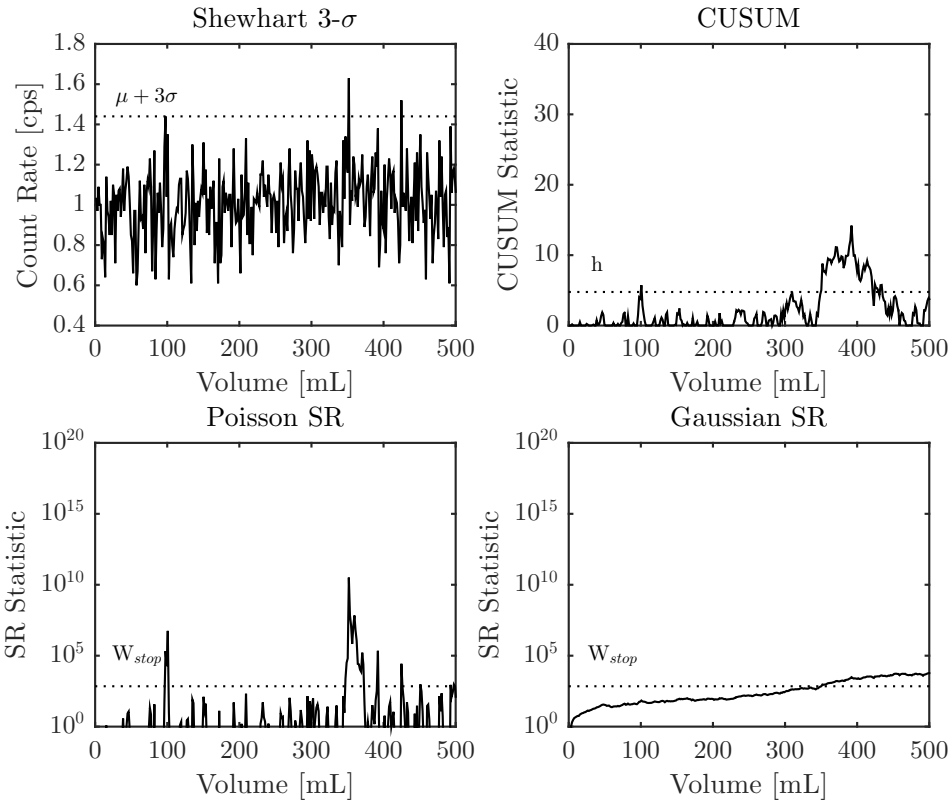

Figure 5.4: Shewhart 3-σ, CUSUM, and Poisson and Gaussian SR control charts for 470 mL 0.110 Bq/L solution preceded by 30 mL 0.01 M HCl. Only the Gaussian SR control exhibits a continuous increasing trend at this activity concentration, an important quality for a control chart used for on-line environmental radiation monitoring using extractive scintillating resin.

When implementing the SR method for on-line environmental radiation monitoring, the desired results from the monitoring scheme will need to be considered prior to choosing a distribution to estimate the likelihood ratio. The main factors

to consider are volume to control limit exceedance, false positive rate, and whether a continuous increasing trend immediately after control limit exceedance is desired. The Poisson SR will exceed the control limit using less solution volume; however, more false positives will occur, which could be an annoyance to the user. Unfortunately, the Poisson SR does not consistently exhibit a continuous increasing trend at the lowest activity concentrations; so, distinguishing between false positives and activity accumulation on the resin will be difficult for an unknown solution. Conversely, the Gaussian SR has a much lower false positive rate; but, this leads to more volume needed to exceed the control limit, which can cause a detection delay and thus delay remedial action. This can be countered though, because the Gaussian SR exhibits a continuous increasing trend after exceeding the control limit even at low activity concentrations. This allows the user to be certain that there was an increase in count rate and remedial action may need to occur depending on the extent of the contamination.

Since environmental radiation measurements are typically low-level measurements, the ideal control chart for on-line environmental radiation monitoring using extractive scintillating resin should be able to do the following: 1) detect changes in the mean count rate quickly, 2) consistently detect low activity concentrations, and 3) have a continuous increasing trend after exceeding the control limit to distinguish between a false positive and activity accumulating on the resin. The Poisson and Gaussian SR methods required less volume to exceed the control limit than the Shewhart 3-σ and CUSUM methods in most cases and were the only two methods to consistently detect the 0.1 Bq/L test solutions. Based on these criteria, the SR method is thus better suited for low-level on-line environmental radiation monitoring than the Shewhart 3-σ and CUSUM methods.

5.2 Activity Concentration Estimation

In statistical process control, the control chart is typically stopped once the control limit is exceeded. The process is then put back on track, and the control chart is restarted as an in-control process. Unfortunately, this does not provide information about the state of the process mean except that it is out-of-control. Since on-line environmental radiation monitoring is not a process that can simply be put back on track, further information regarding the state of the mean is desired so that appropriate remedial action can be implemented. Hughes et al. (2008) was able to estimate the activity concentration in a solution from the CUSUM and EWMA control charts after the control limit was exceeded, because the magnitude of the control chart was dependent on the activity concentration of the solution. The magnitude of the Poisson and Gaussian SR control charts appears to have a similar dependency on activity concentration, as illustrated in Fig. 5.5 for 2.50 Bq/L, 1.51 Bq/L, and 0.497 Bq/L solutions. Because of the dependency on activity concentration, it was hypothesized that the Poisson and Gaussian SR control charts can likely be used to estimate the activity concentration using a similar method to those developed for the CUSUM and EWMA control charts (Hughes et al. 2008).

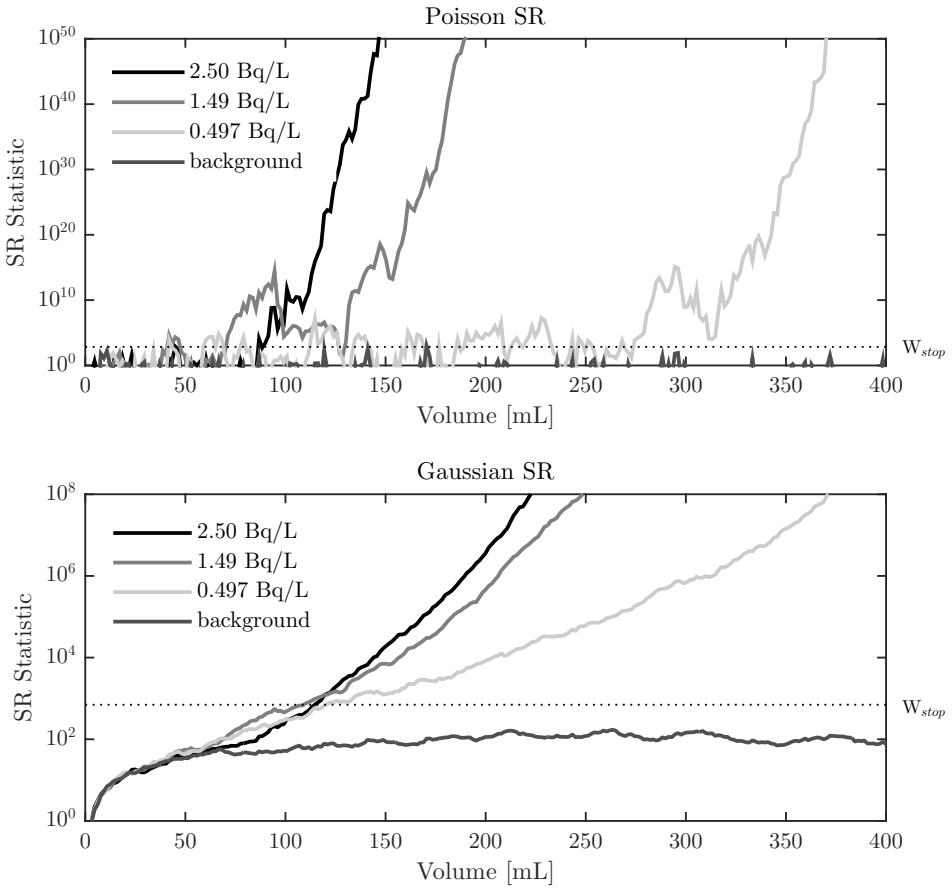

Figure 5.5: Poisson and Gaussian SR control charts for 2.50 Bq/L, 1.49 Bq/L, 0.497 Bq/L, and background solutions

Figure 5.5 suggests that the logarithmic value of the SR statistic and volume have a linear relationship after the control limit was exceeded. In the case of the Poisson SR, a linear trend did not necessarily exist until the control limit was exceeded and a continuous increasing trend was evident. The magnitude of the linear slope for the SR control charts also appears to be dependent on activity concentration. Given this, activity concentration was related to the slope of the SR control chart on a semi-logarithmic scale to estimate activity concentration in a solution. The slope

of the Poisson SR control chart, m_p, was calculated by

$$m_p = \frac{\log(W_i) - \log(W_p)}{\Delta V_p}$$

where W_i is an SR statistic after the stopping threshold was exceeded, W_p is the Poisson SR statistic that exceeded the stopping threshold and exhibited a continuous increasing trend thereafter, and ΔV_p is the volume that passed through the flow cell from W_p to W_i. The slope of the Gaussian SR control chart, m_g, was calculated by

$$m_g = \frac{\log(W_i) - \log(W_g)}{\Delta V_g}$$

where W_g is the Gaussian SR statistic that exceeded the stopping threshold, and ΔV_g is the volume that passed through the flow cell from W_g to W_i. This method was derived only for the situation where activity continuously accumulates on the resin; it could not be used in a situation for stop-flow, plume passes, or resin capacity exceedance. These events caused the count rate to "level-off" at a constant rate, causing the Poisson and Gaussian SR to increase at a different rate than during activity accumulation.

Activity concentration and the slope of the SR control charts had an empirical relationship; so, a calibration curve was required for this method. The calibration curve was constructed by randomly selecting one test solution from each activity concentration grouping (0.1 Bq/L, 0.5 Bq/L, 1 Bq/L, 1.5 Bq/L, 2.5 Bq/L, and 5 Bq/L). Separate calibration curves were necessary for the Poisson and Gaussian SR curves, because they did not increase in magnitude at the same rate for a given activity concentration. Their respective calibration curves are pictured in Fig. 5.6. No 0.1 Bq/L test solutions were included in the Poisson SR calibration curve, because a

slope could not be calculated due to the lack of a continuous increasing trend. Values of W_i investigated for the Poisson SR were approximately 10^{50}, 10^{60}, and 10^{70}, and values of W_i investigated for the Gaussian SR were approximately 10^5, 10^6, 10^7, and 10^8. Slope values were not calculated for smaller values than $W_i = 10^{50}$ and $W_i = 10^5$ for the Poisson and Gaussian SR methods, respectively, because the SR statistics varied considerably in many cases up until this point, particularly for the Poisson SR method. In order to have consistent responses to construct an acceptable calibration curve, larger statistic values were needed despite the consequential delay in estimating the activity concentration. The value $W_i = 10^{50}$ was ultimately chosen for the Poisson method, because the R^2 value of 0.83 for calibration curve did not improve for $W_i = 10^{60}$ or $W_i = 10^{70}$; so, this value was chosen for more rapid quantification. The value $W_i = 10^8$ was chosen for the Gaussian SR method, because it was the only value to produce an R^2 value greater than 0.9 for the calibration curve, indicating the linear model was a good fit to the data.

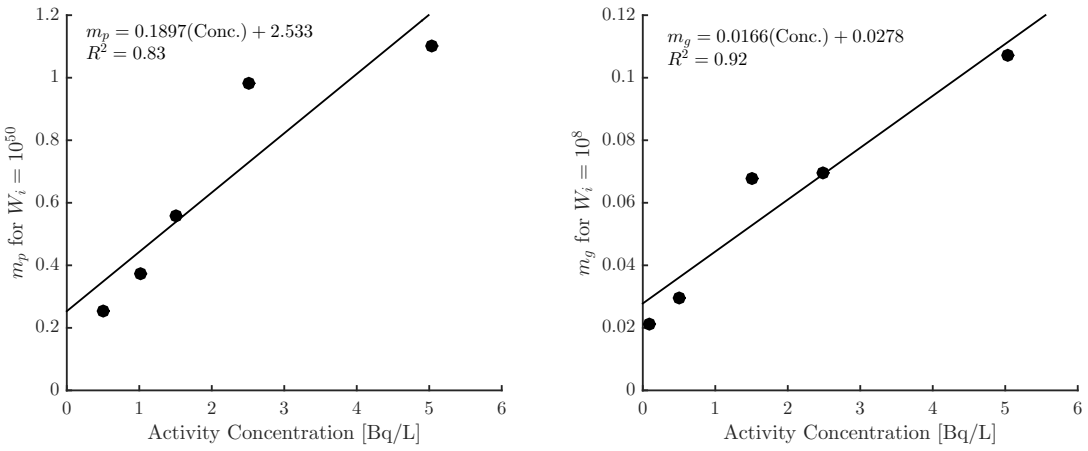

Figure 5.6: Calibration curves to estimate the activity concentration using the slope of the Poisson (left) and Gaussian (right) Shiryaev-Roberts procedure control charts

The error in the calibration curve likely stemmed from variation in the control charts for solutions with approximately equal activity concentrations. Figure 5.7 illustrates this variation for test solutions of about 0.5 Bq/L (left) and 1 Bq/L (right). For the Poisson SR control charts, the test solutions were statistically different from each other for both activity concentrations. This likely introduced significant error in the calibration curve, because the calibration curve was constructed assuming that the control charts would be statistically similar and thus reproducible for similar activity concentrations. Since the control charts were not necessarily reproducible, a trend among various activity concentrations was difficult to define for the calibration curve due to the lack of a trend for similar activity concentrations. The Gaussian control charts were overall less statistically different from each other from each other than the Poisson SR control charts; however, there were notable outliers, particularly the 0.497 Bq/L test solution. The linear fit to the calibration curve was thus better for the Gaussian SR method, because the control charts had better agreement with each other for similar activity concentrations and thus better reproducibility. A trend was then easier to define for different activity concentrations since control charts for similar activity concentrations appeared to be comparable.

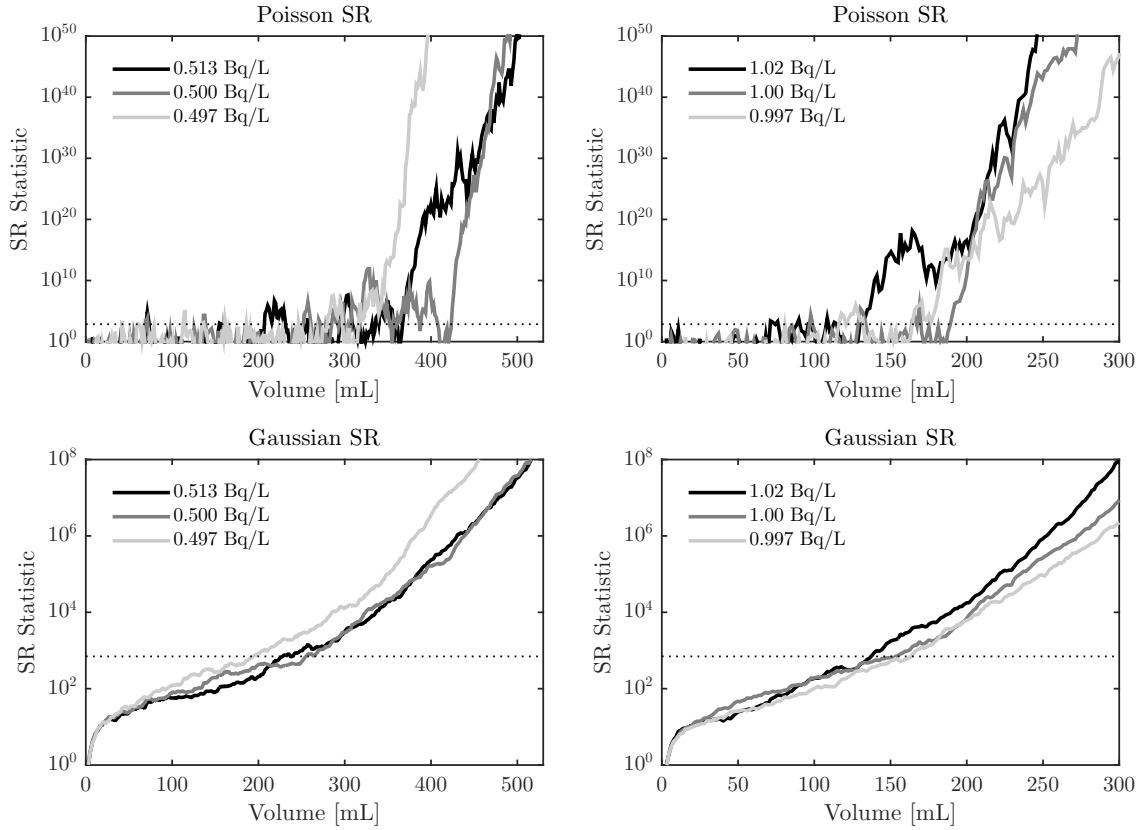

Figure 5.7: Comparison of test solutions containing approximately 0.5 Bq/L (left) and 1 Bq/L (right) for Poisson and Gaussian SR control charts

The activity concentration was estimated for nine solutions using the Poisson SR calibration curve and eight solutions using the Gaussian SR calibration curve. The results displayed in Table 5.2 include the slope calculated from the respective Poisson and Gaussian SR calibration curves, the volume that passed through the flow cell between W_p and $W_i = 10^{50}$ for the Poisson SR method and W_g and $W_i = 10^8$ for the Gaussian SR method, the estimated activity concentration for each method from the fit to the calibration curve, and the percent deviation of the estimated activity concentration from the actual activity concentration. Gaussian SR statistic values for the 2.53 Bq/L test solution did not reach $W_i = 10^8$, because the volume

of test solution that was passed through the flow was not sufficient to produce SR statistic values greater than this; so, an activity concentration estimation was not be calculated for this solution.

Activity concentration estimations for the Poisson SR method were within approximately 30% of the actual value for five of nine solutions. The least precise estimation for the Poisson SR method was the 0.497 Bq/L test solution, which had an estimated value 263.2% different than the actual value. The poor results for four of the nine estimations likely resulted from inconsistencies among control charts at the same activity concentration for reasons similar to the error in the calibration curve. The poor reproducibility of the Poisson SR control for similar activity concentrations likely caused the imprecise slope estimates, because the control charts were not necessarily the same as the solution used for the calibration curve.

Activity concentration estimates for the Gaussian SR method were much better than the Poisson SR method. Six of eight estimations were within 30% of the actual value, and all estimations were within 76% of the actual value. The more precise estimates likely stemmed from better control chart reproducibility for the Gaussian SR method than the Poisson SR method. The Gaussian SR calibration curve was able to identify a strong trend among different activity concentrations, because the control charts were comparable for similar activity concentrations. This ultimately led to better activity concentration estimations using the slope of the Gaussian SR control chart, because the control charts were reproducible for similar activity concentrations.

Table 5.2: Activity concentration estimations using the slope of the Poisson SR control chart, m_p, and Gaussian SR control chart, m_g, on a semi-logarithmic scale for test solutions containing approximately 0.5-5 Bq/L of ^{99}Tc.

Activity Conc. (Bq/L)	Poisson Slope, m_p, at $W_i = 10^{50}$	Volume, (mL) $(W_i > W_{stop})$	Poisson SR Est. (Bq/L)	Poisson SR % Deviation of Means	Gaussian Slope, m_g, at $W_i = 10^8$	Volume, (mL) $(W_i > W_{stop})$	Gaussian SR Est. (Bq/L)	Gaussian SR % Deviation of Means
4.97	0.72	69.8	2.38	52.1	0.091	55.8	3.65	26.6
2.53	0.78	58.9	2.66	-5.2	n/a	n/a	n/a	n/a
2.50	0.84	57.4	2.94	-17.5	0.095	51.2	3.87	-54.7
1.53	0.63	74.4	2.01	-31.6	0.057	91.5	1.79	-16.7
1.49	0.59	76.0	1.82	-21.8	0.047	110.1	1.24	16.5
1.00	0.56	82.2	1.71	-71.2	0.043	120.9	1.00	0.1
0.997	0.35	138.0	0.79	20.4	0.056	89.9	1.75	-75.2
0.513	0.40	119.4	1.00	-94.4	0.036	141.1	0.66	-29.1
0.497	0.58	80.6	1.81	-263.2	0.026	200.0	0.12	76.0

Overall, the estimations produced using this method were mediocre for the Poisson SR method and satisfactory for the Gaussian SR method. A more complex method that accounts for variation among control charts with similar activity concentrations would likely produce better estimates for the SR control charts. These results demonstrate, however, that a relationship exists between activity concentration and the magnitude of the SR control chart that can be exploited to determine the activity concentration using the control chart.

5.3 Additional Studies

Nitric acid (0.01 M) was initially used for the test solutions, because it was previously used for ^{99}Tc uptake using MDOA as the extracting ligand (Seliman et al. 2011); however, the loading efficiency was inconsistent with the resin used for this study. Control chart plots for data collected using nitric acid as the test solution are in Appendix C. Liquid scintillation counting confirmed the loading efficiency for $^{99}TcO_4^-$ was consistently 100% using 0.01 M HCl. These results were consistent with Seliman et al. (2013).

5.4 Future Work

Additional distributions should be considered to estimate the likelihood ratio in the SR statistic. The 'alpha' distribution, a simplified variant of the Gamma distribution, and log-normal distribution have previously been studied as prior distributions for Bayesian statistical analysis of radiation measurements (Miller et al. 2001). These distributions could improve the fit of the distribution to the data, which would likely improve SR control chart performance.

The performance of the SR procedure should also be tested using environmental samples, such as groundwater samples. A previous study used synthetic groundwater samples to test the performance of the Shewhart 3-σ, CUSUM, and EWMA methods against samples prepared using 0.01 M HNO_3 (Hughes et al. 2008). The control charts performed comparably using the synthetic groundwater samples as the nitric acid samples; however, the activity concentration estimations were not always precise, unlike the samples prepared using nitric acid (Hughes et al. 2008). Varying the pH of the test solution and introducing ions competitive with $^{99}TcO_4^-$ into the solution should be considered to compare the performance of the SR curves to a 0.01 M HCl solution used in this study.

Additional methods should also be investigated to improve activity concentration estimation for the Poisson and Gaussian SR control charts. More complex methods that account for variation among control charts with similar activity concentrations would likely produce better estimates for the SR control charts. These methods should include using three or more points on the SR control chart to average the slope from several points on the curve. Improving the activity concentration estimation method is important in order to determine the state of the mean after the control limit is exceeded for on-line environmental radiation monitoring.

Further studies should be performed to determine the cause of the inconsistent loading efficiency using nitric acid as the test solution for this extractive scintillating resin. This was an unexpected result, as nitric acid had previously been used with the extracting ligand used for ^{99}Tc uptake in this extractive scintillating resin. A loading efficiency of 100% was measured in this study, and no inconsistencies were reported regarding uptake (Seliman et al. 2011). Conditioning protocols should be considered to swell the beads prior to passing a radioactive solution through them. This would help properly wetted them and provide access to more binding sites.

Chapter 6

Conclusions

The SR procedure is the best suited control chart for low-level on-line environmental radiation monitoring with an accumulating signal. Both the Poisson and Gaussian SR methods required less solution volume to exceed the control limit than the Shewhart 3-σ method in most cases, which is analogous to having a smaller ARL_δ. The CUSUM method and Gaussian SR method required comparable solution for activity concentrations of at least 1.5 Bq/L. For activity concentration less than 1.5 Bq/L, the Gaussian SR method required less solution volume than the CUSUM method. This finding was consistent with previous studies that indicated that the Gaussian SR detects small changes in the process mean more quickly than the CUSUM. Both SR methods also consistently detected test solutions containing approximately 0.1 Bq/L, the lowest activity concentration tested, whereas the Shewhart 3-σ and CUSUM methods were not able to consistently detect solutions containing this activity concentration. A continuous increasing trend was exhibited for all Gaussian SR control charts and most Poisson SR and CUSUM control charts for test solutions with an activity concentration greater than 0.1 Bq/L; however, the Shewhart 3-σ control charts only exhibited an increasing trend on control charts for

test solutions containing greater than 1 Bq/L. This is an important feature of a control chart for on-line environmental radiation monitoring, because it allows the user to distinguish between activity accumulation on the resin and a false positive caused by statistical variation in radioactive decay.

Although both the Poisson and Gaussian SR methods are excellent tools for on-line environmental radiation monitoring, the desired results from the monitoring scheme need to be considered prior to choosing a distribution to estimate the likelihood ratio. The Poisson SR method required less solution volume to exceed the control limit than the Gaussian SR method; however, the Gaussian SR method had a lower false positive rate than the Poisson SR method, making it easier to distinguish between false positives and actual activity accumulation on the resin. The Poisson SR also does not always immediately exhibit a continuous increasing trend after initially exceeding the control limit, because it bounces around the control limit until the measured count rate increases enough above the background count rate for it to exhibit the increasing trend. Conversely, the Gaussian SR method does exhibit a continuous increasing trend after initially exceeding the control limit for all test solutions, even solutions containing 0.1 Bq/L. Overall, the Poisson SR method will detect a change in the mean count rate faster than the Gaussian SR method, but the control chart may not always be detecting activity accumulation on the resin due to the lack of immediate continuous increasing trend after exceeding the control limit in many cases. Conversely, the Gaussian SR method consistently distinguishes between a false positive and activity accumulation on the resin by exhibiting a continuous increasing trend, but requires more volume to detect a change in the process mean.

Estimating the activity concentration using the slope of the SR statistic on a semi-logarithmic scale produced mediocre results for the Poisson SR method and satisfactory results for the Gaussian SR method; however, the relationship between

activity concentration and SR curve magnitude can be used to determine the activity concentration. More complex methods should thus be considered to improve the activity concentration estimations from the Poisson and Gaussian SR curves.

Appendices

Appendix A MATLAB Algorithms

CRchange.m

```
% Re-bin 10-s intervals to 100-s intervals
clear all;
data=xlsread('insert file name here','insert cells here');
newd=[];
j=1;
for x=1:10:length(data)
    k=1;
    num=0;
    while k<11
        num=num+data(x+k-1);
        k=k+1;
    end
    newd(j)=num;
    j=j+1;
end
newd=newd';
```

analysis.m

```
clear all;

% Input file information for analysis
file=input('Enter the file name?','s');
cells=input('Which cells will be accessed?','s');
data=xlsread(file,cells);

a=input('Enter the average background count rate:  ');
s=input('Enter the standard deviation of the background count rate:  ');
v=input('Enter the volumetric flow rate [mL/min]:  ');

% Analyze data for the Shewhart, CUSUM, and SR methods
shew3=Shewhart(data,a,s); % Shewhart.m
[cus,c]=CUSUM(data,a,s); % CUSUM.m
[SRp,Wp]=SRpoi(data,a,s); % SRpoi.m
[SRn,Wn]=SRnorm(data,a,s); % SRnorm.m

% Display the results
disp(['The Shewart method responded after ',shew3,'measurements.']);
disp(['The CUSUM method responded after ',cus,'measurements.']);
disp(['The Poisson SR method responded after ',SRp,'measurements.']);
disp(['The normal SR method responded after ',SRn,'measurements.']);

% Horizontal axis
x=1:length(data);
x=x.*100./60.*v;

% Subplot
```

```
29 fig=figure('Position',[100 100 400 575]);
30 set(0, 'defaultTextInterpreter', 'latex');
31 set(groot, 'defaultAxesTickLabelInterpreter','latex')
32
33 % Plot Shewhart 3-sigma
34 fig1=subplot(4,1,1); % subplot 1
35 data=data./100;
36 plot(fig1,x,data,'black')
37 high=refline(0,a/100+3*s/100);
38 set(high,'LineStyle',':','Color','black');
39 title('Shewhart 3-sigma')
40 xlabel('Volume [mL]');
41 ylabel('Count Rate [cps]');
42
43 % Plot CUSUM statistic
44 fig2=subplot(4,1,2); % subplot 2
45 plot(fig2,x,c,'black')
46 h=refline(0,4.77);
47 set(h,'LineStyle',':','Color','black');
48 title('CUSUM')
49 xlabel('Volume [mL]');
50 ylabel('CUSUM Statistic');
51
52 % Plot Poisson SR statistic
53 fig3=subplot(4,1,3); % subplot 3
54 semilogy(fig3,x,Wp,'black')
55 Wstop=refline(0,700);
56 set(Wstop,'LineStyle',':','Color','black');
57 title('Poisson Shiryaev-Roberts')
58 xlabel('Volume [mL]');
59 ylabel('SR Statistic');
```

```
60
61 % Plot Gaussian SR statistic
62 fig4=subplot(4,1,4); % subplot 3
63 semilogy(fig4,x,Wn,'black')
64 Wstop=refline(0,700);
65 set(Wstop,'LineStyle',':','Color','black');
66 title('Gaussian Shiryaev-Roberts')
67 xlabel('Volume [mL]');
68 ylabel('SR Statistic');
```

Shewhart.m

```
function [i]=Shewhart(data,a,s)
% Turn counts into count rate
data=data./100;
a=a/100;
s=s/100;

% Shewhart parameters
d=3;

% Alarm location
for i=1:size(data,1)
    if data(i)>a+d*s
        step=i;
        return;
    end
end
end
```

CUSUM.m

```
function [k,c]=CUSUM(data,a,s)
% CUSUM parameters
k=0.5;
h=4.77;
t=size(data,1);
c=zeros(t,1);
ndata=(data-a)./s; %normalize data
for j=1:t
    if j==1
        c(j)=max(0,ndata(j)-k); % c(0)=0
    else
        c(j)=max(0,ndata(j)-k+c(j-1));
    end
end

% Alarm location
for k=1:size(data,1)
    if c(k)>h
        step=k;
        return;
    end
end
end
```

SRpoi.m

```
function [p,W]=SRpoi(data,a,s)
% Poisson SR parameters
n=1;
Wstop=700;
Δ=3;
rho=(a+Δ*sqrt(a))/a;

% SR statistic calculation
W=zeros(length(data),1);
for m=2:length(data)
    s1=0;
    wm=0;
    for i=1:m-1
        s1=s1+data(m-i+1);
        wm=wm+exp(-i*Δ*sqrt(a)+log(rho)*s1);
    end
    W(m)=wm;
end

% Alarm location
for p=1:size(W,1)
    if W(p)>Wstop
        p;
        return;
    end
end
```

SRnorm.m

```
function [p,W]=SRnorm(data,a,s)
% Gaussian SR parameters
n=1;
Wstop=700;
Δ=1;
d2=Δ^2;
s2=s^2;

% SR statistic calculation
W=zeros(length(data),1);
for m=2:length(data)
    wm=0;
    sum=0;
    for i=1:m-1
        sum=sum+data(m-i+1)-a;
        wm=wm+exp(-i*n*d2/(2*s2)+n*Δ*sum/s2);
    end
    W(m)=wm;
end

% Alarm location
for p=1:size(W,1)
    if W(p)>Wstop
        p;
        return;
    end
end
end
```

Appendix B Control Chart Plots (HCl Data)

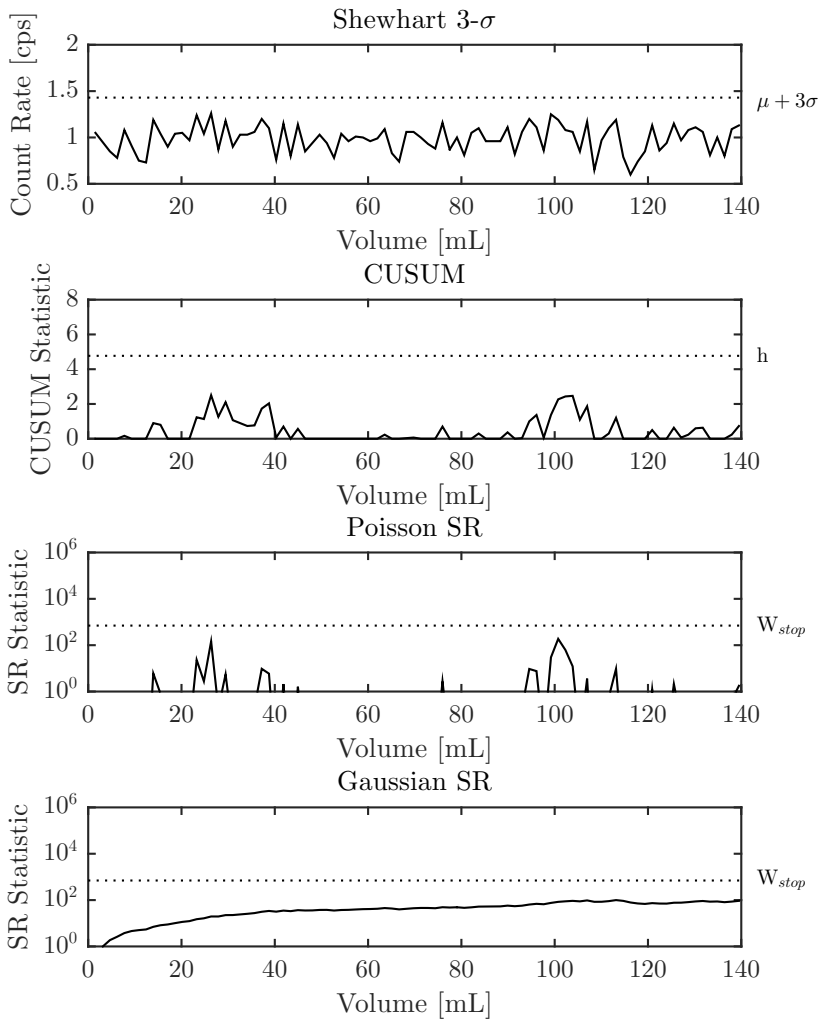

Figure B.1: Shewhart, CUSUM, S-R control charts for background 1; 140 mL of 0.01 M HCl

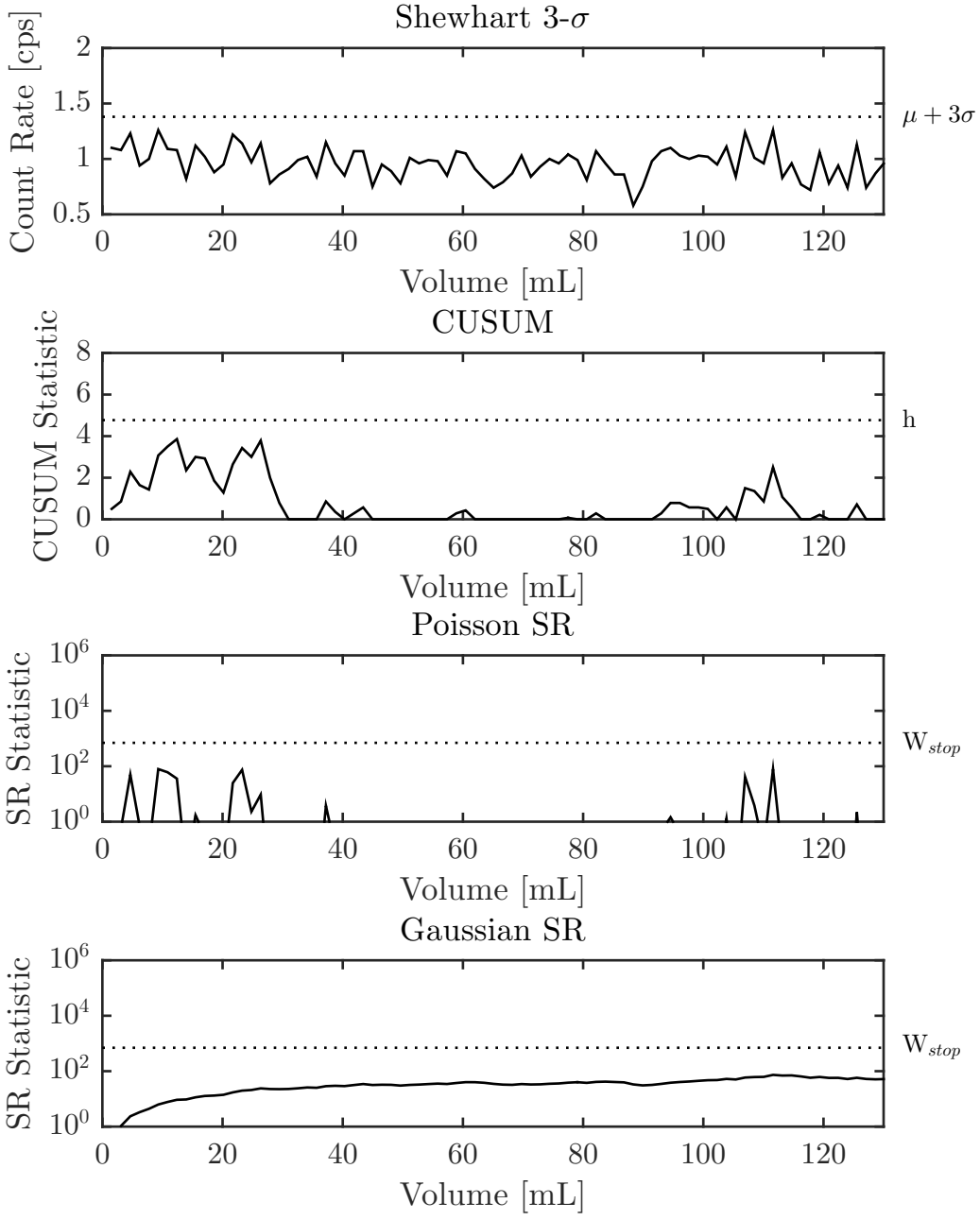

Figure B.2: Shewhart, CUSUM, S-R control charts for background 2; 130 mL of 0.01 M HCl

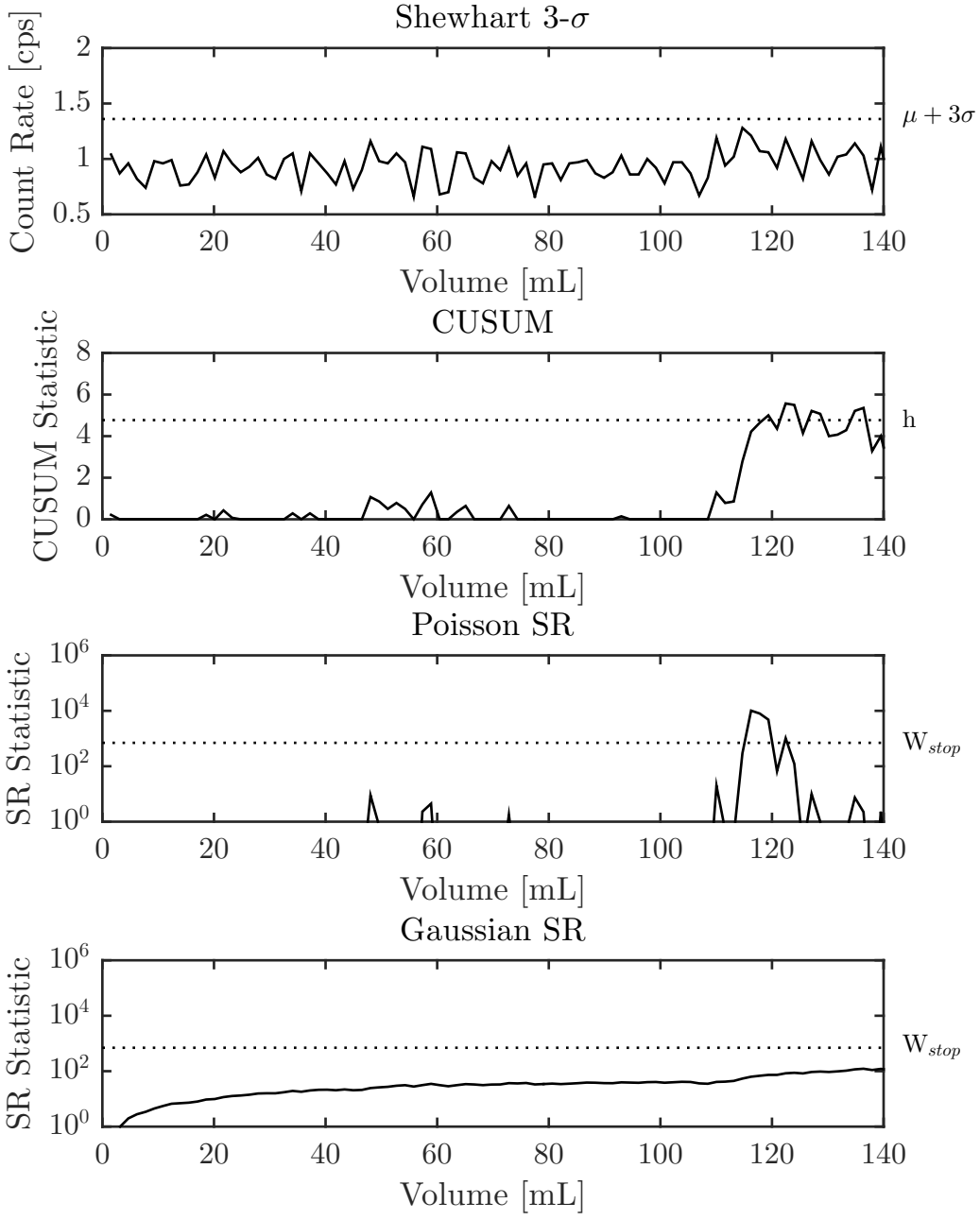

Figure B.3: Shewhart, CUSUM, S-R control charts for background 3; 140 mL of 0.01 M HCl

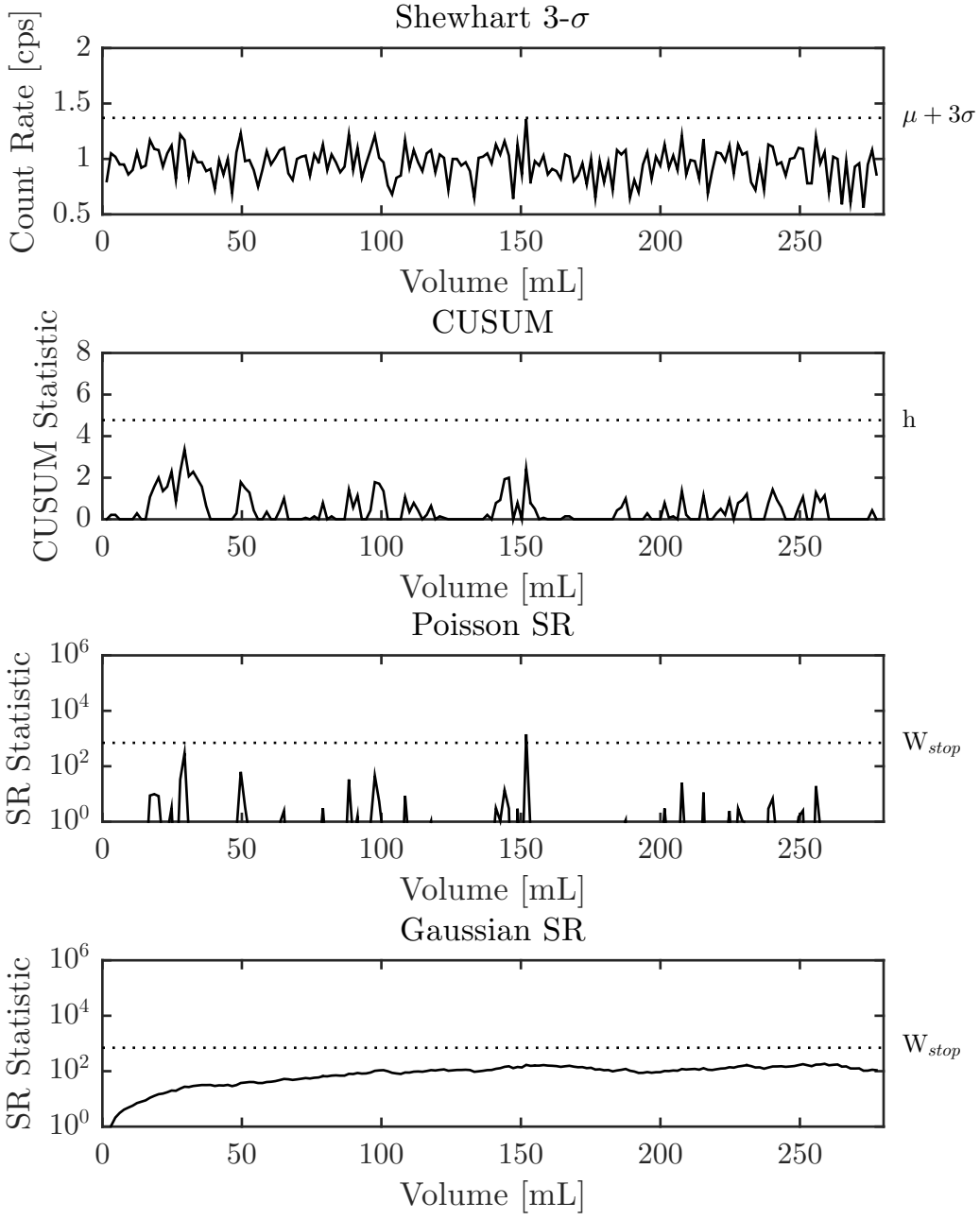

Figure B.4: Shewhart, CUSUM, S-R control charts for background 4; 280 mL of 0.01 M HCl

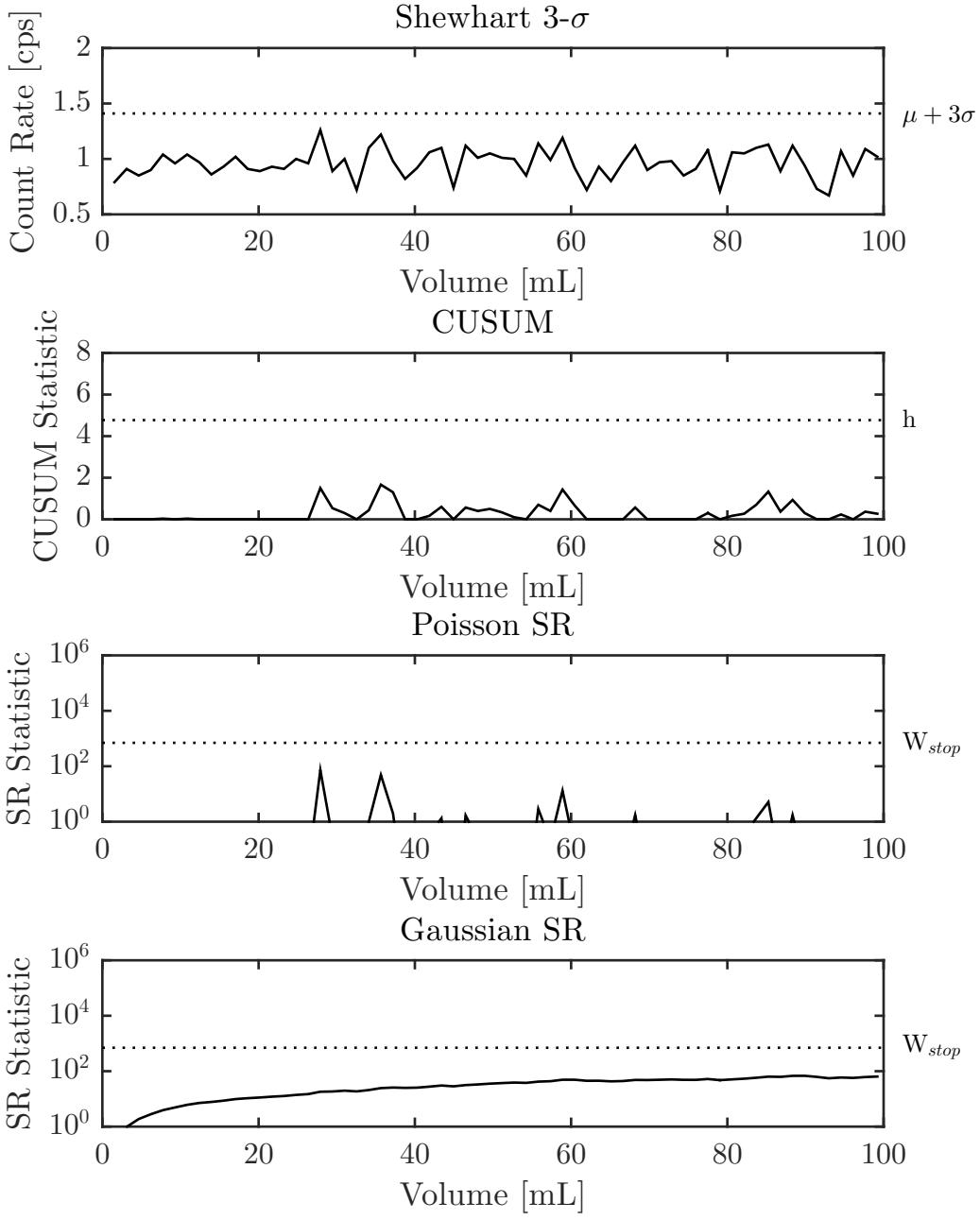

Figure B.5: Shewhart, CUSUM, S-R control charts for background 5; 100 mL of 0.01 M HCl

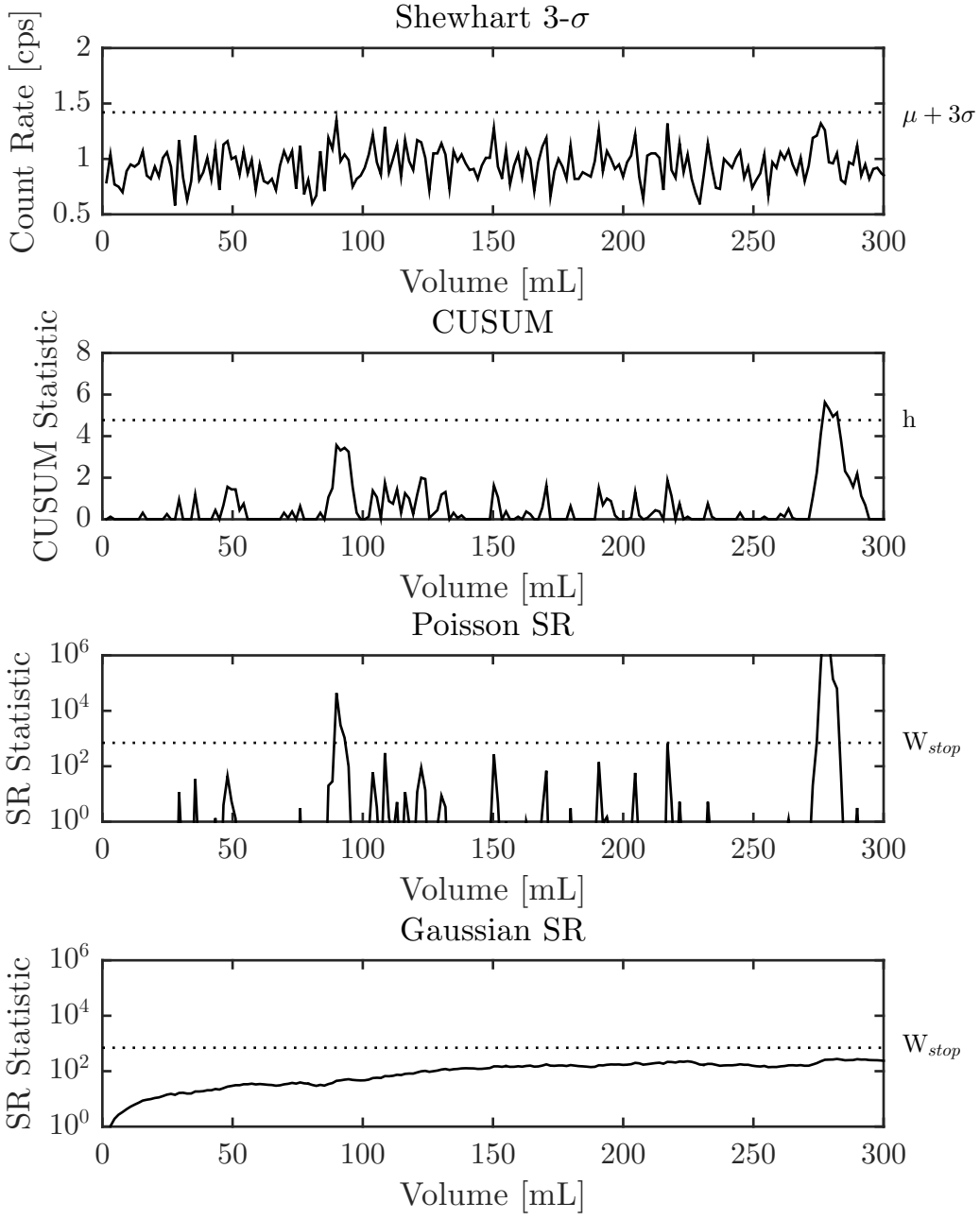

Figure B.6: Shewhart, CUSUM, S-R control charts for background 6; 300 mL of 0.01 M HCl

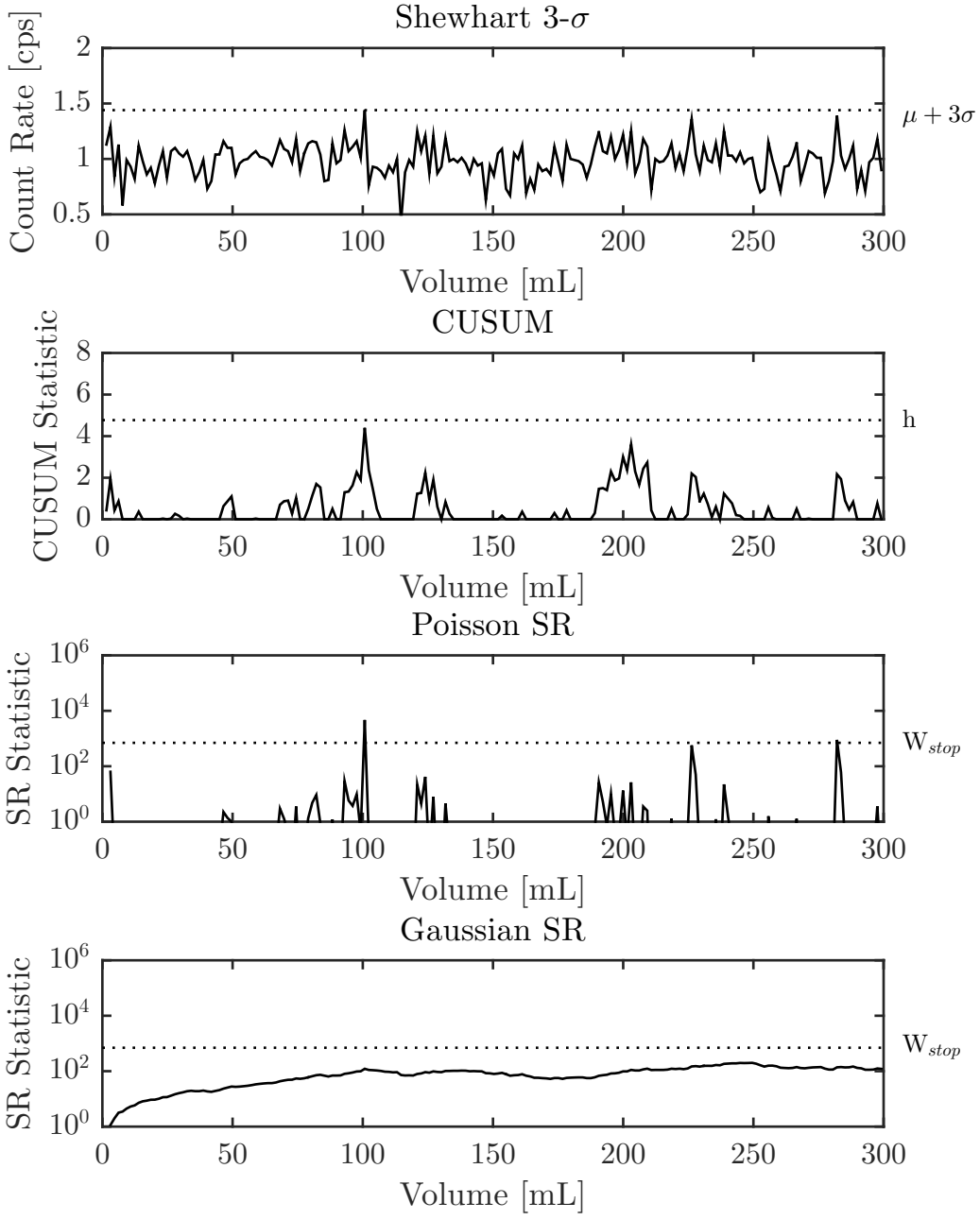

Figure B.7: Shewhart, CUSUM, S-R control charts for background 7; 300 mL of 0.01 M HCl

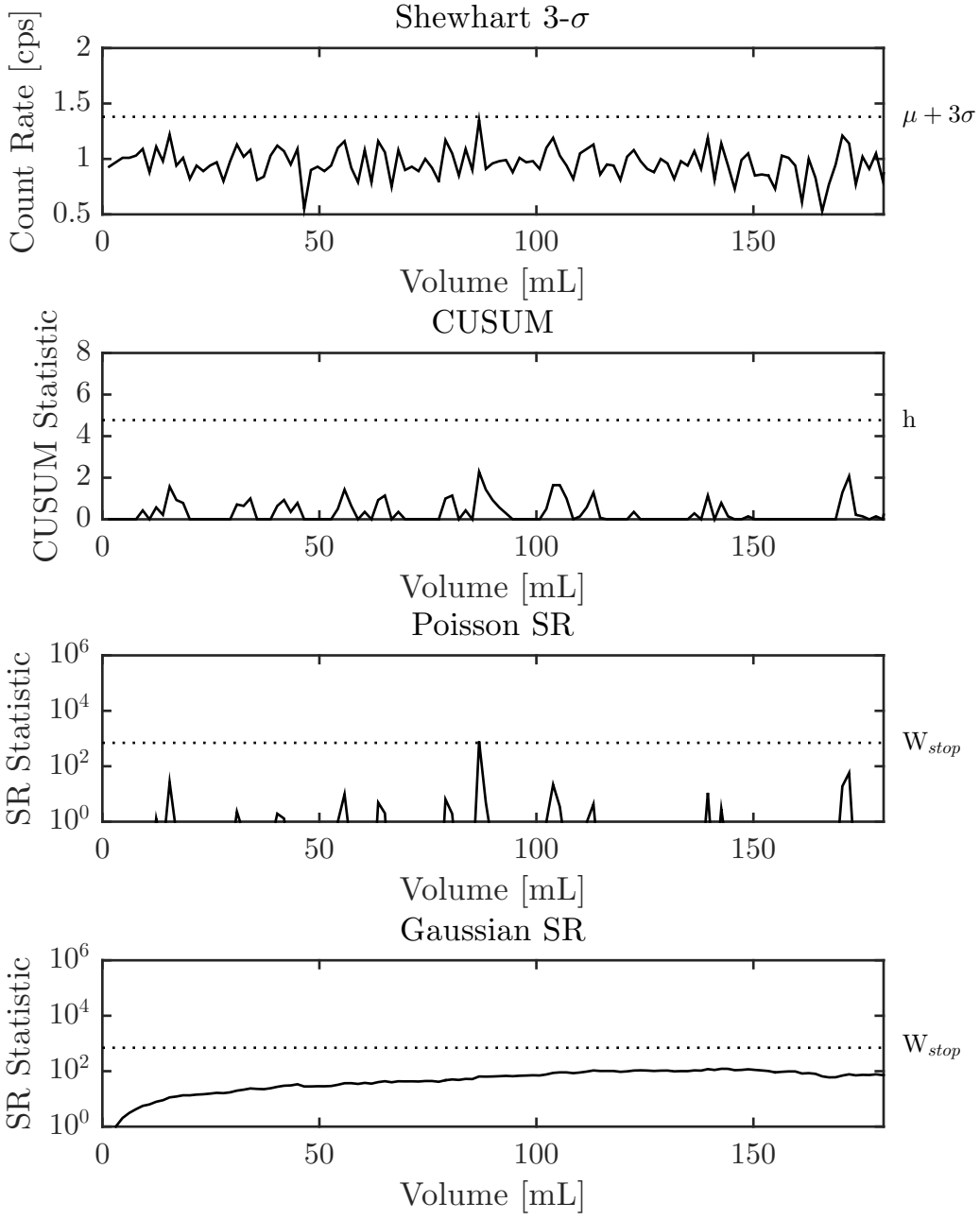

Figure B.8: Shewhart, CUSUM, S-R control charts for background 8; 180 mL of 0.01 M HCl

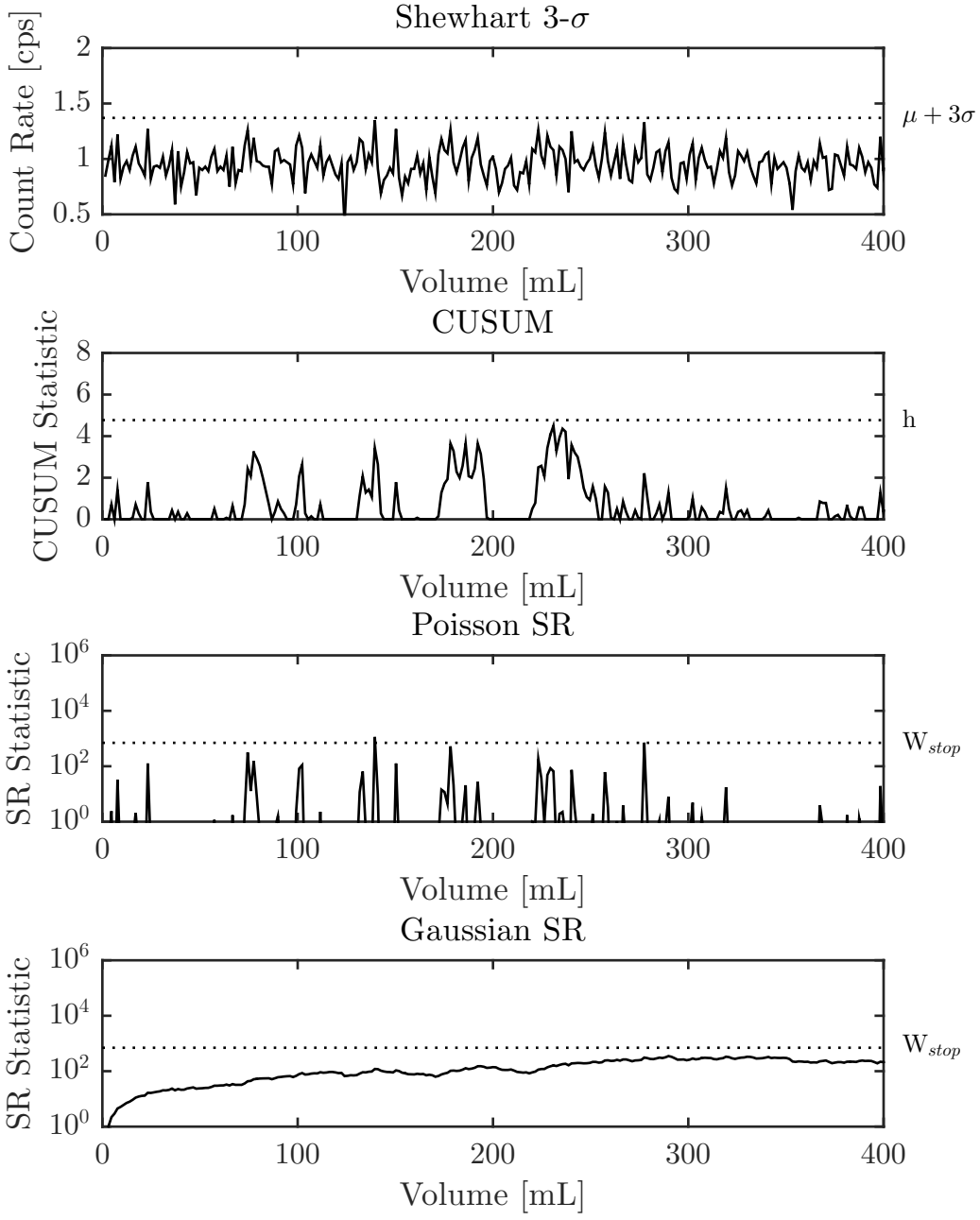

Figure B.9: Shewhart, CUSUM, S-R control charts for background 9; 400 mL of 0.01 M HCl

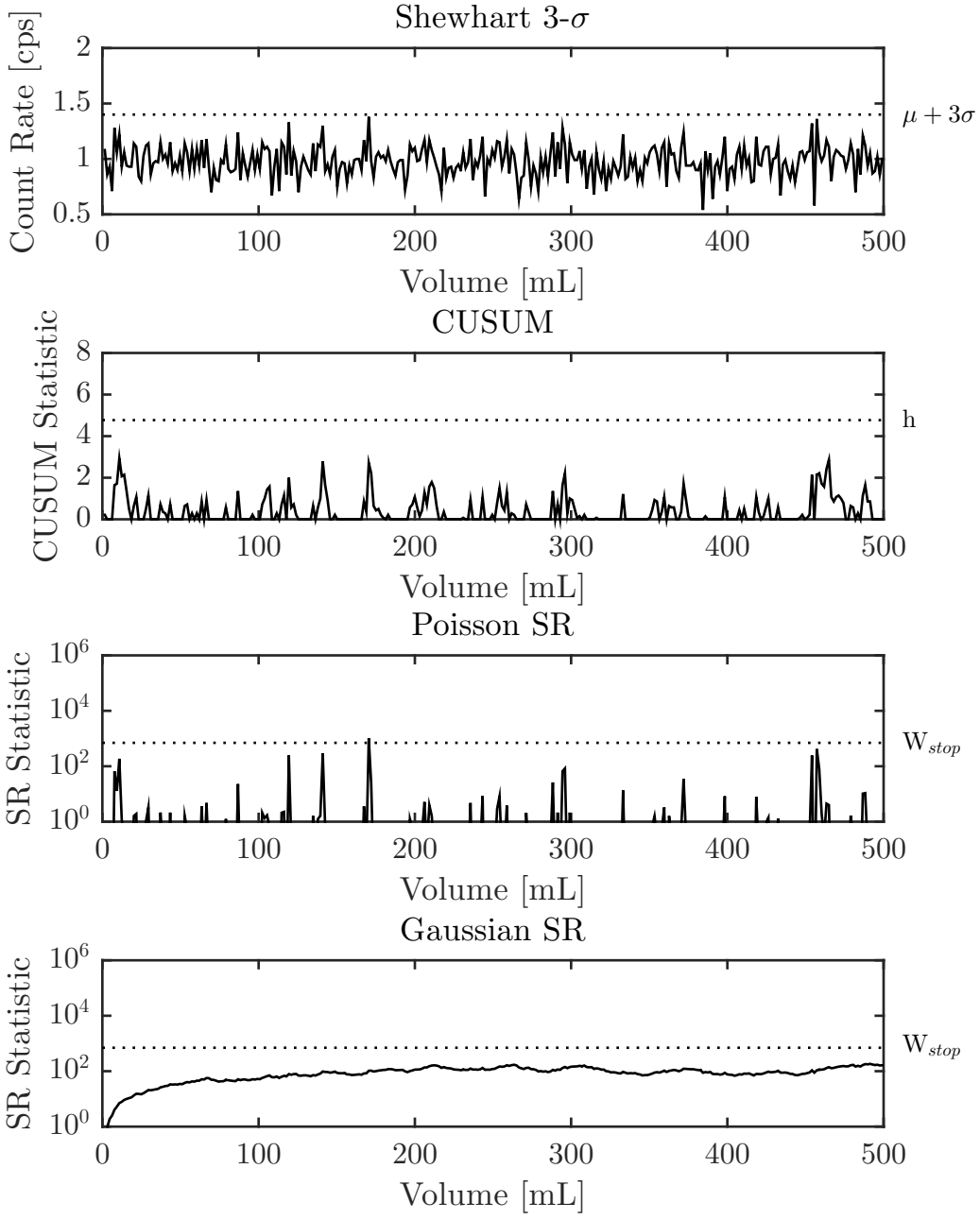

Figure B.10: Shewhart, CUSUM, S-R control charts for background 10; 500 mL of 0.01 M HCl

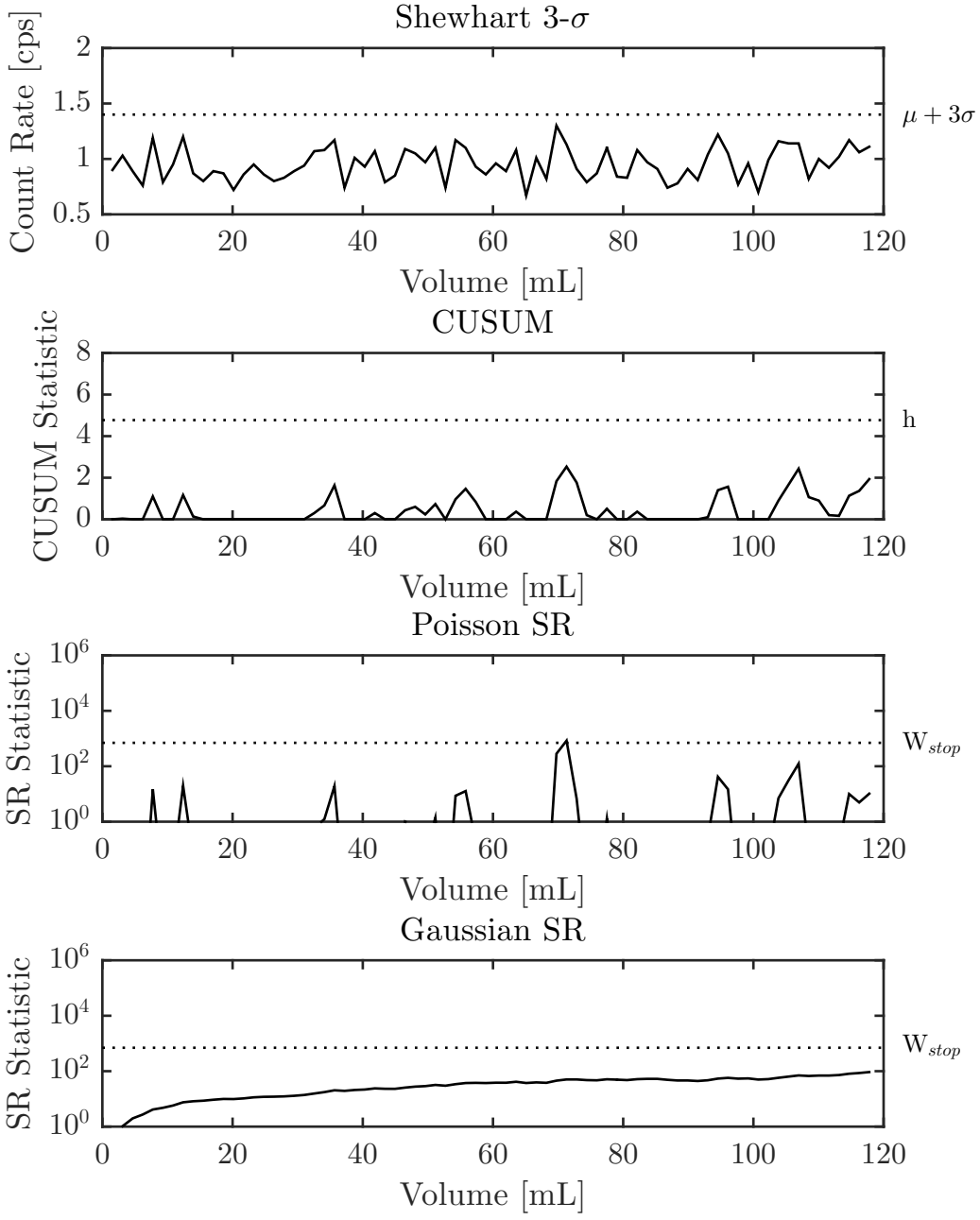

Figure B.11: Shewhart, CUSUM, S-R control charts for background 11; 120 mL of 0.01 M HCl

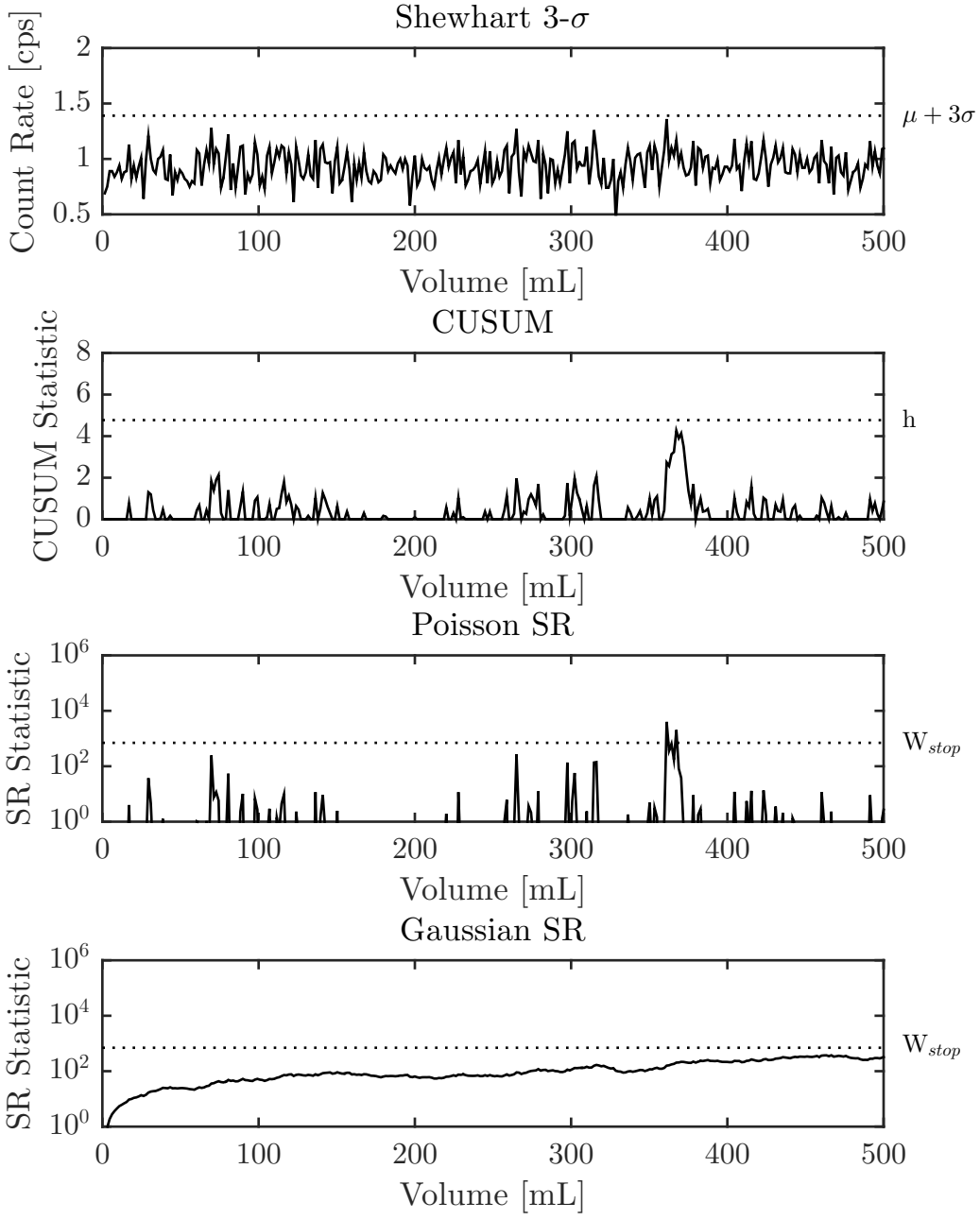

Figure B.12: Shewhart, CUSUM, S-R control charts for background 12; 500 mL of 0.01 M HCl

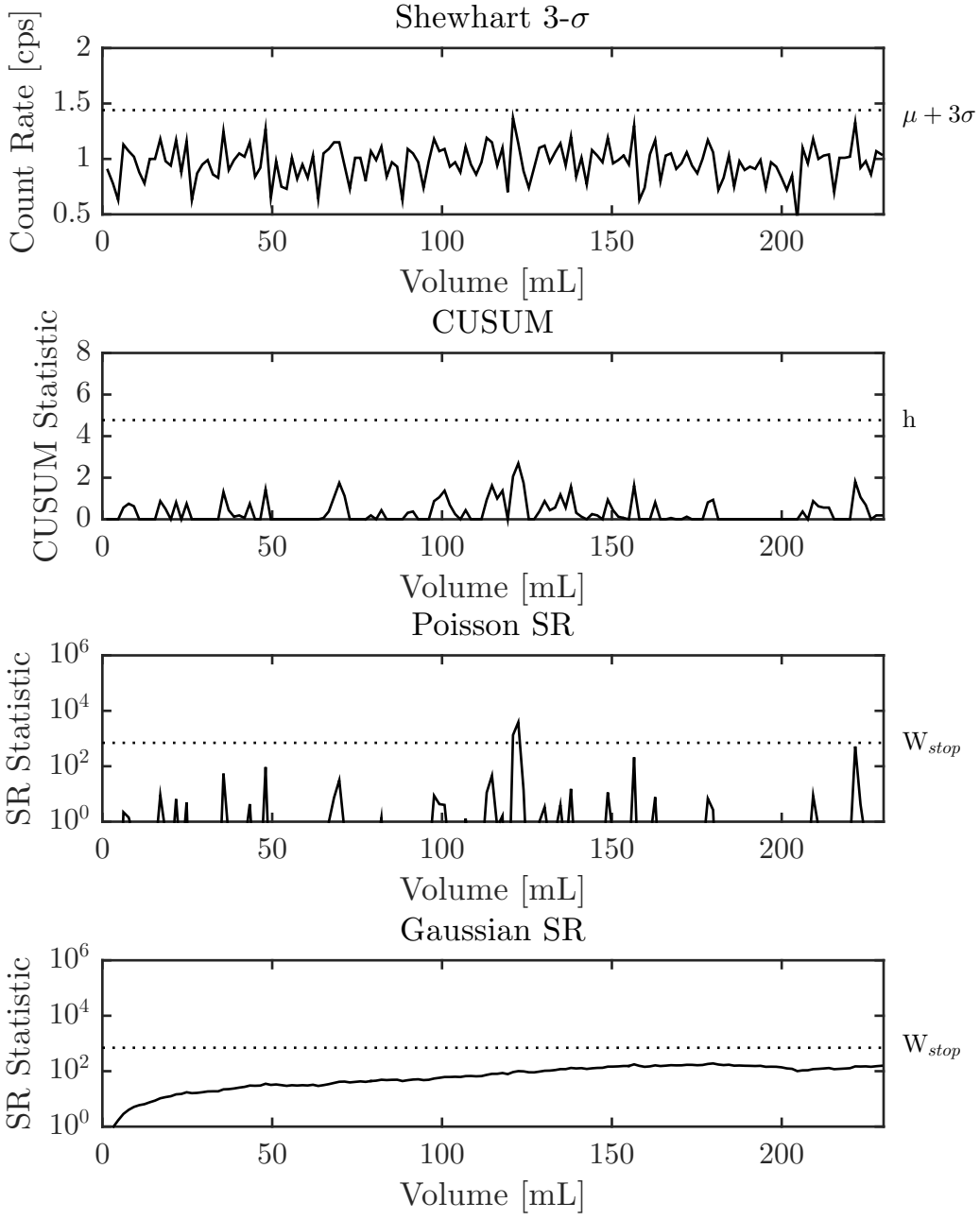

Figure B.13: Shewhart, CUSUM, S-R control charts for background 13; 230 mL of 0.01 M HCl

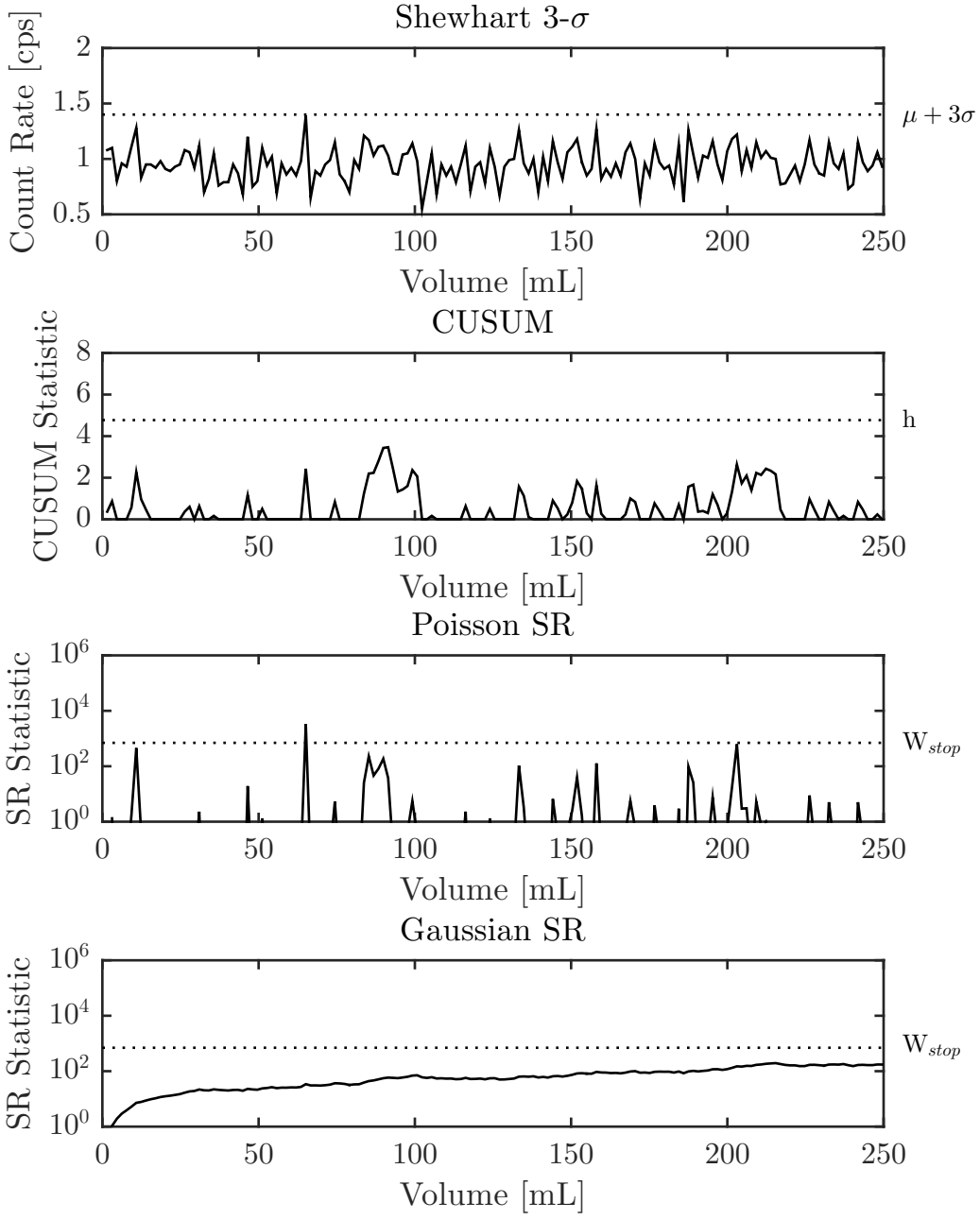

Figure B.14: Shewhart, CUSUM, S-R control charts for background 14; 250 mL of 0.01 M HCl

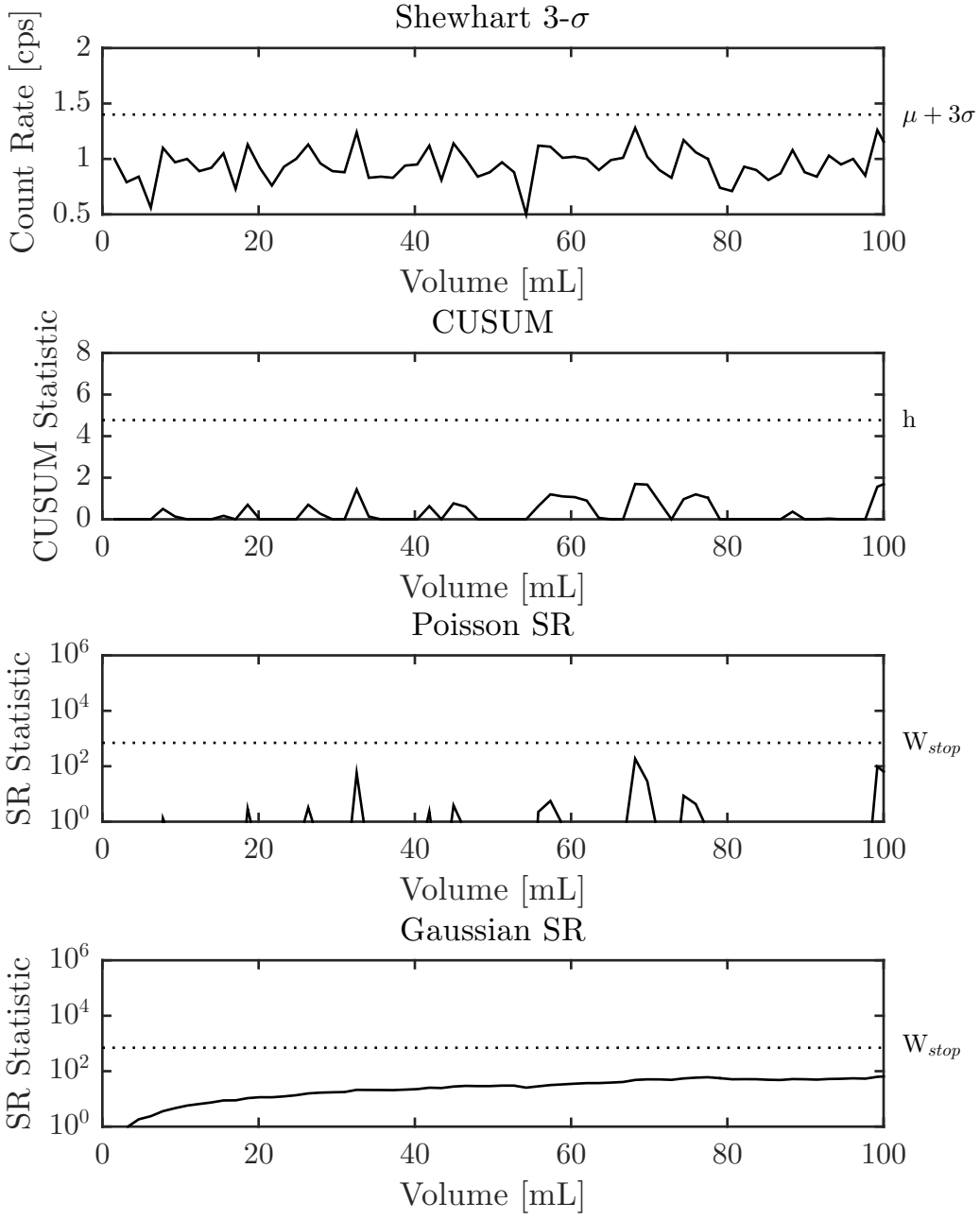

Figure B.15: Shewhart, CUSUM, S-R control charts for background 15; 100 mL of 0.01 M HCl

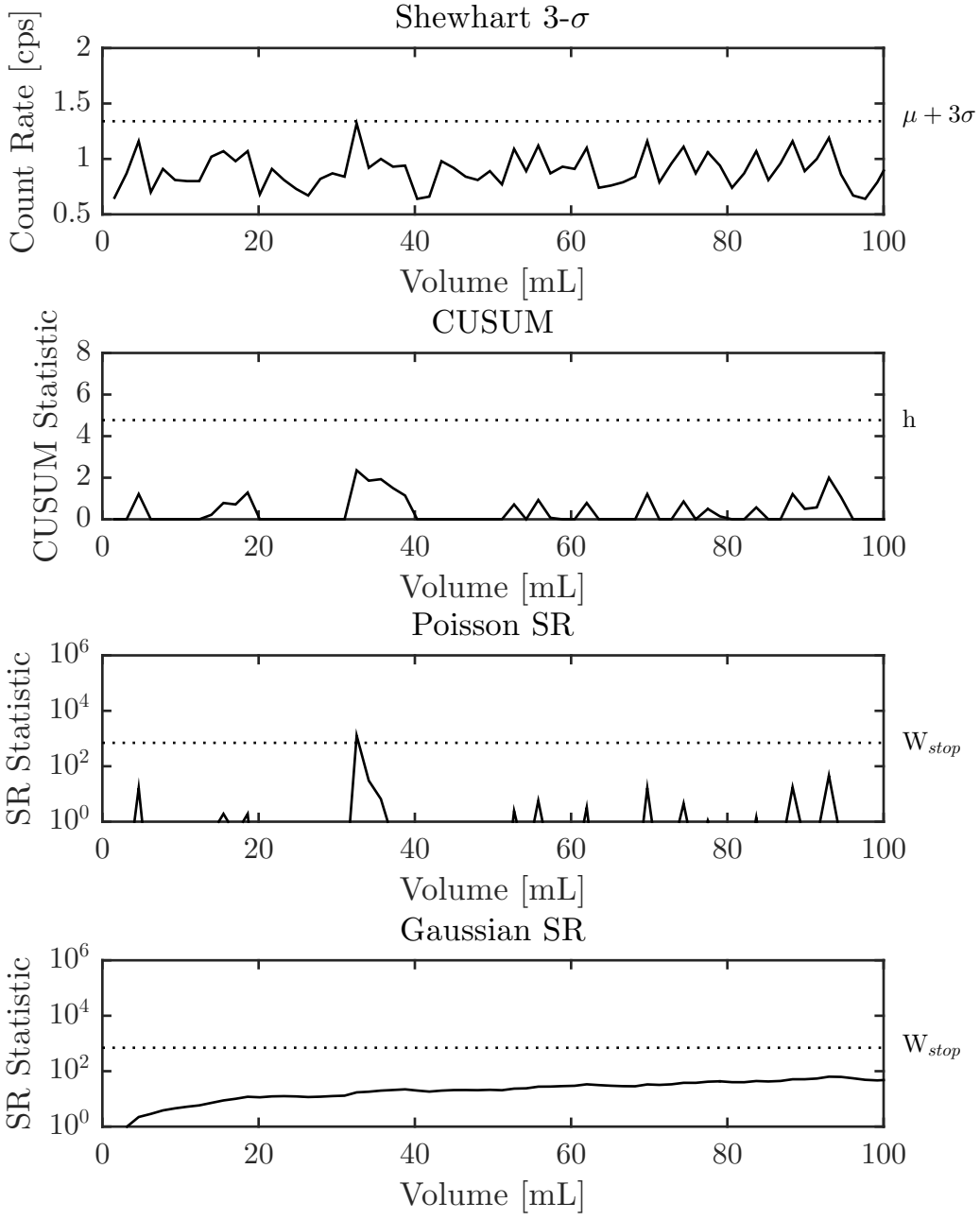

Figure B.16: Shewhart, CUSUM, S-R control charts for background 16; 100 mL of 0.01 M HCl

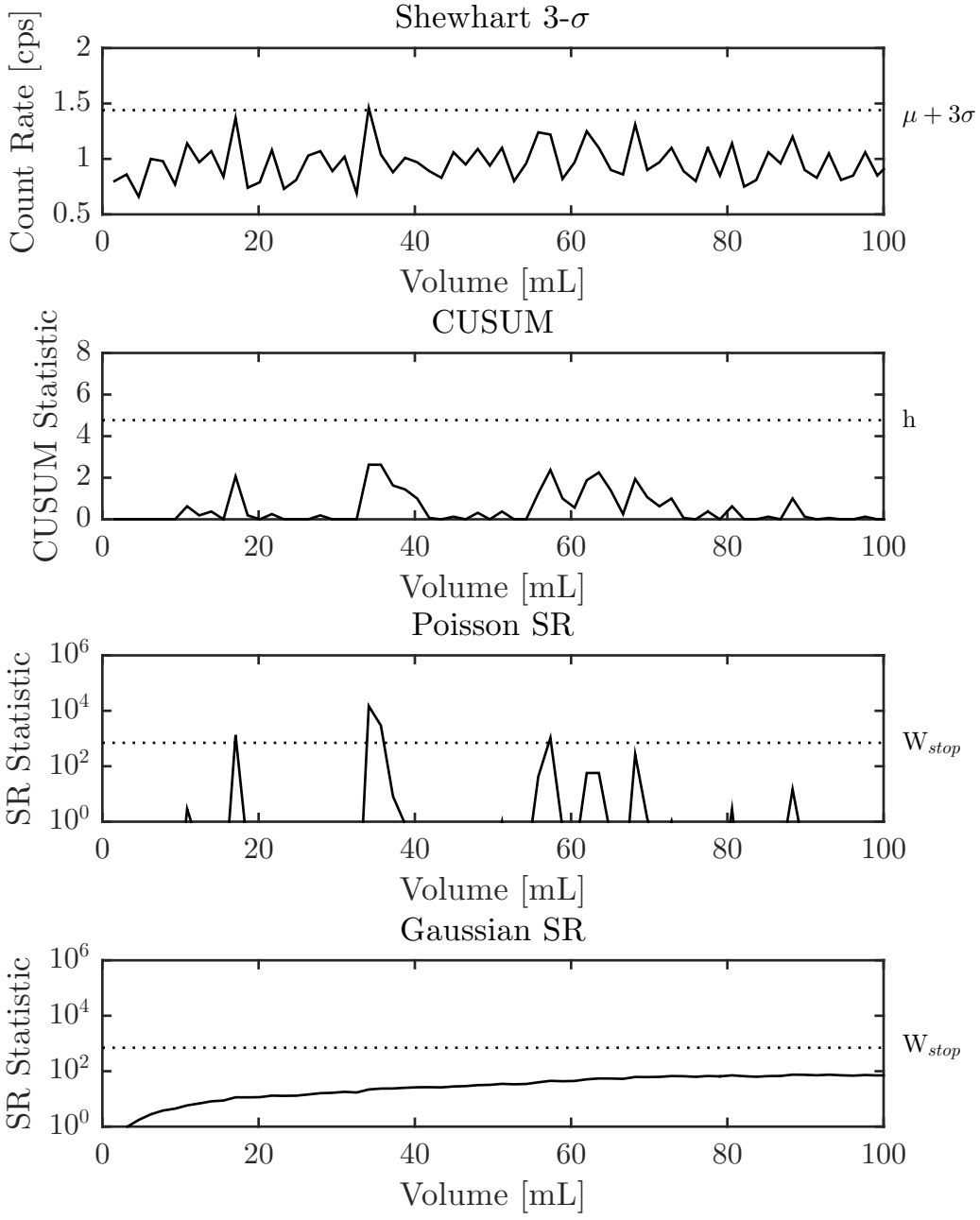

Figure B.17: Shewhart, CUSUM, S-R control charts for background 17; 100 mL of 0.01 M HCl

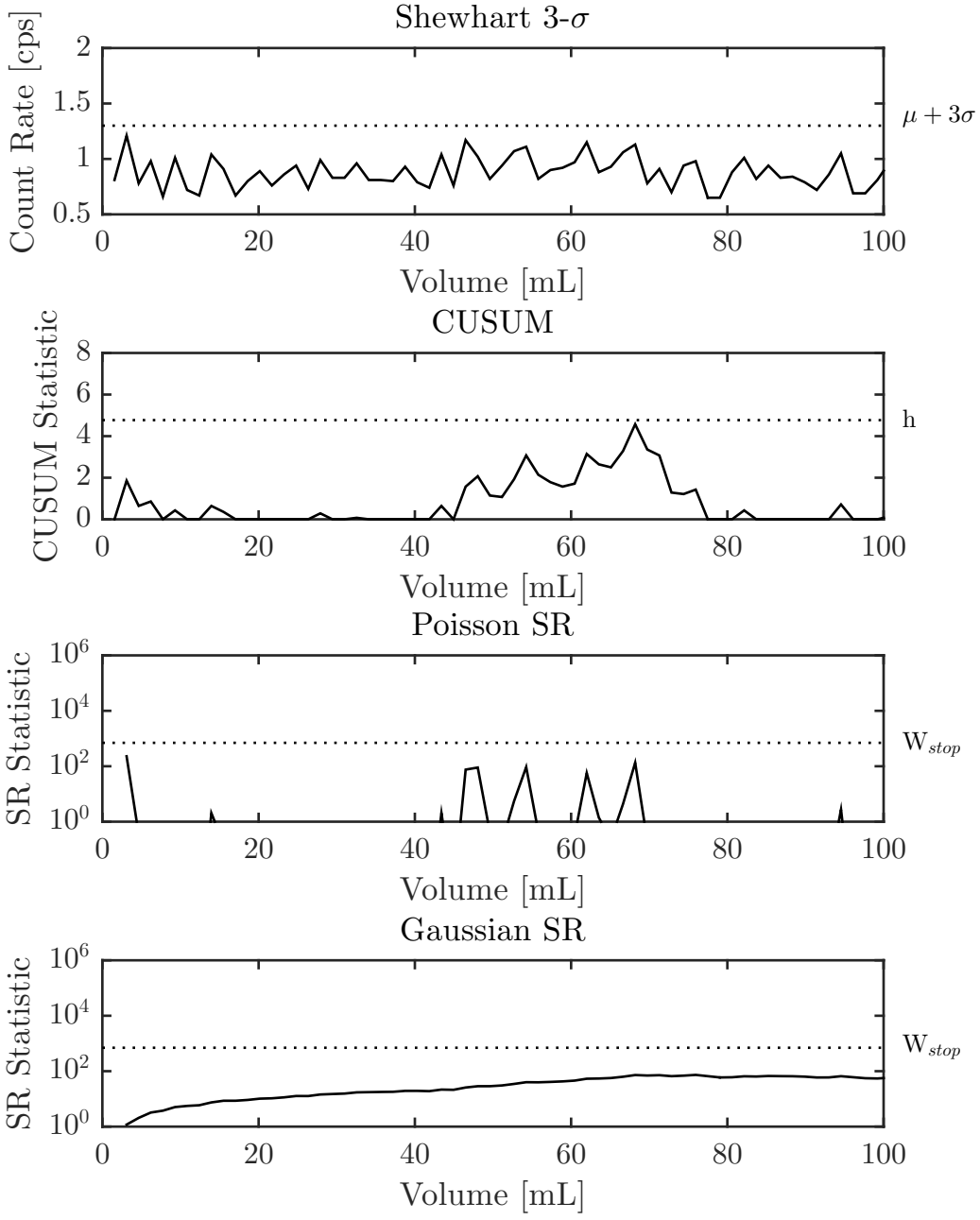

Figure B.18: Shewhart, CUSUM, S-R control charts for background 18; 100 mL of 0.01 M HCl

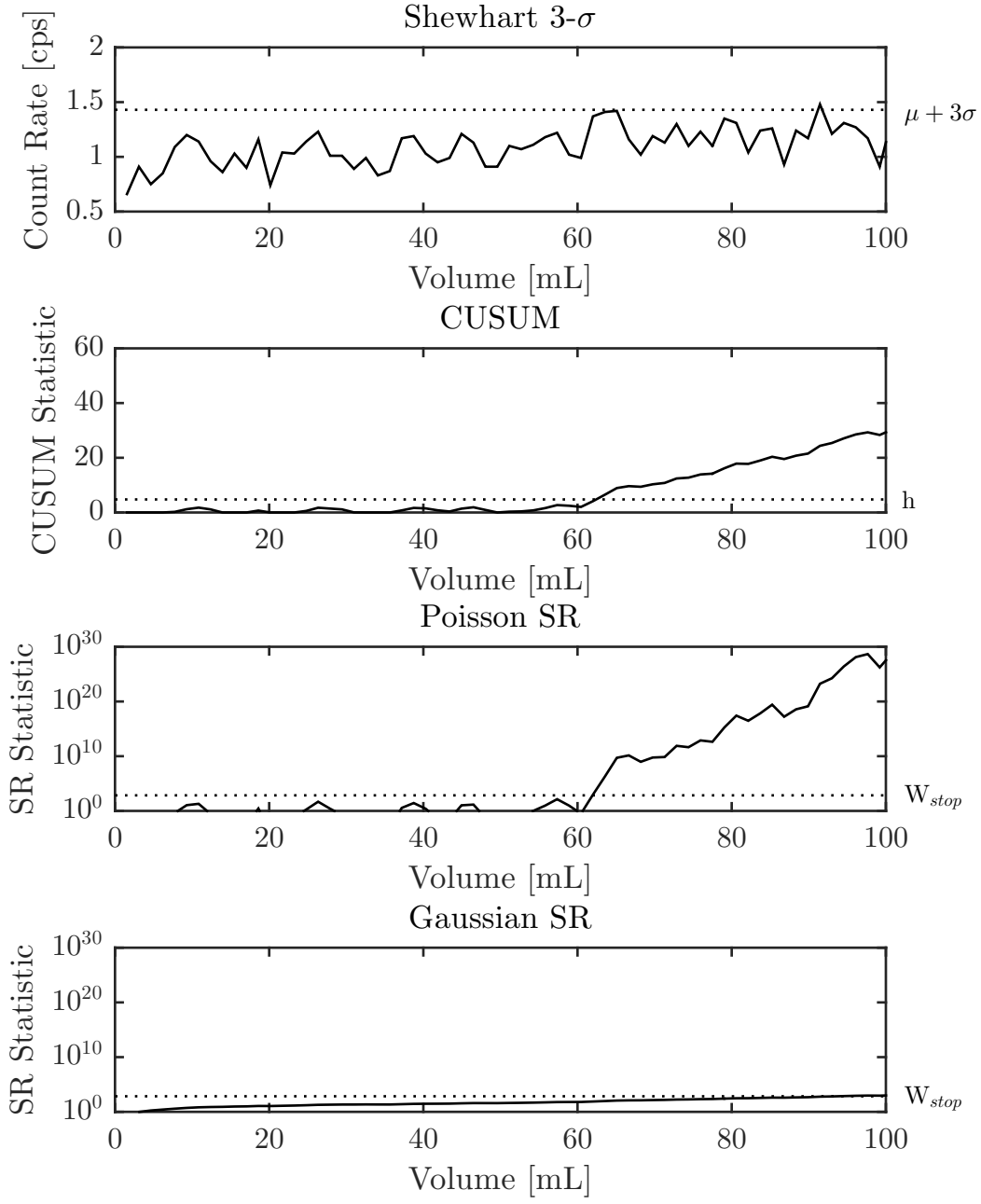

Figure B.19: Shewhart, CUSUM, S-R control charts 70 mL of 5.08 Bq/L $^{99}TcO_4^-$ preceded by 30 mL of 0.01 M HCl

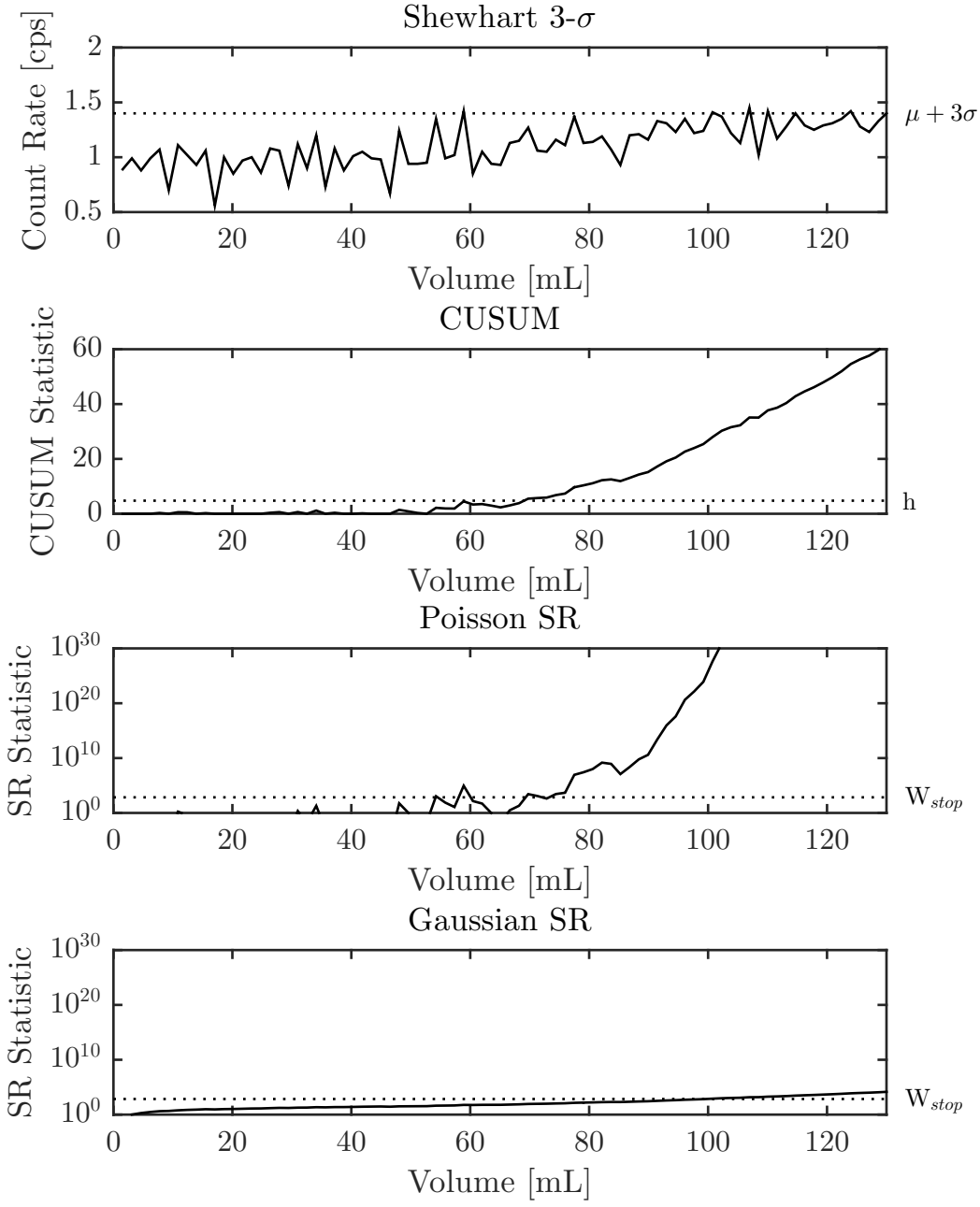

Figure B.20: Shewhart, CUSUM, S-R control charts 100 mL of 5.03 Bq/L $^{99}TcO_4^-$ preceded by 30 mL of 0.01 M HCl

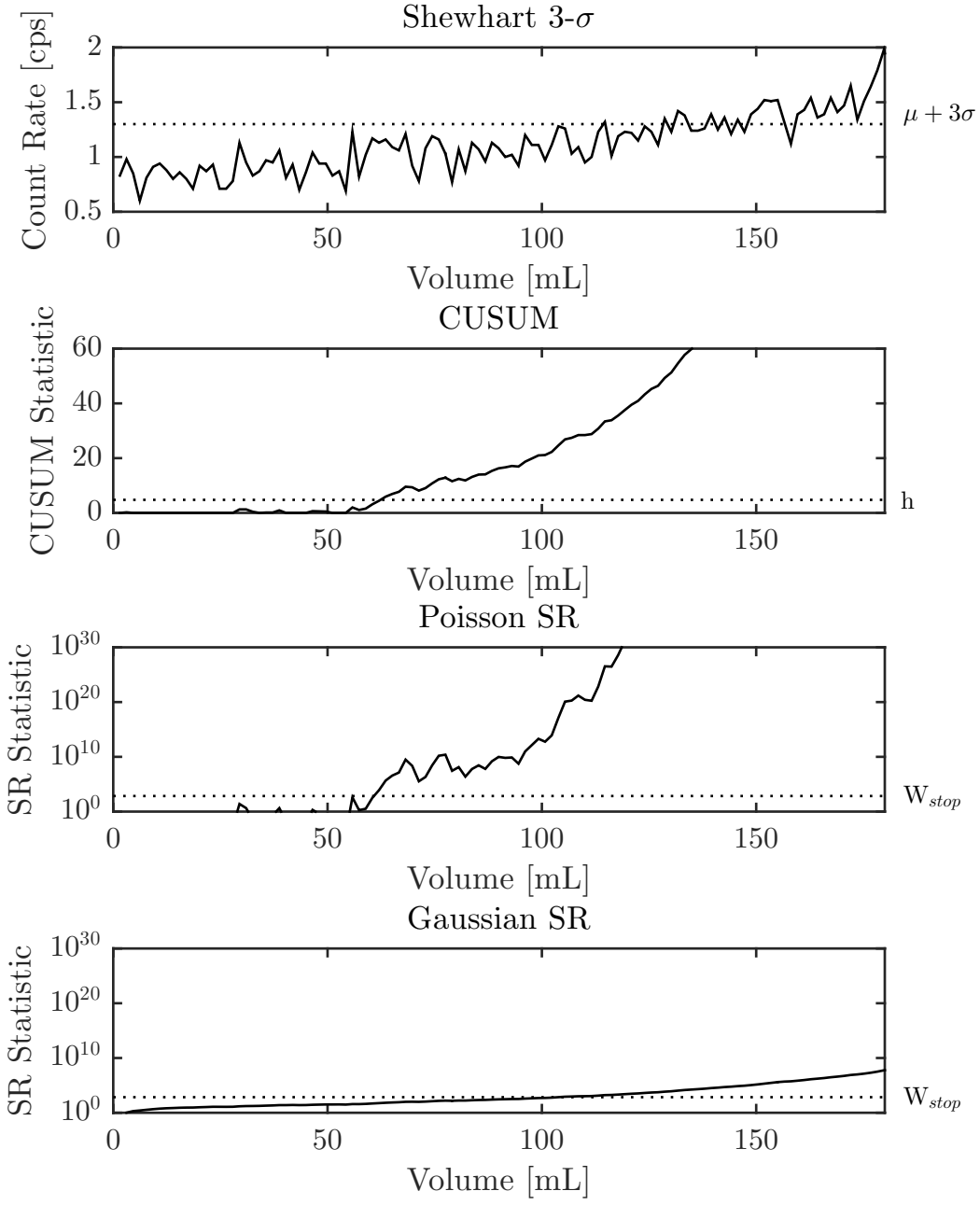

Figure B.21: Shewhart, CUSUM, S-R control charts for 150 mL of 4.97 Bq/L $^{99}TcO_4^-$ preceded by 30 mL of 0.01 M HCl

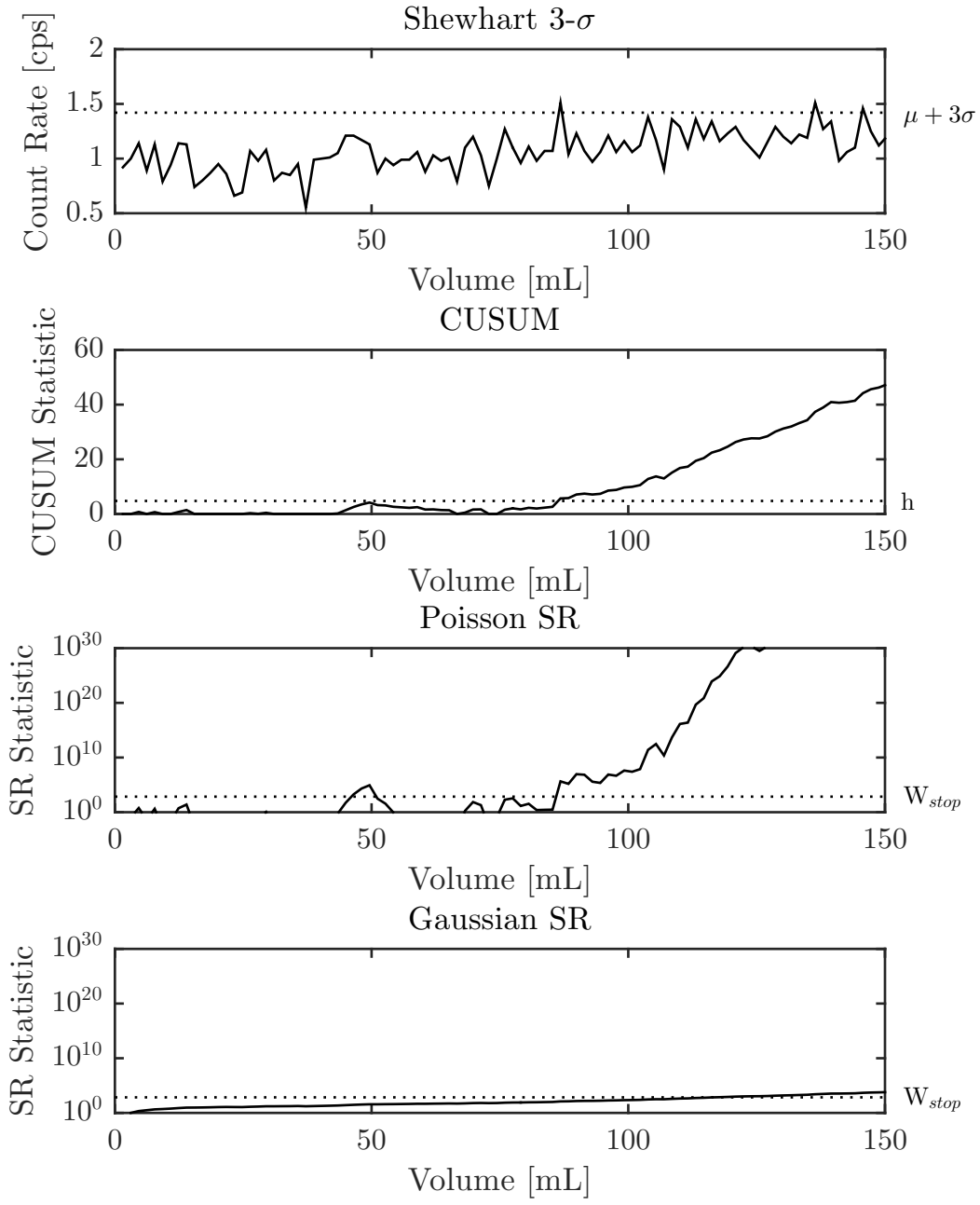

Figure B.22: Shewhart, CUSUM, S-R control charts for 120 mL of 2.54 Bq/L $^{99}TcO_4^-$ preceded by 30 mL of 0.01 M HCl

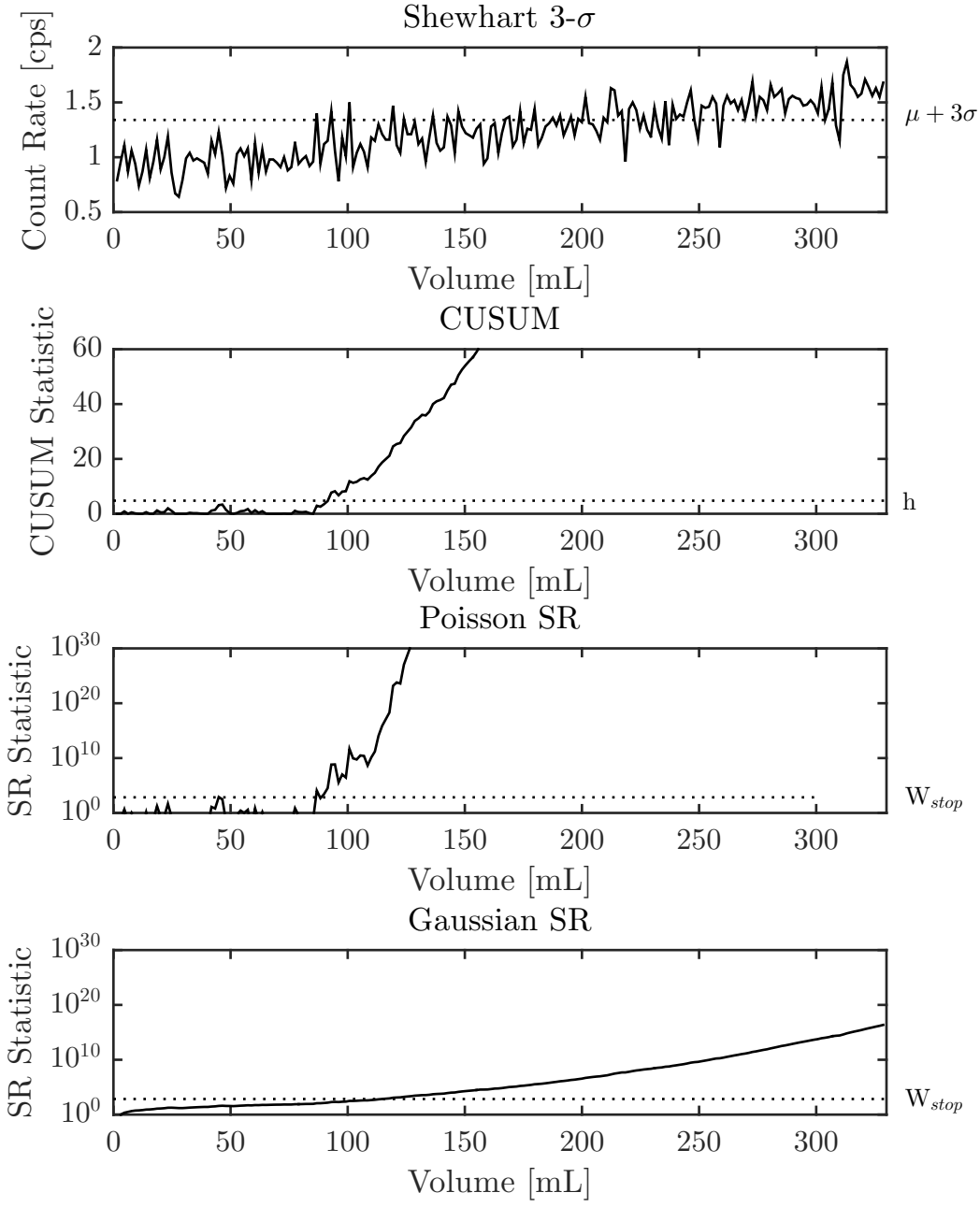

Figure B.23: Shewhart, CUSUM, S-R control charts for 300 mL of 2.50 Bq/L $^{99}TcO_4^-$ preceded by 30 mL of 0.01 M HCl

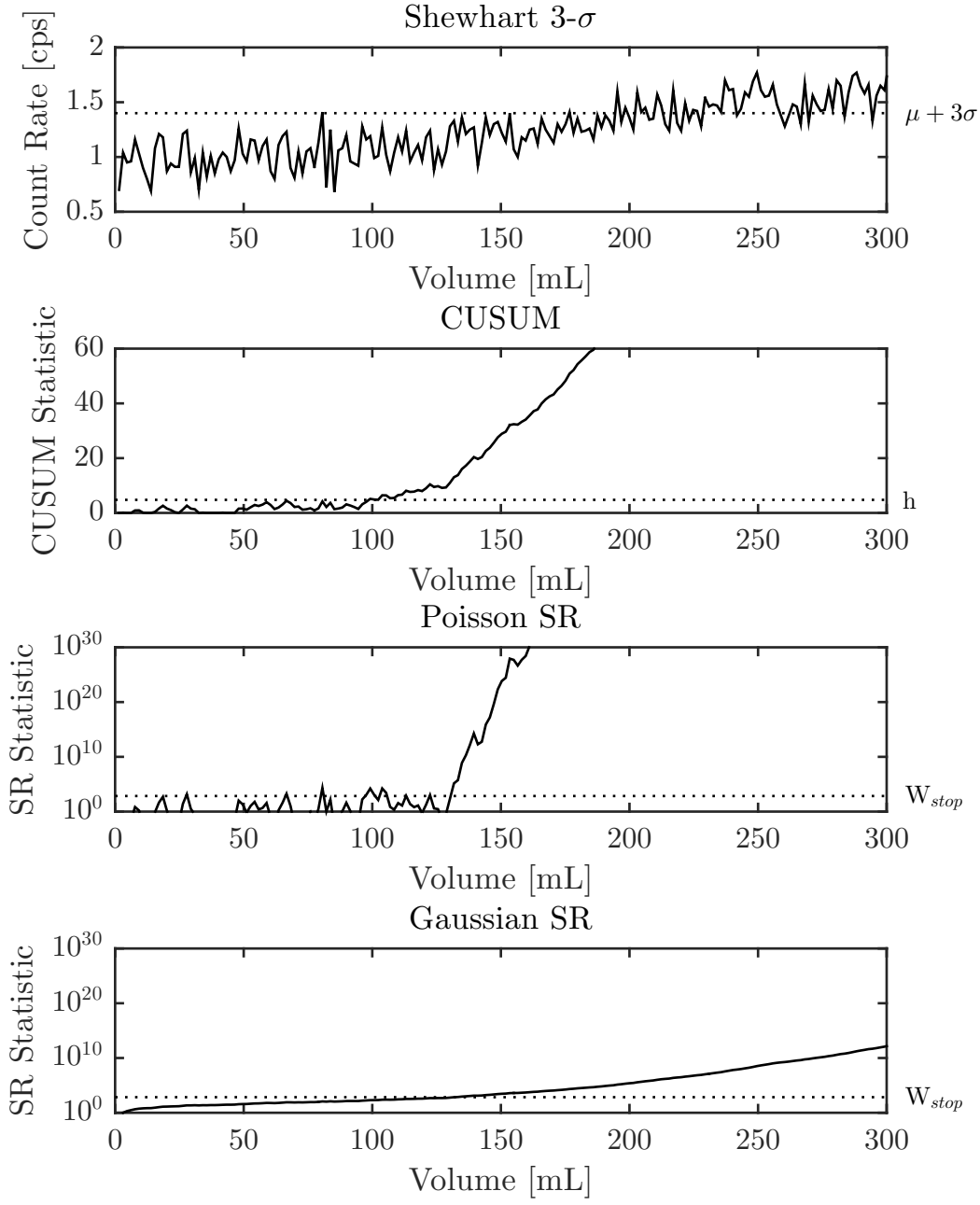

Figure B.24: Shewhart, CUSUM, S-R control charts for 270 mL of 2.49 Bq/L $^{99}TcO_4^-$ preceded by 30 mL of 0.01 M HCl

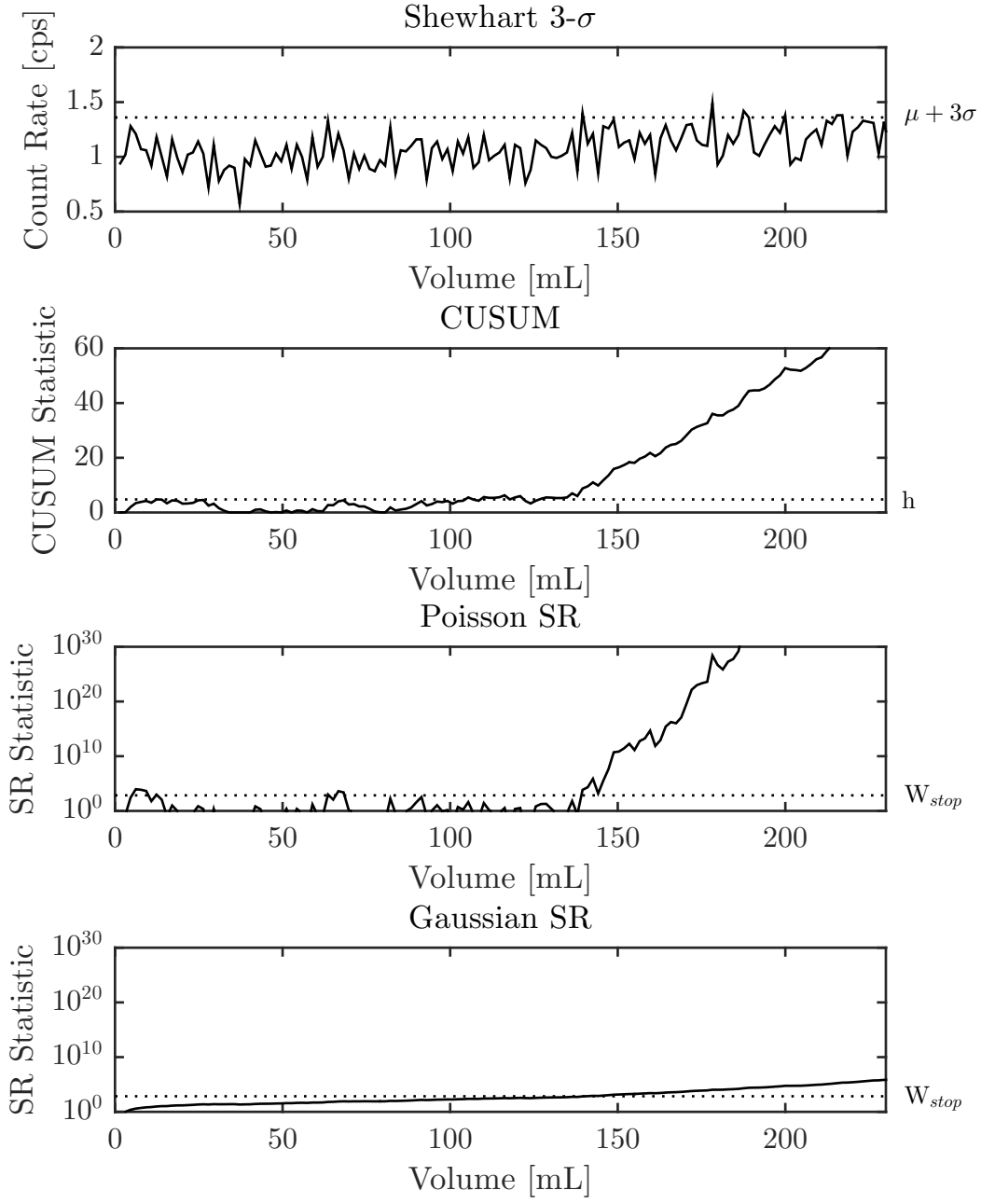

Figure B.25: Shewhart, CUSUM, S-R control charts for 200 mL of 1.53 Bq/L $^{99}TcO_4^-$ preceded by 30 mL of 0.01 M HCl

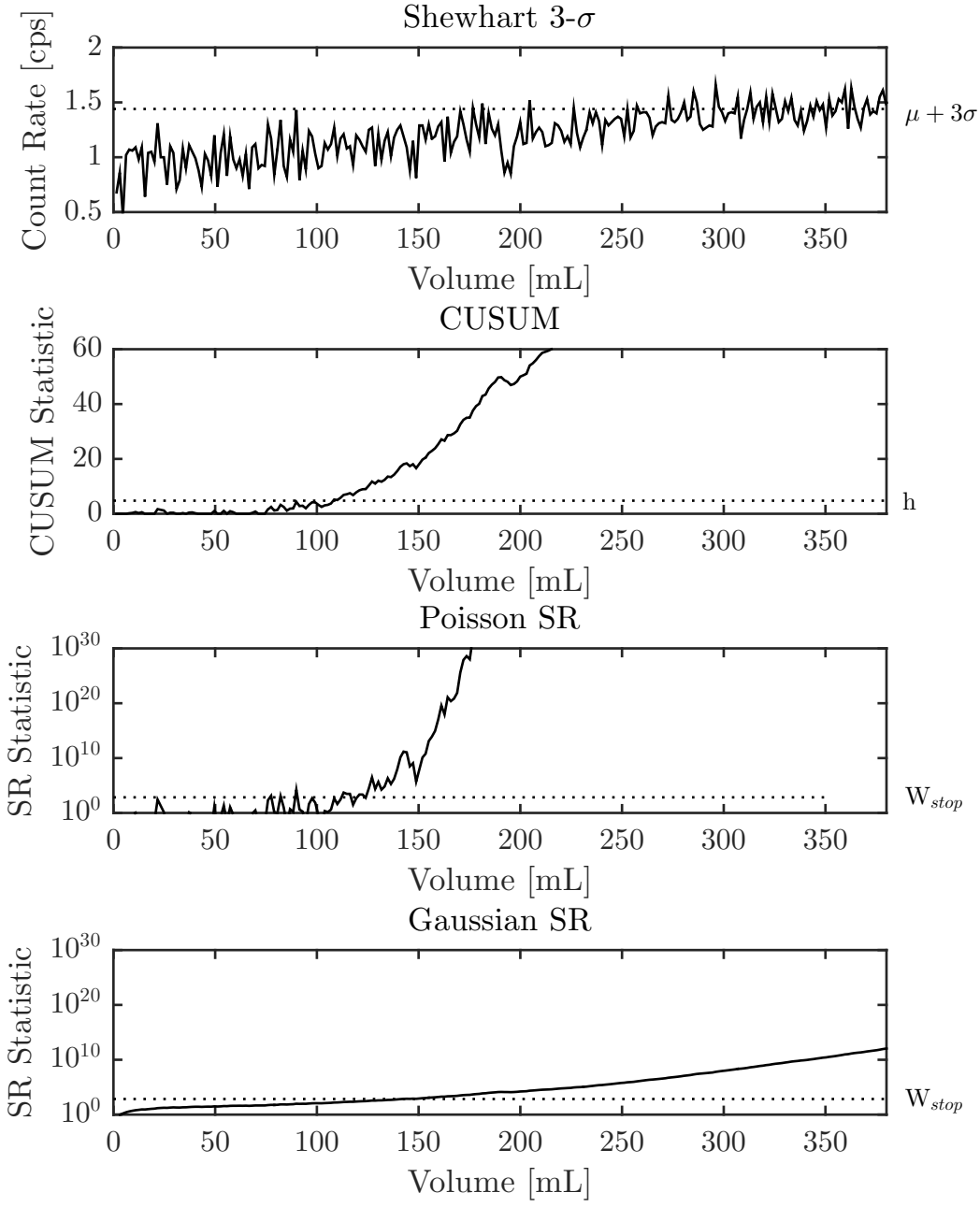

Figure B.26: Shewhart, CUSUM, S-R control charts for 350 mL of 1.51 Bq/L $^{99}TcO_4^-$ preceded by 30 mL of 0.01 M HCl

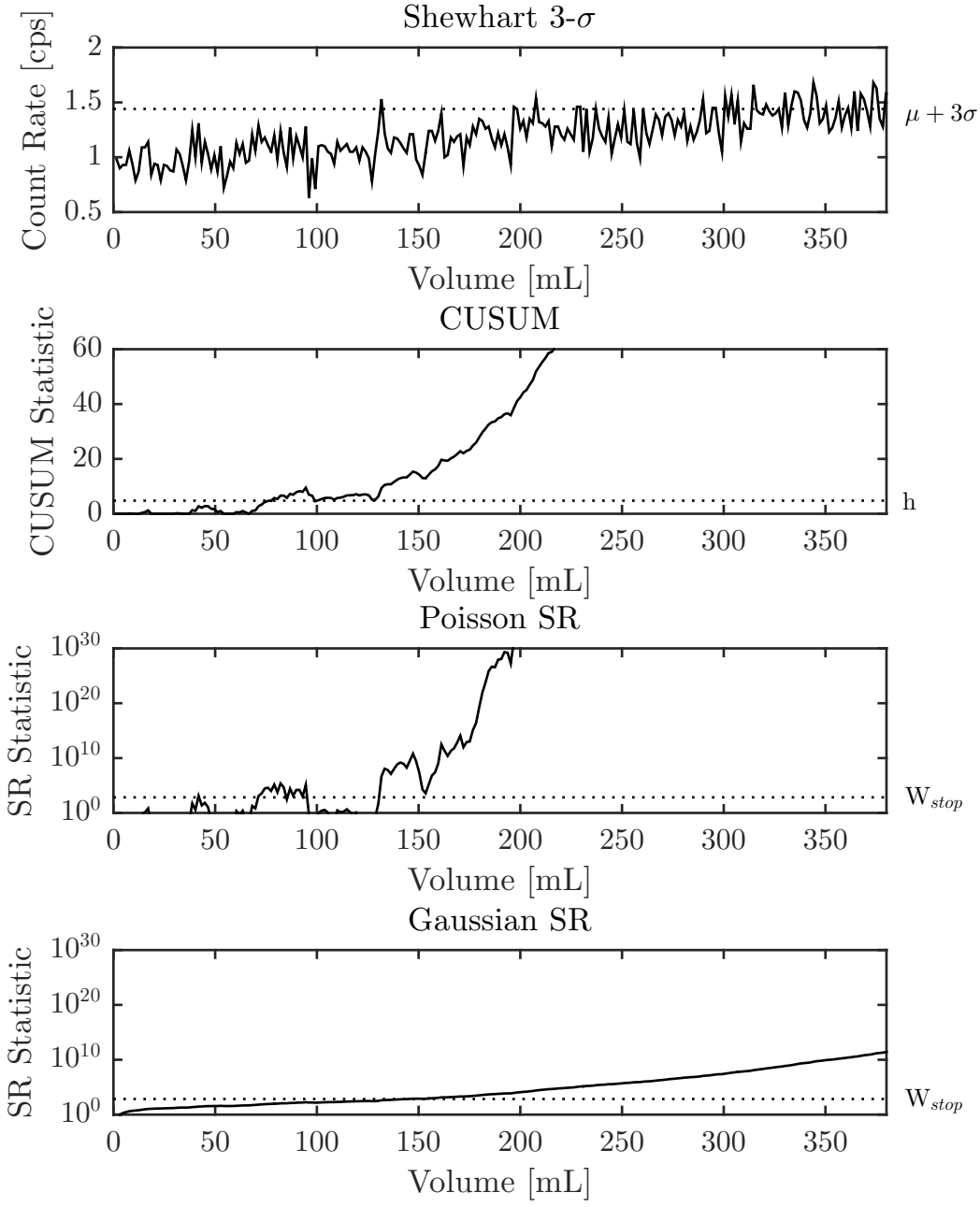

Figure B.27: Shewhart, CUSUM, S-R control charts for 350 mL of 1.49 Bq/L $^{99}TcO_4^-$ preceded by 30 mL of 0.01 M HCl

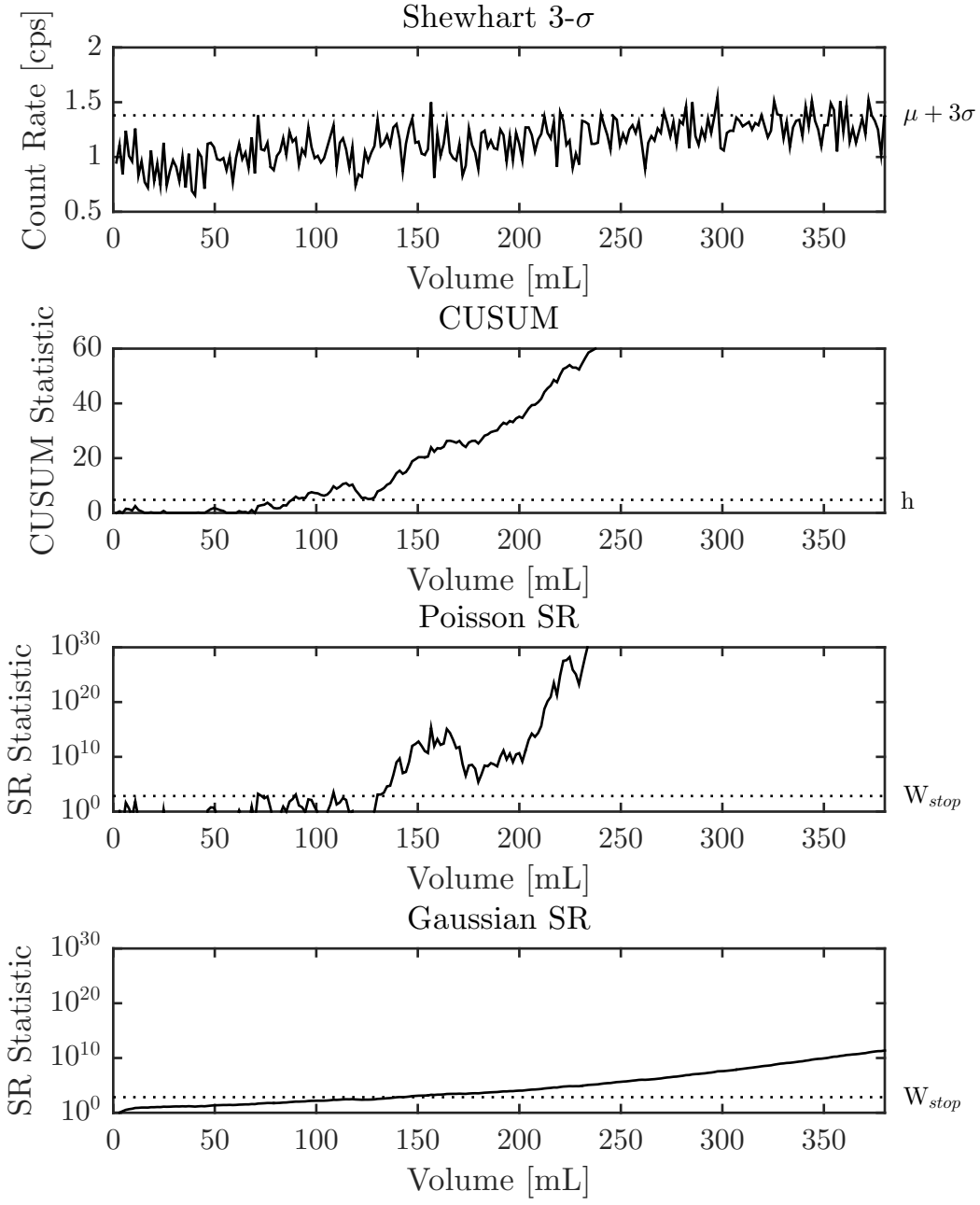

Figure B.28: Shewhart, CUSUM, S-R control charts for 350 mL of 1.02 Bq/L $^{99}TcO_4^-$ preceded by 30 mL of 0.01 M HCl

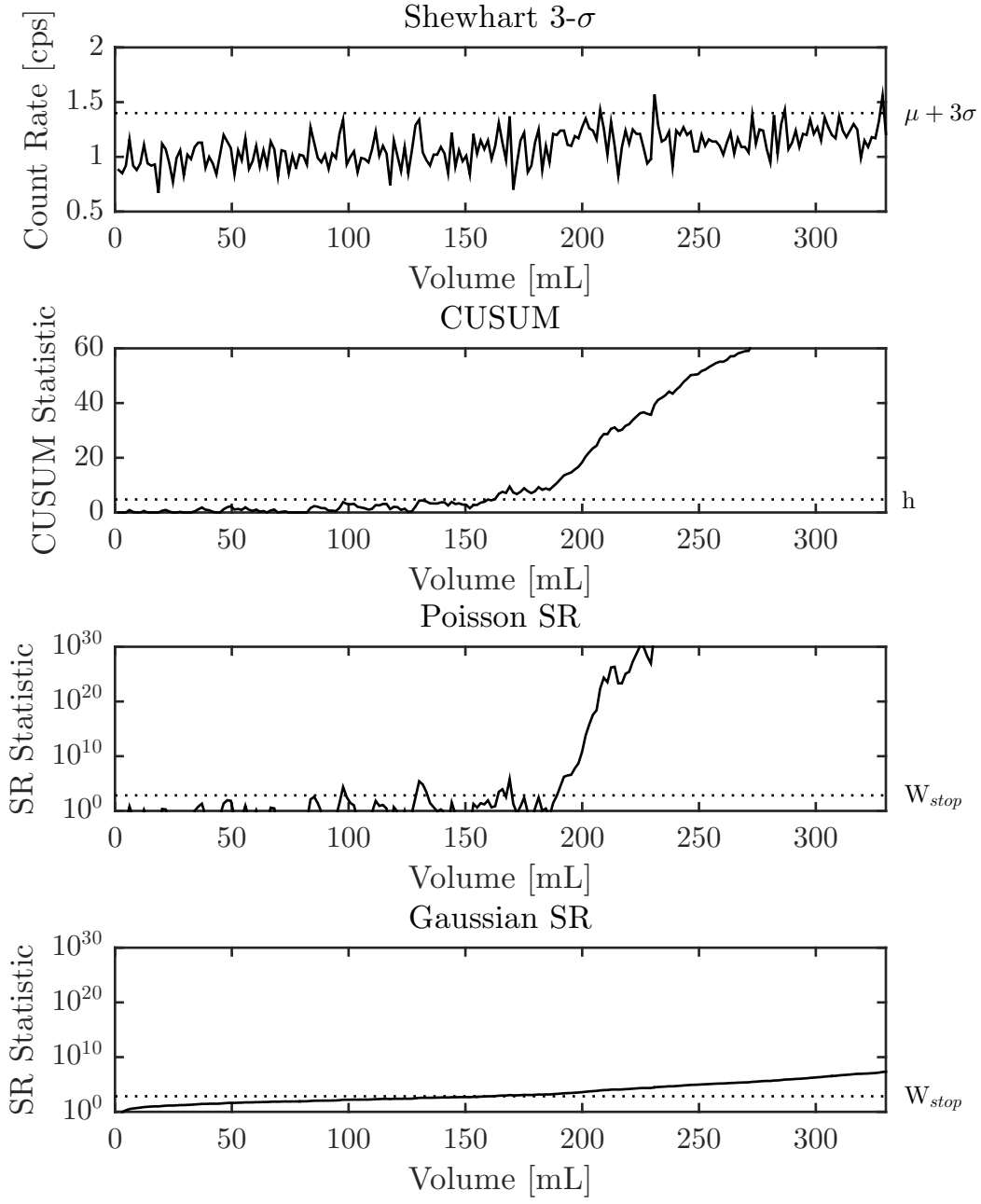

Figure B.29: Shewhart, CUSUM, S-R control charts for 300 mL of 1.00 Bq/L $^{99}TcO_4^-$ preceded by 30 mL of 0.01 M HCl

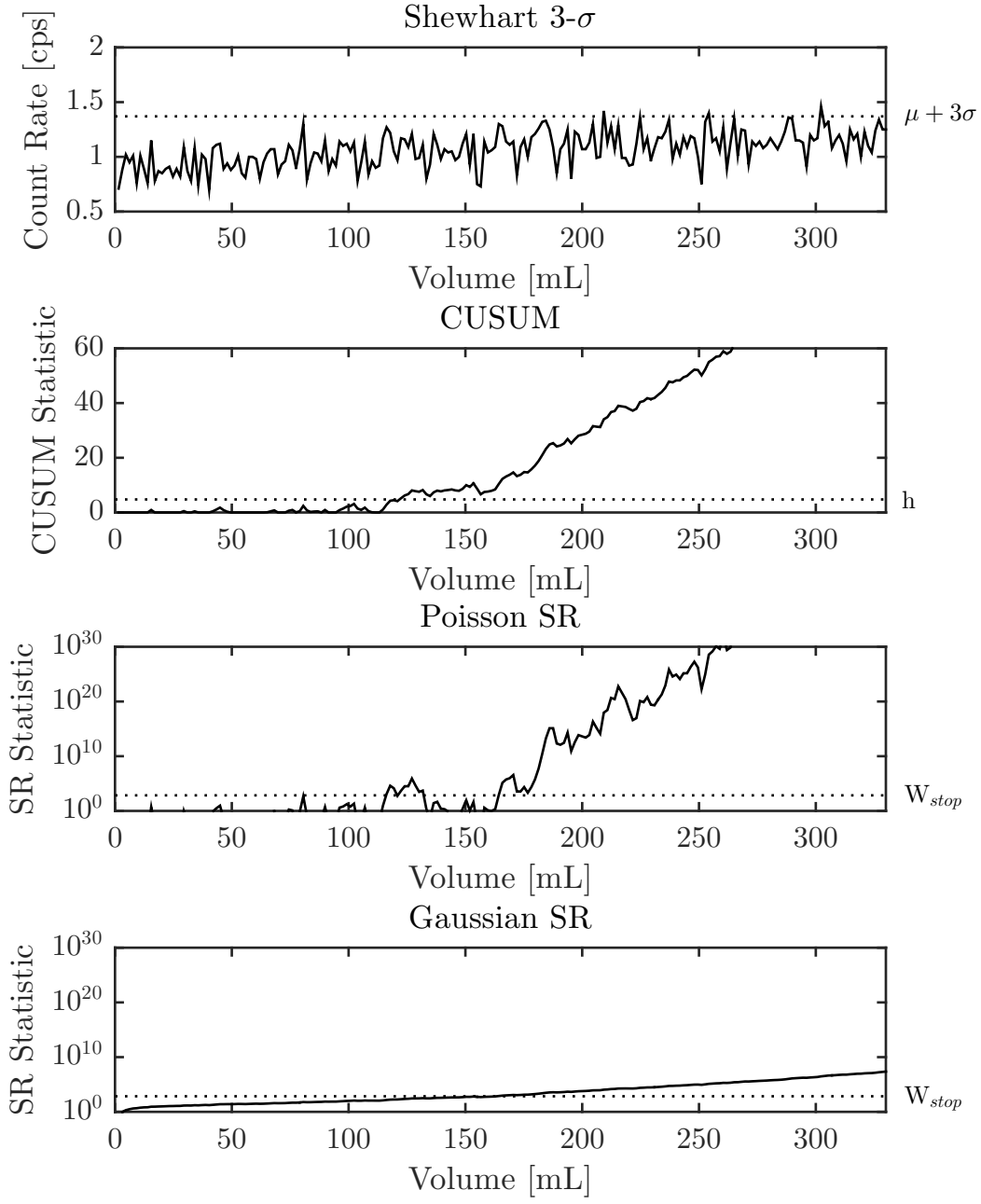

Figure B.30: Shewhart, CUSUM, S-R control charts for 300 mL of 0.997 Bq/L $^{99}TcO_4^-$ preceded by 30 mL of 0.01 M HCl

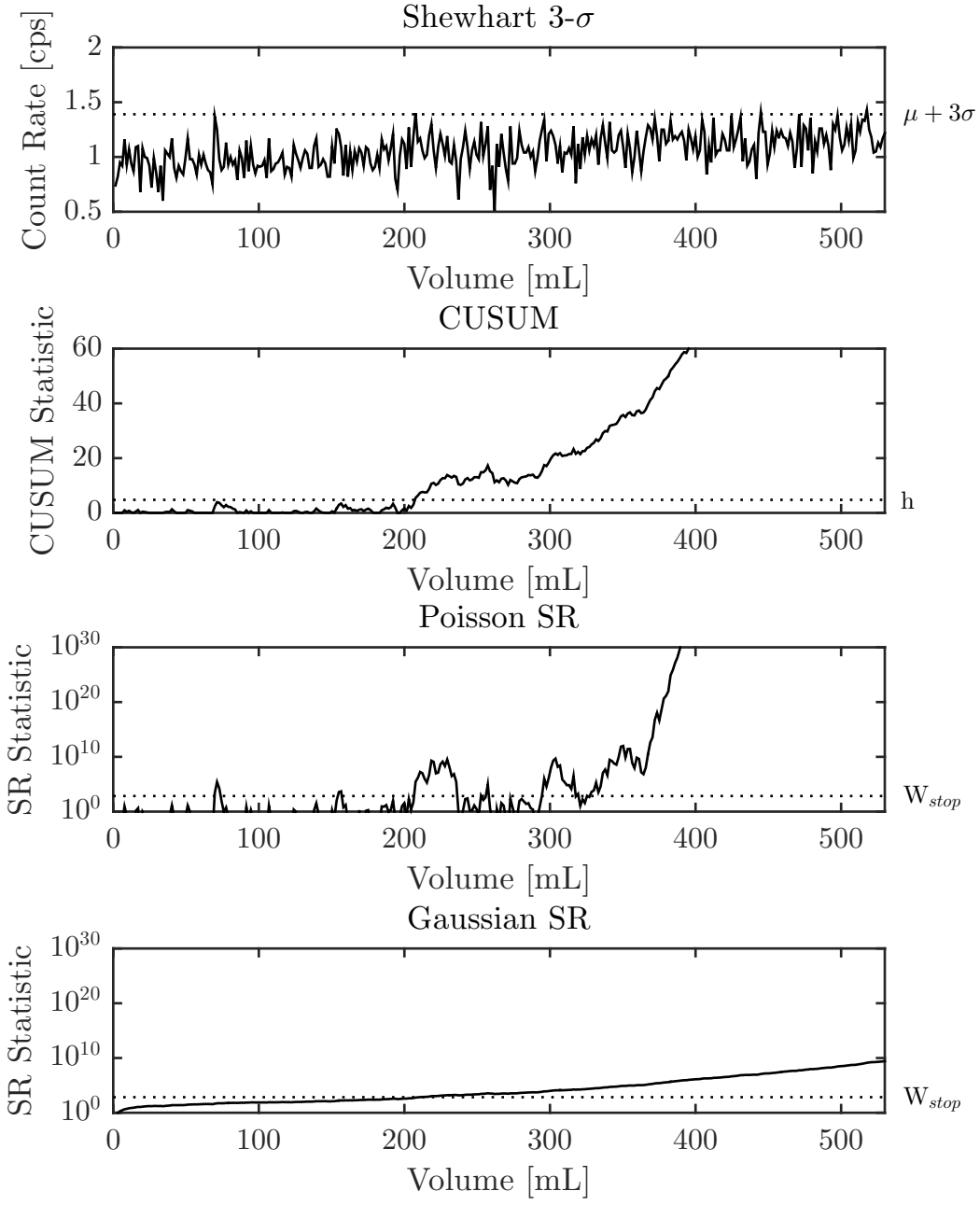

Figure B.31: Shewhart, CUSUM, S-R control charts for 500 mL of 0.513 Bq/L $^{99}TcO_4^-$ preceded by 30 mL of 0.01 M HCl

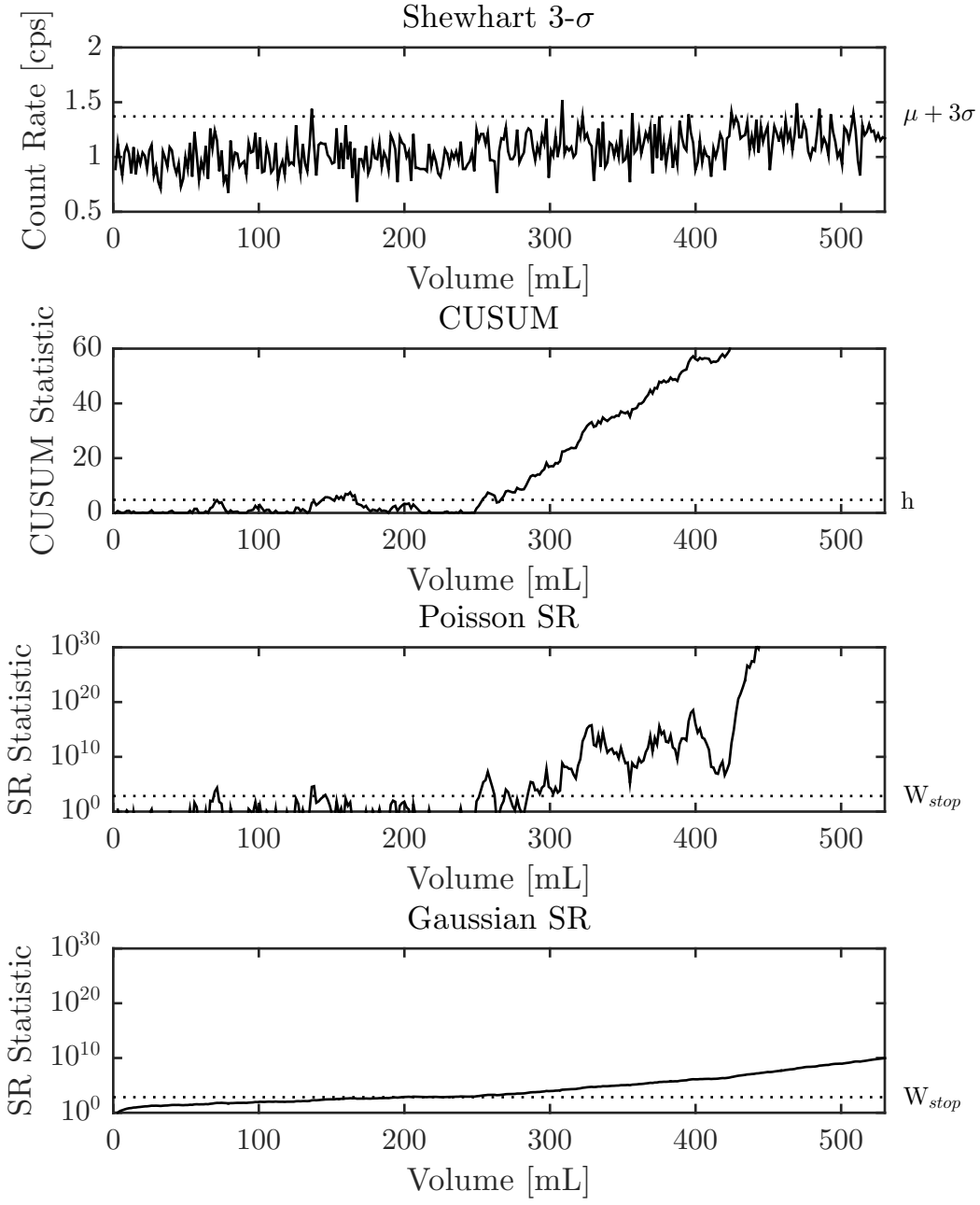

Figure B.32: Shewhart, CUSUM, S-R control charts for 500 mL of 0.500 Bq/L $^{99}TcO_4^-$ preceded by 30 mL of 0.01 M HCl

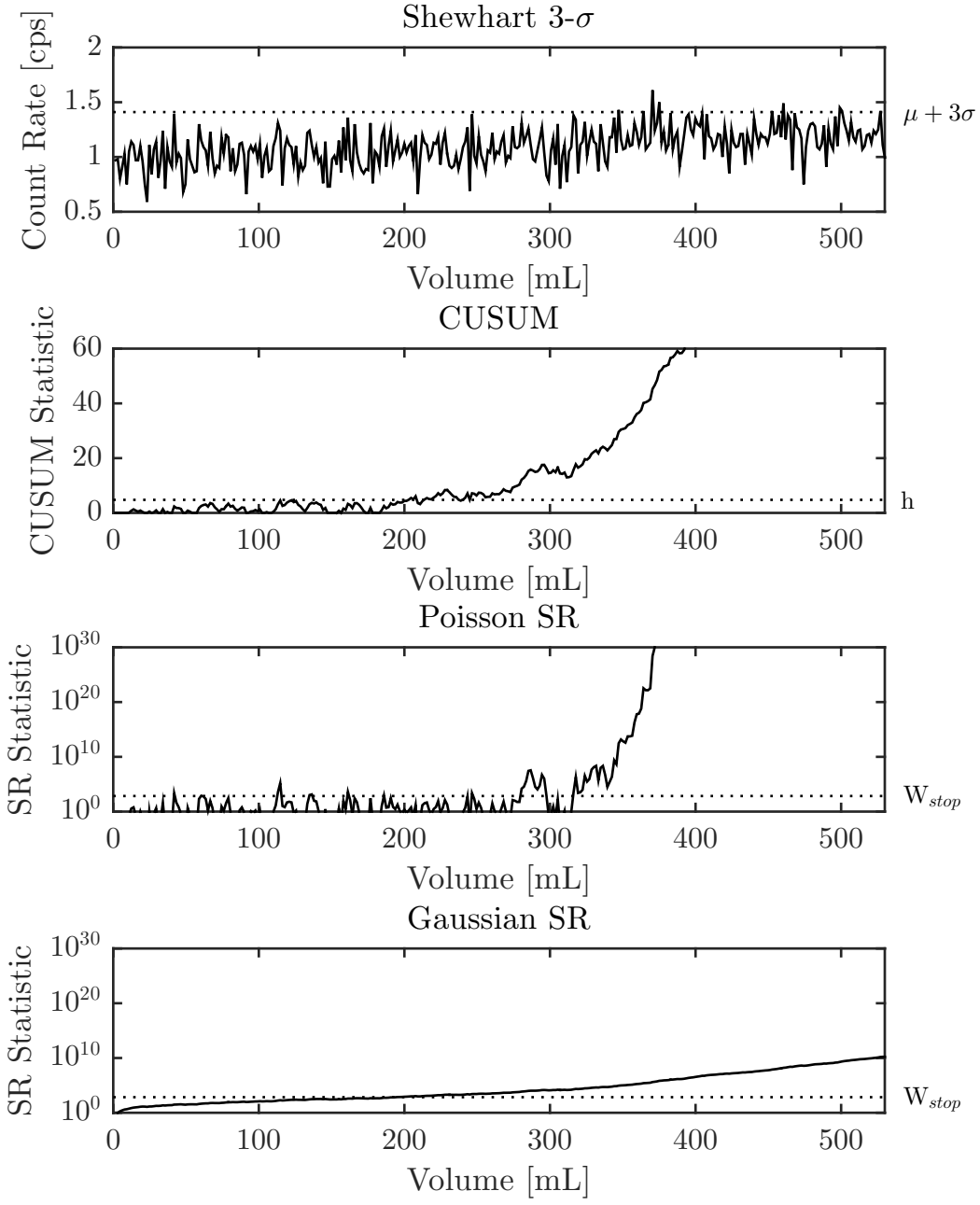

Figure B.33: Shewhart, CUSUM, S-R control charts for 500 mL of 0.497 Bq/L $^{99}TcO_4^-$ preceded by 30 mL of 0.01 M HCl

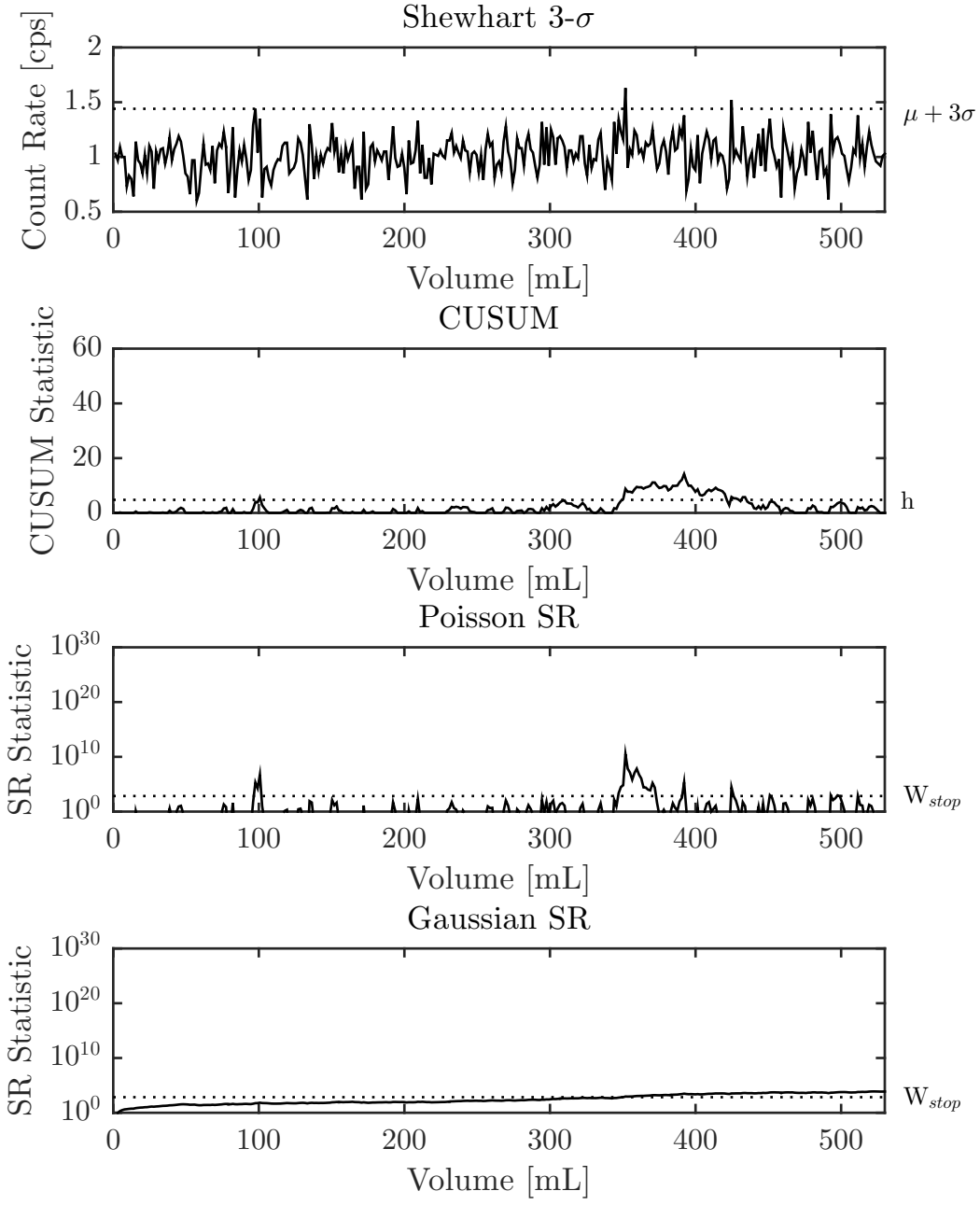

Figure B.34: Shewhart, CUSUM, S-R control charts for 500 mL of 0.110 Bq/L $^{99}TcO_4^-$ preceded by 30 mL of 0.01 M HCl

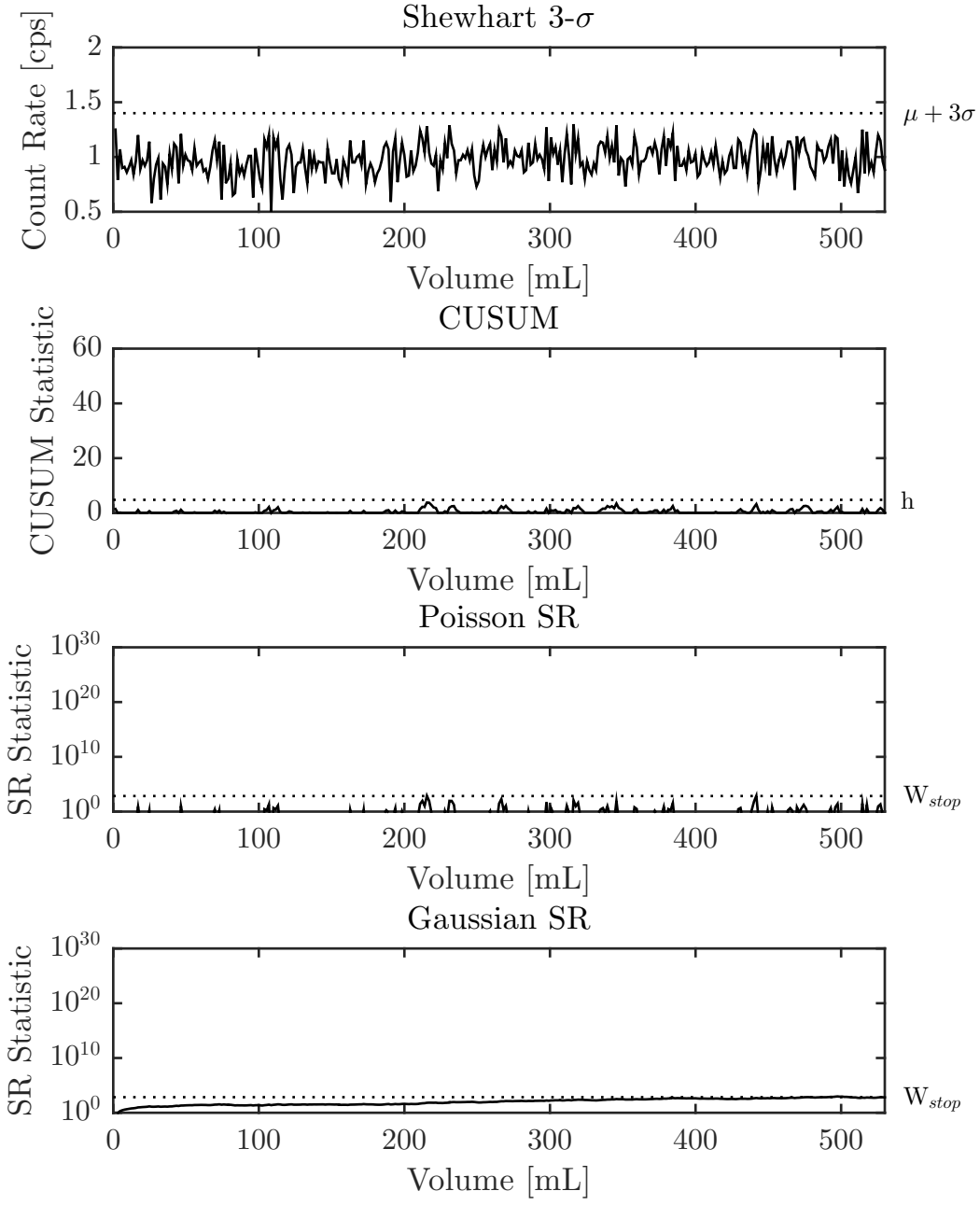

Figure B.35: Shewhart, CUSUM, S-R control charts for 500 mL of 0.103 Bq/L $^{99}TcO_4^-$ preceded by 30 mL of 0.01 M HCl

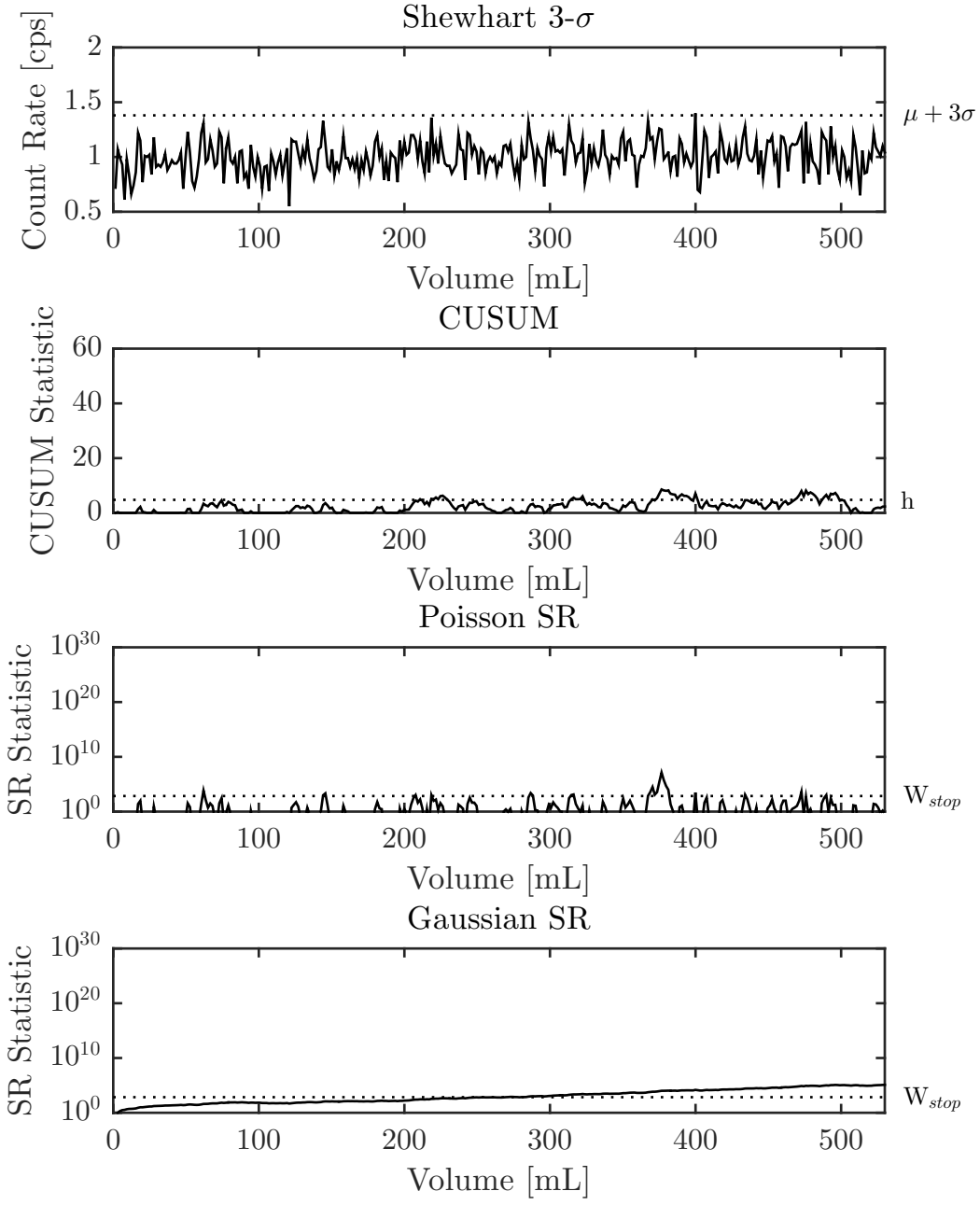

Figure B.36: Shewhart, CUSUM, S-R control charts for 500 mL of 0.0986 Bq/L $^{99}TcO_4^-$ preceded by 30 mL of 0.01 M HCl

Appendix C Control Chart Plots (HNO_3 Data)

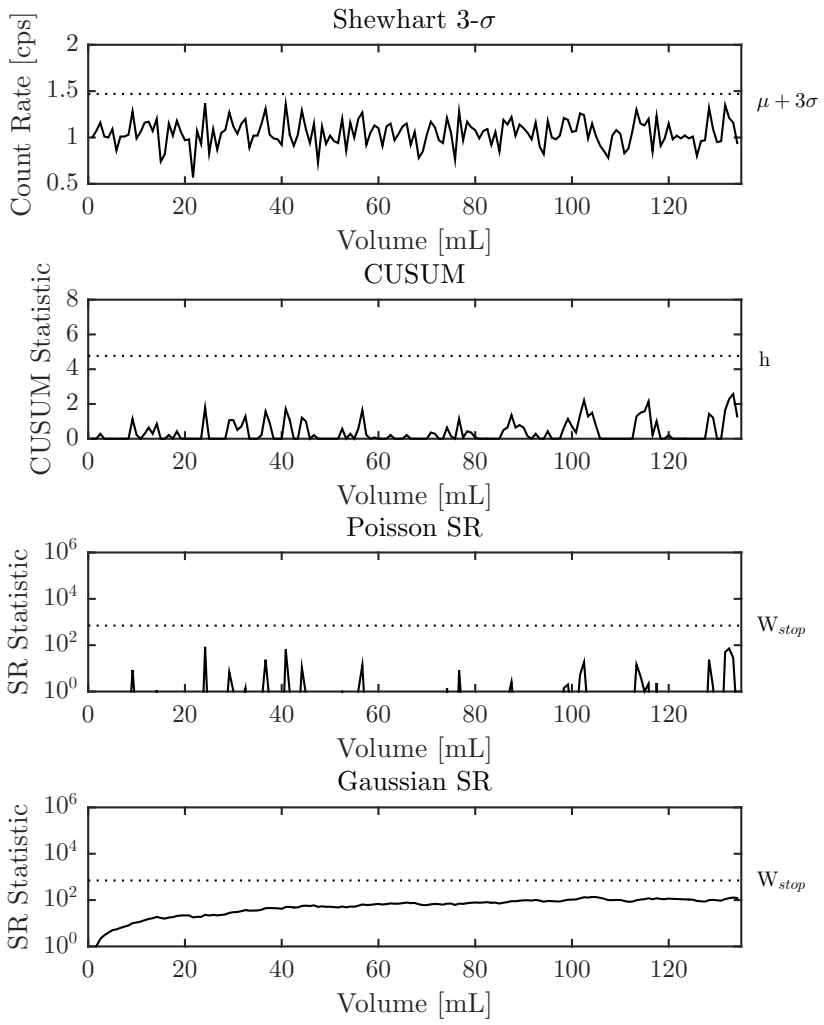

Figure C.1: Shewhart, CUSUM, S-R control charts for background 1; 135 mL of 0.01 M HNO_3

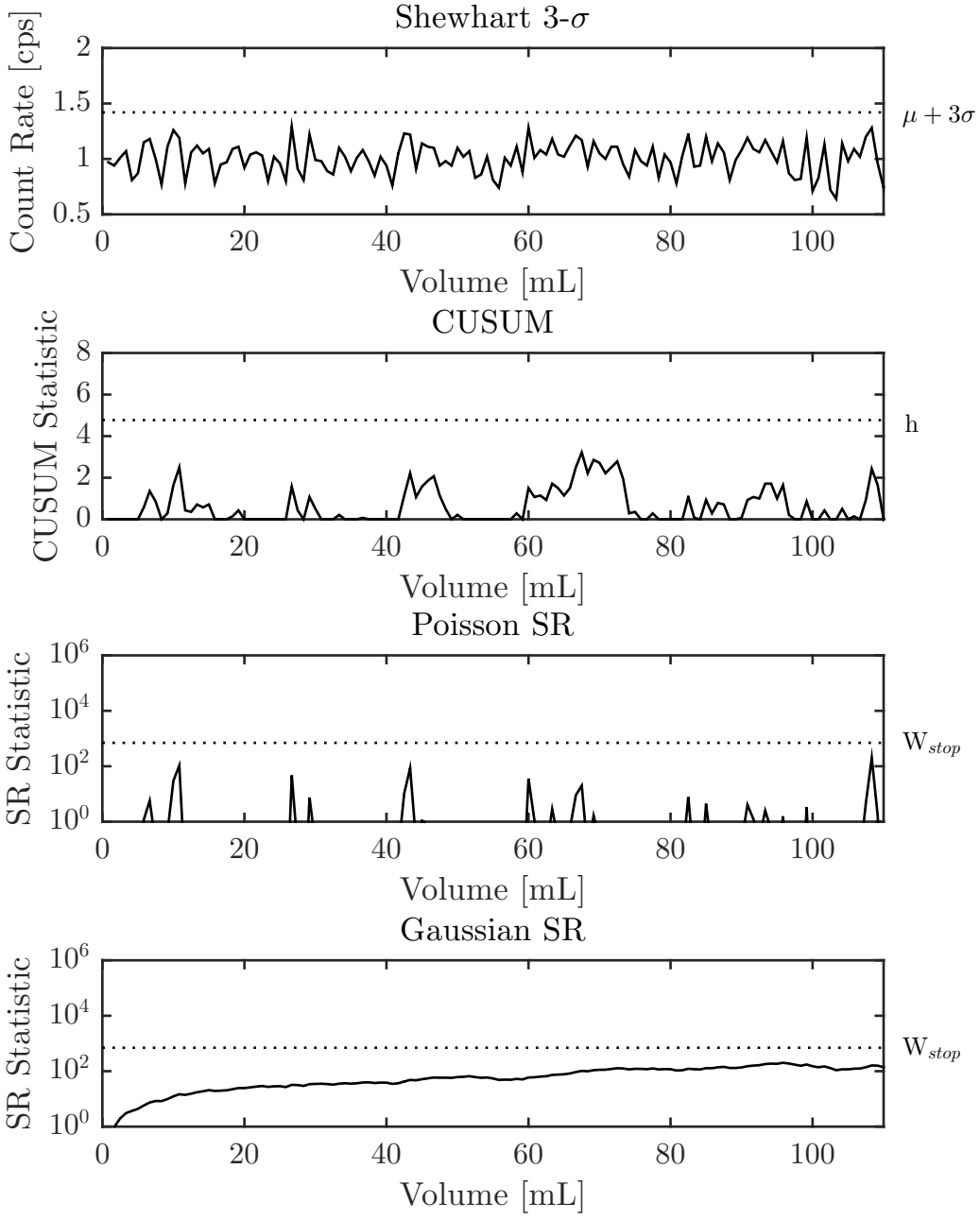

Figure C.2: Shewhart, CUSUM, S-R control charts for background 2; 110 mL of 0.01 M HNO_3

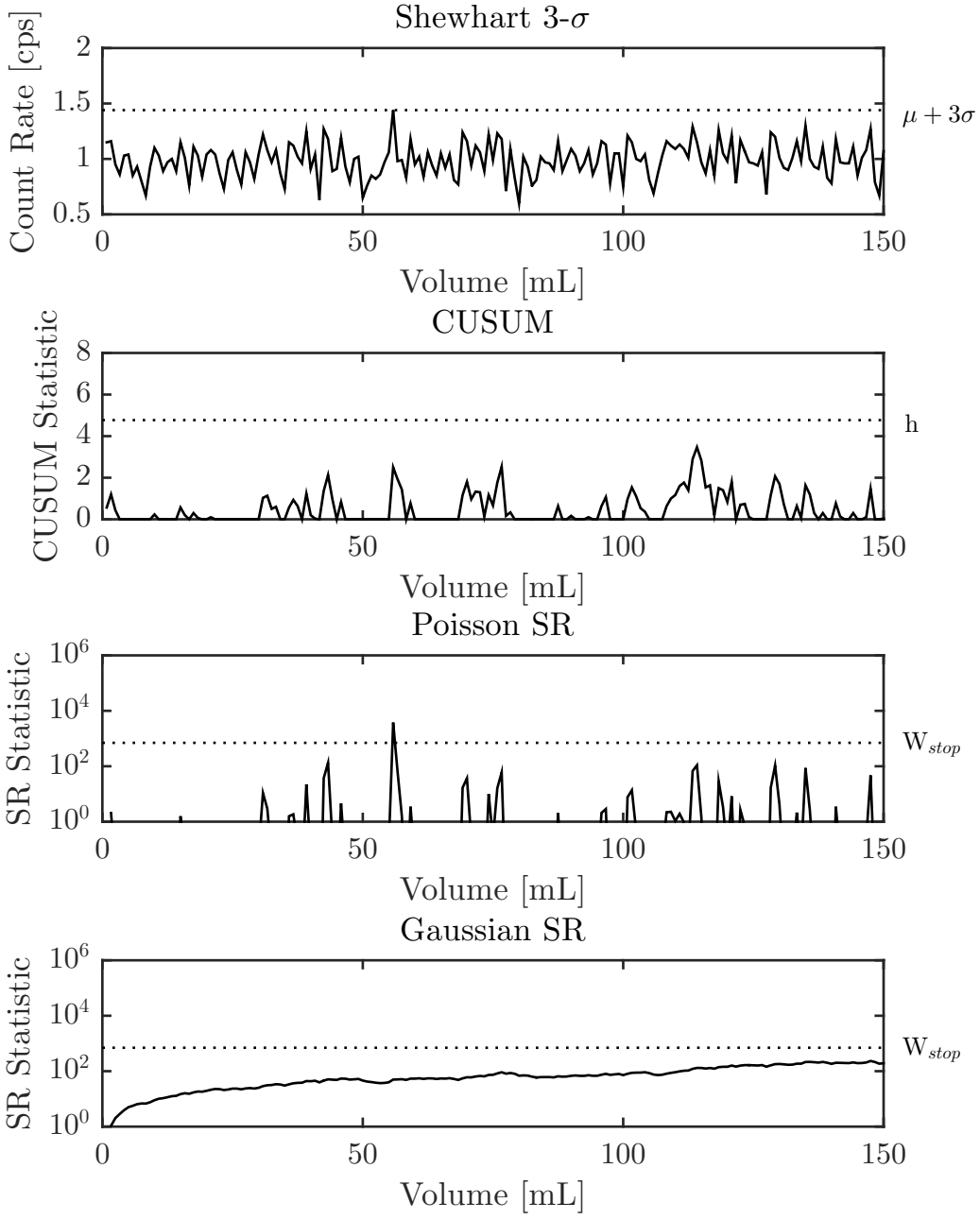

Figure C.3: Shewhart, CUSUM, S-R control charts for background 3; 150 mL of 0.01 M HNO_3

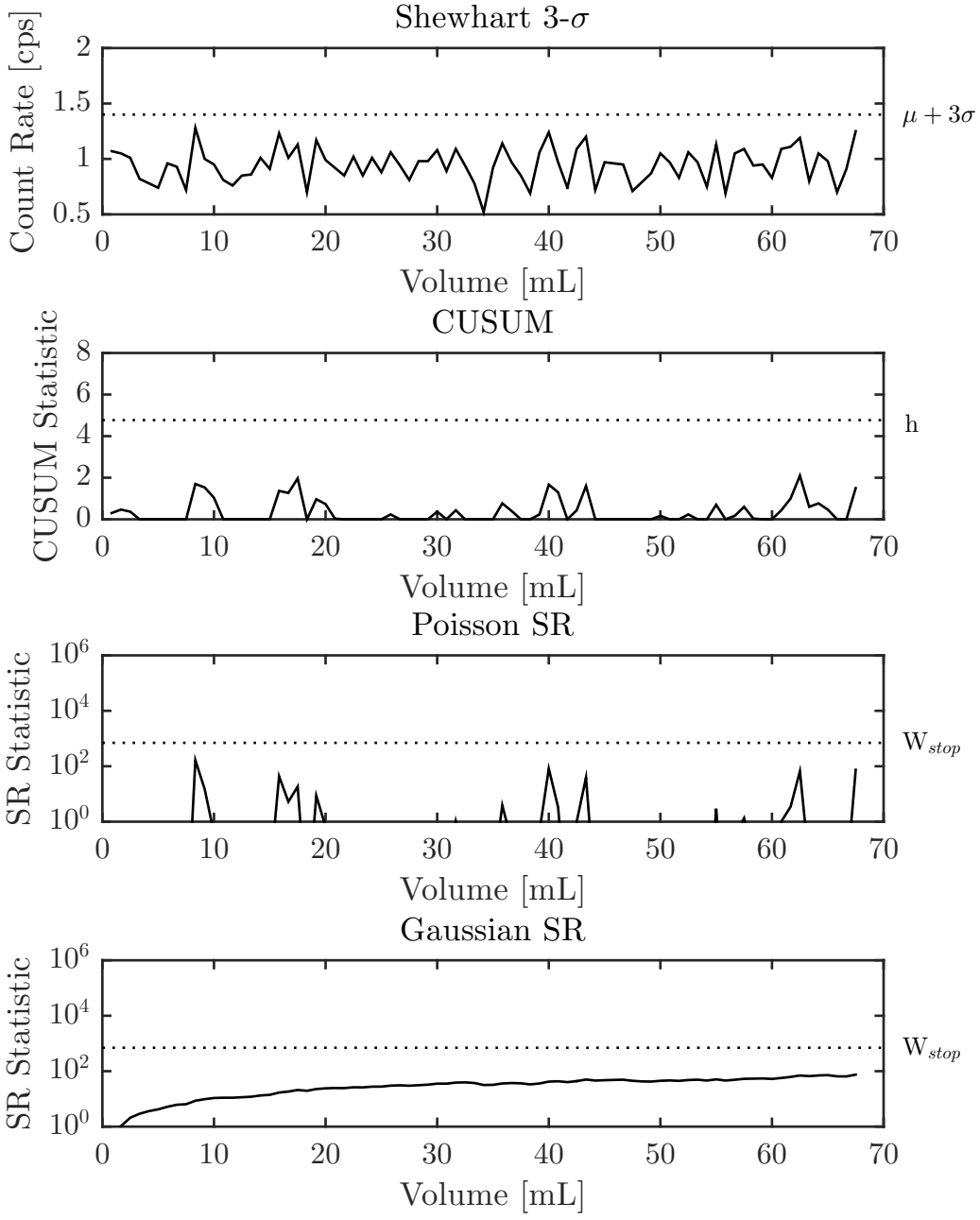

Figure C.4: Shewhart, CUSUM, S-R control charts for background 4; 65 mL of 0.01 M HNO_3

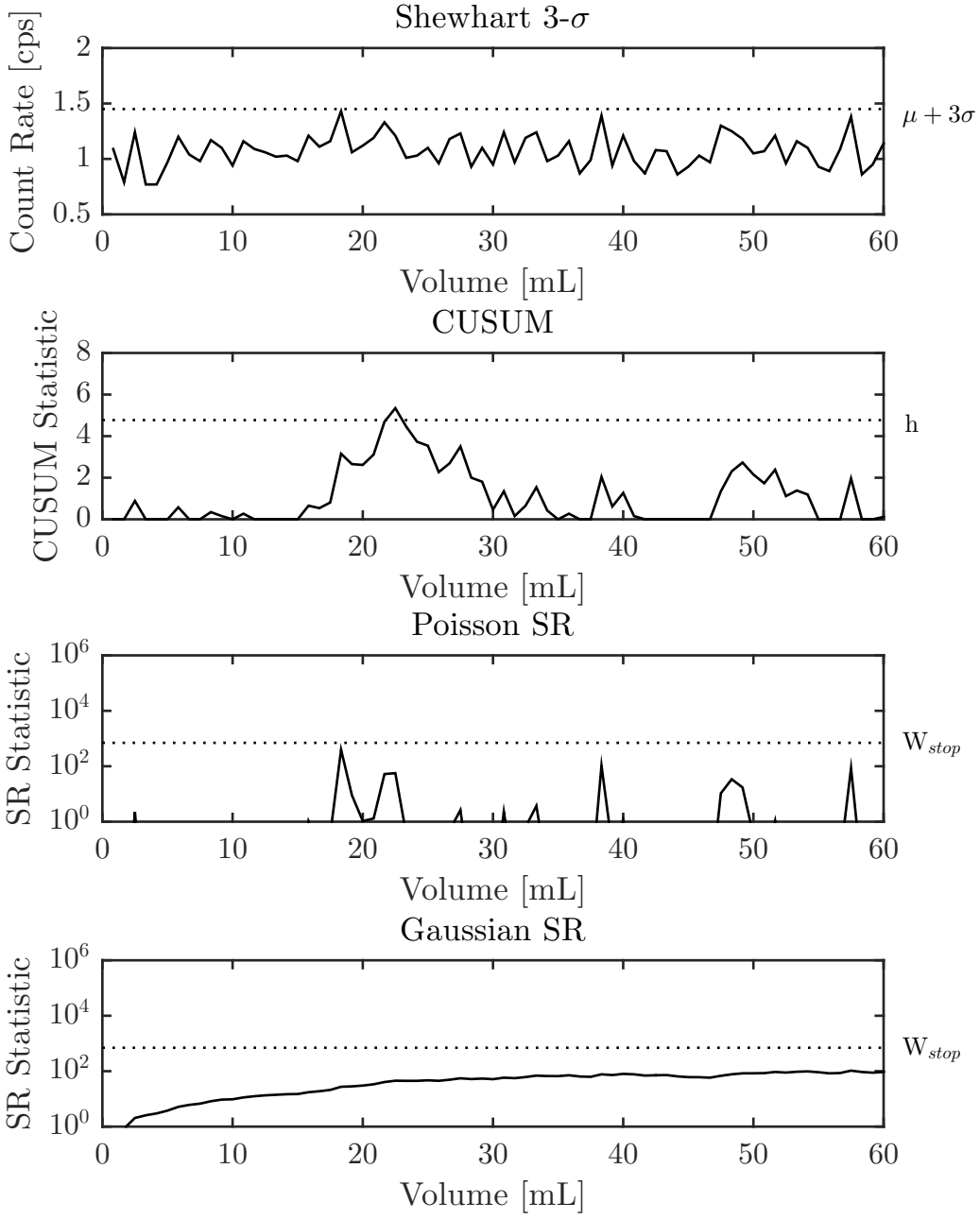

Figure C.5: Shewhart, CUSUM, S-R control charts for background 5; 60 mL of 0.01 M HNO_3

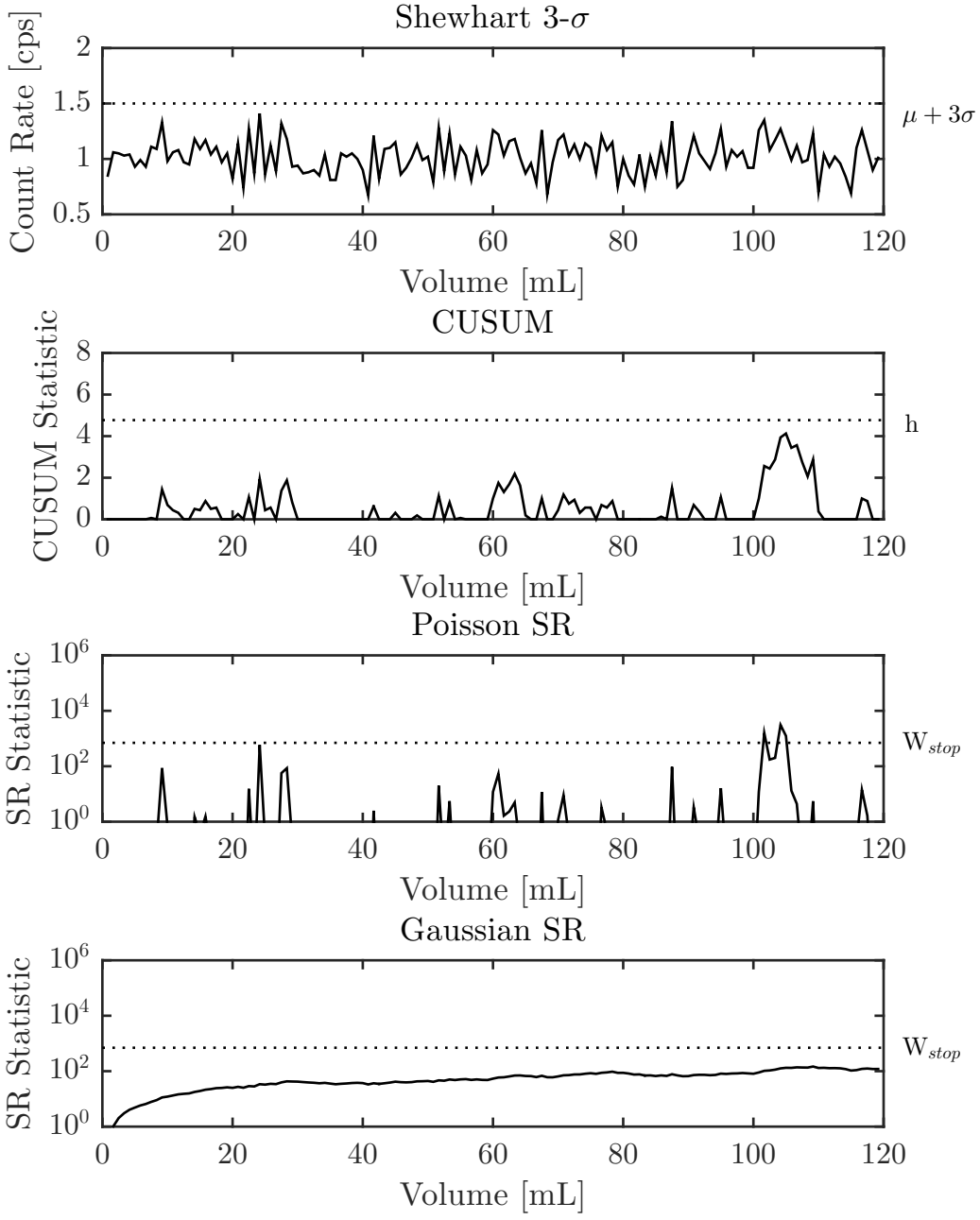

Figure C.6: Shewhart, CUSUM, S-R control charts for background 6; 120 mL of 0.01 M HNO_3

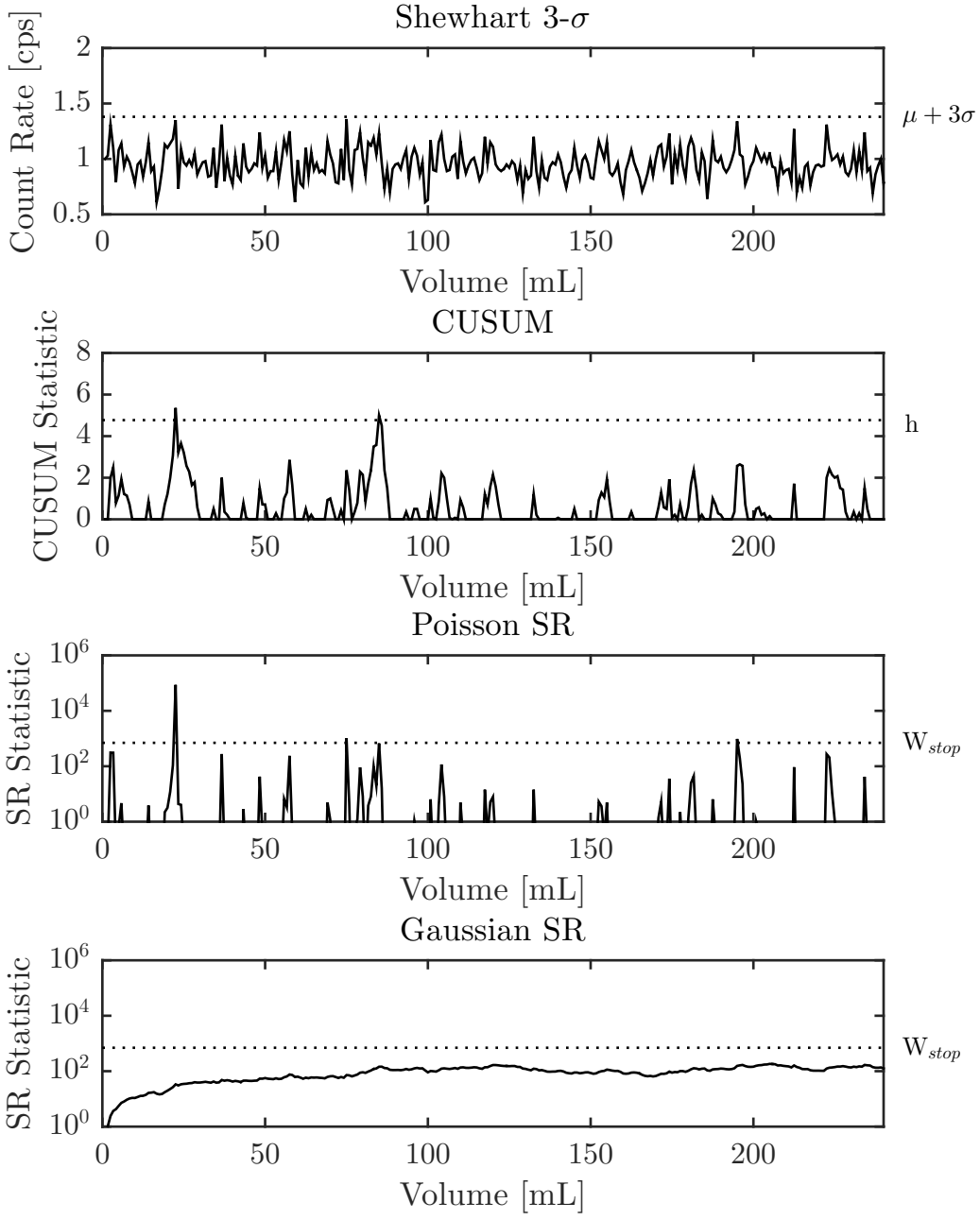

Figure C.7: Shewhart, CUSUM, S-R control charts for background 7; 240 mL of 0.01 M HNO_3

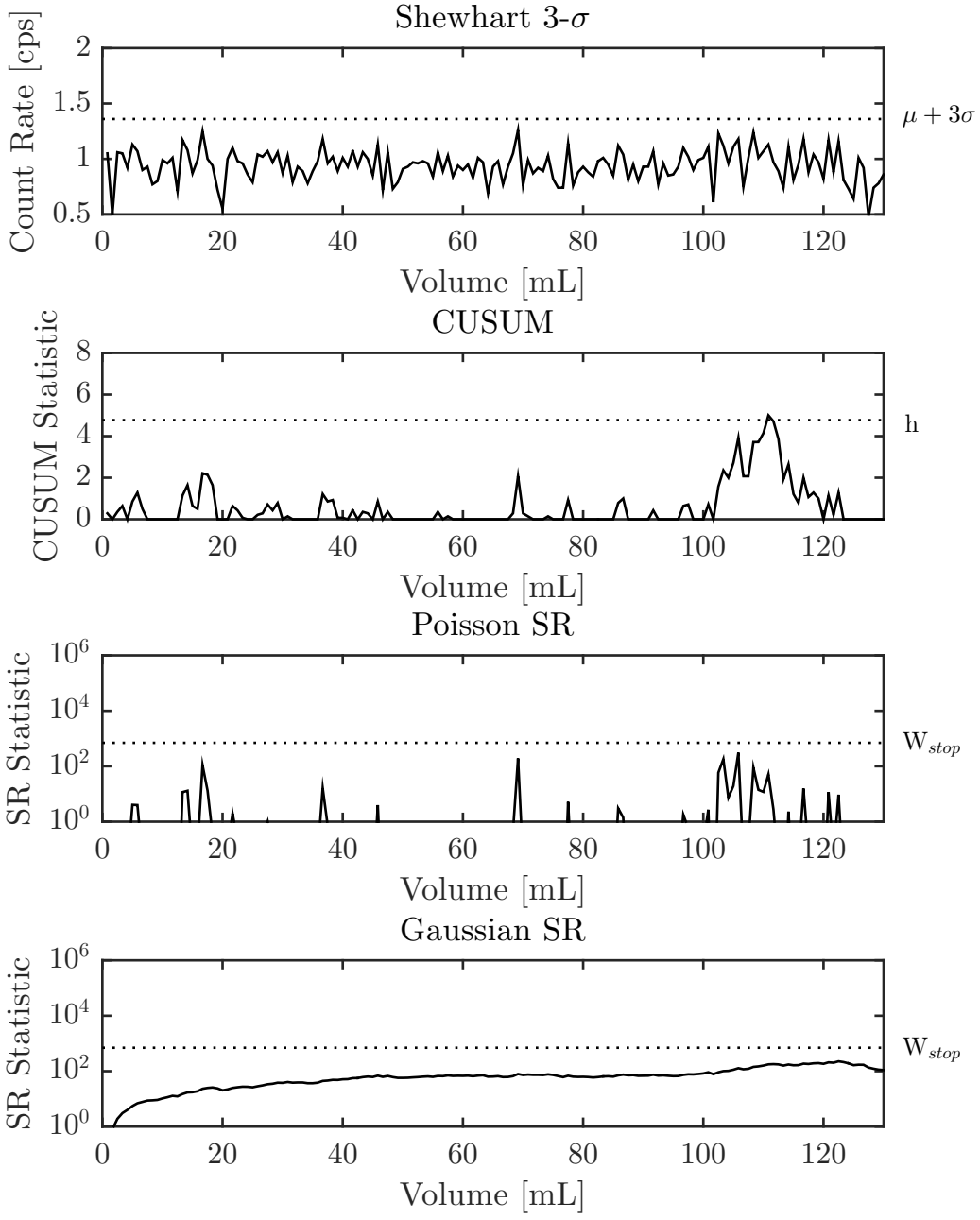

Figure C.8: Shewhart, CUSUM, S-R control charts for background 8; 130 mL of 0.01 M HNO_3

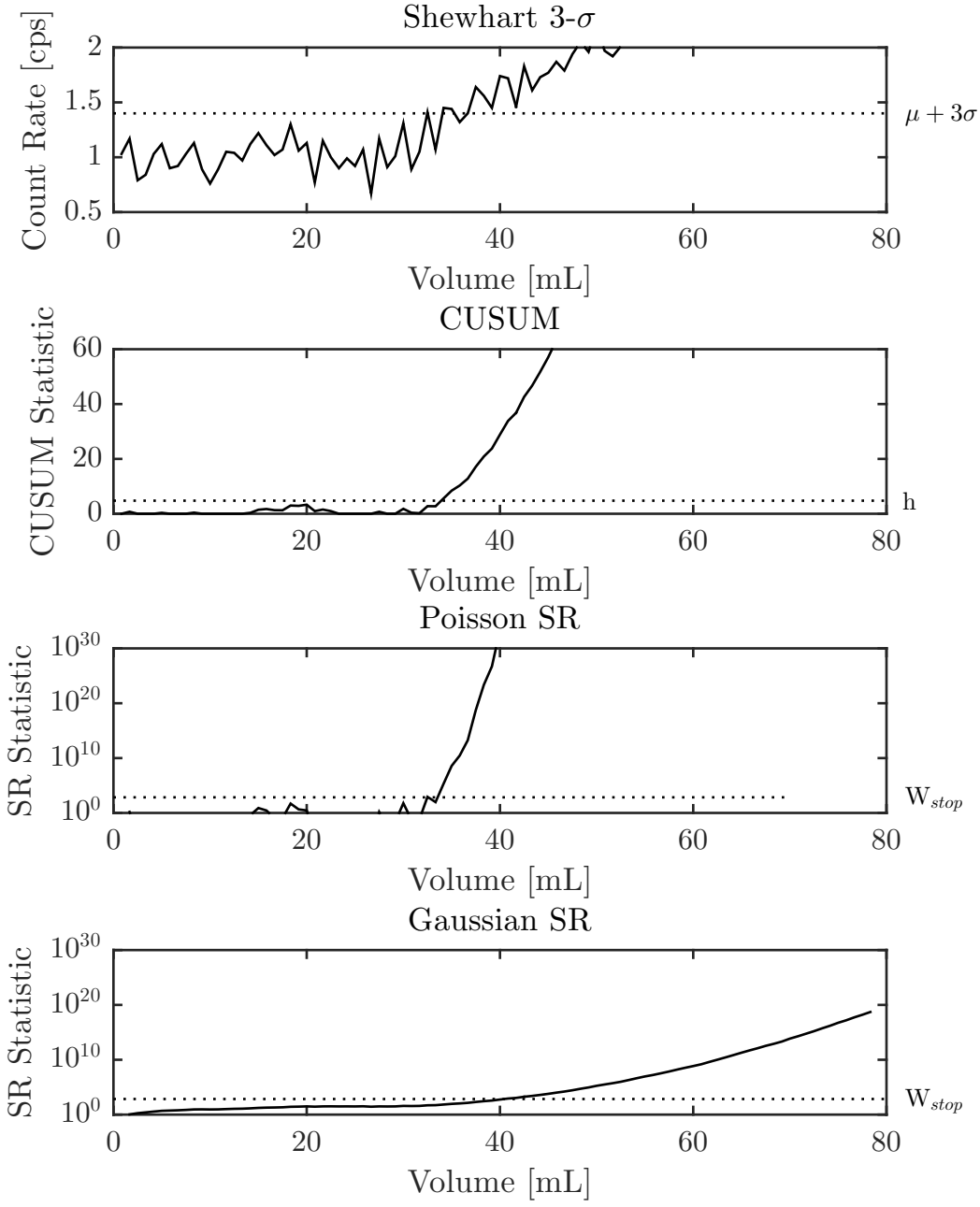

Figure C.9: Shewhart, CUSUM, S-R control charts for 40 mL of 50 Bq/L $^{99}TcO_4^-$ preceded by 30 mL of 0.01 M HNO_3

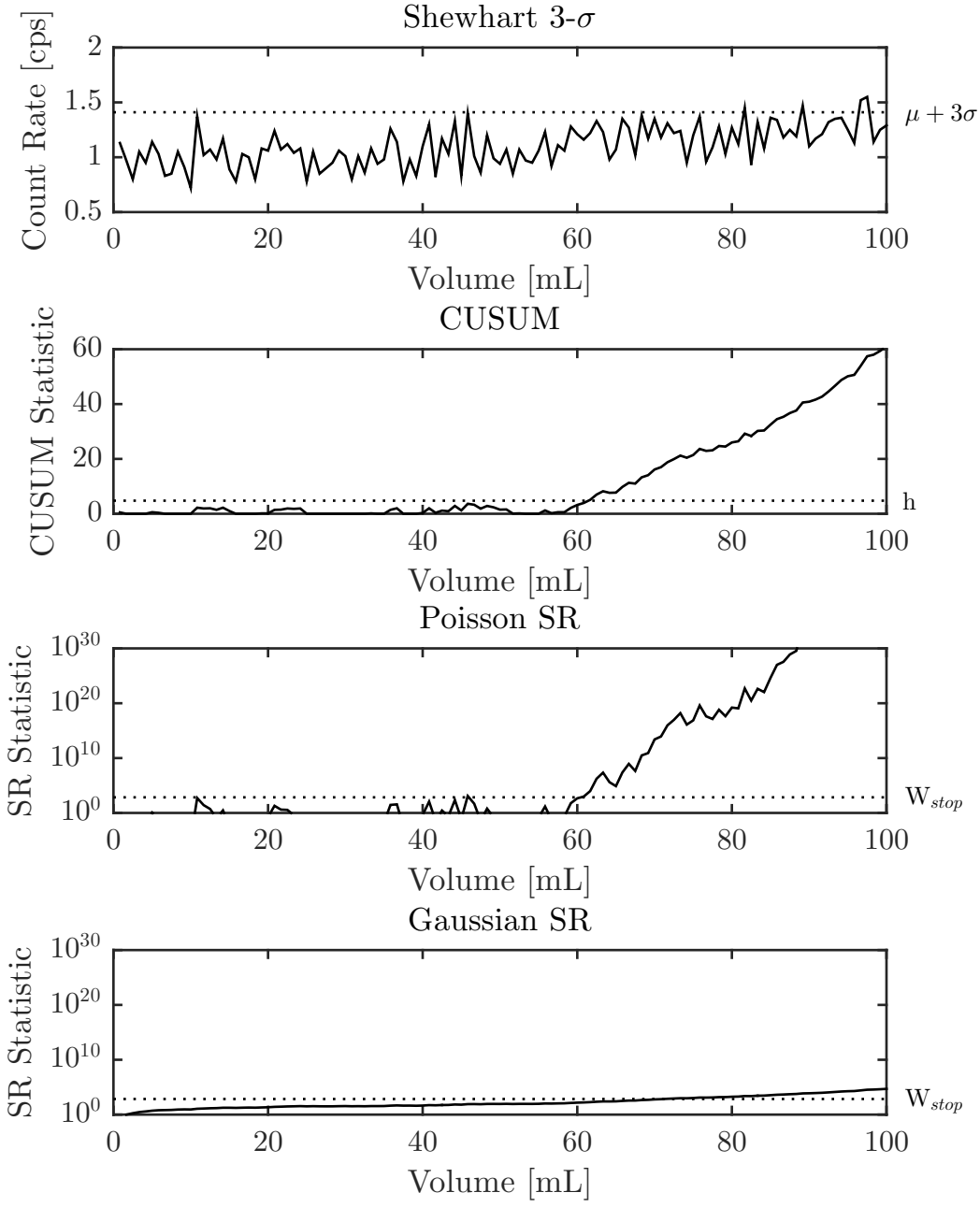

Figure C.10: Shewhart, CUSUM, S-R control charts for 70 mL of 5 Bq/L $^{99}TcO_4^-$ preceded by 30 mL of 0.01 N M HNO_3

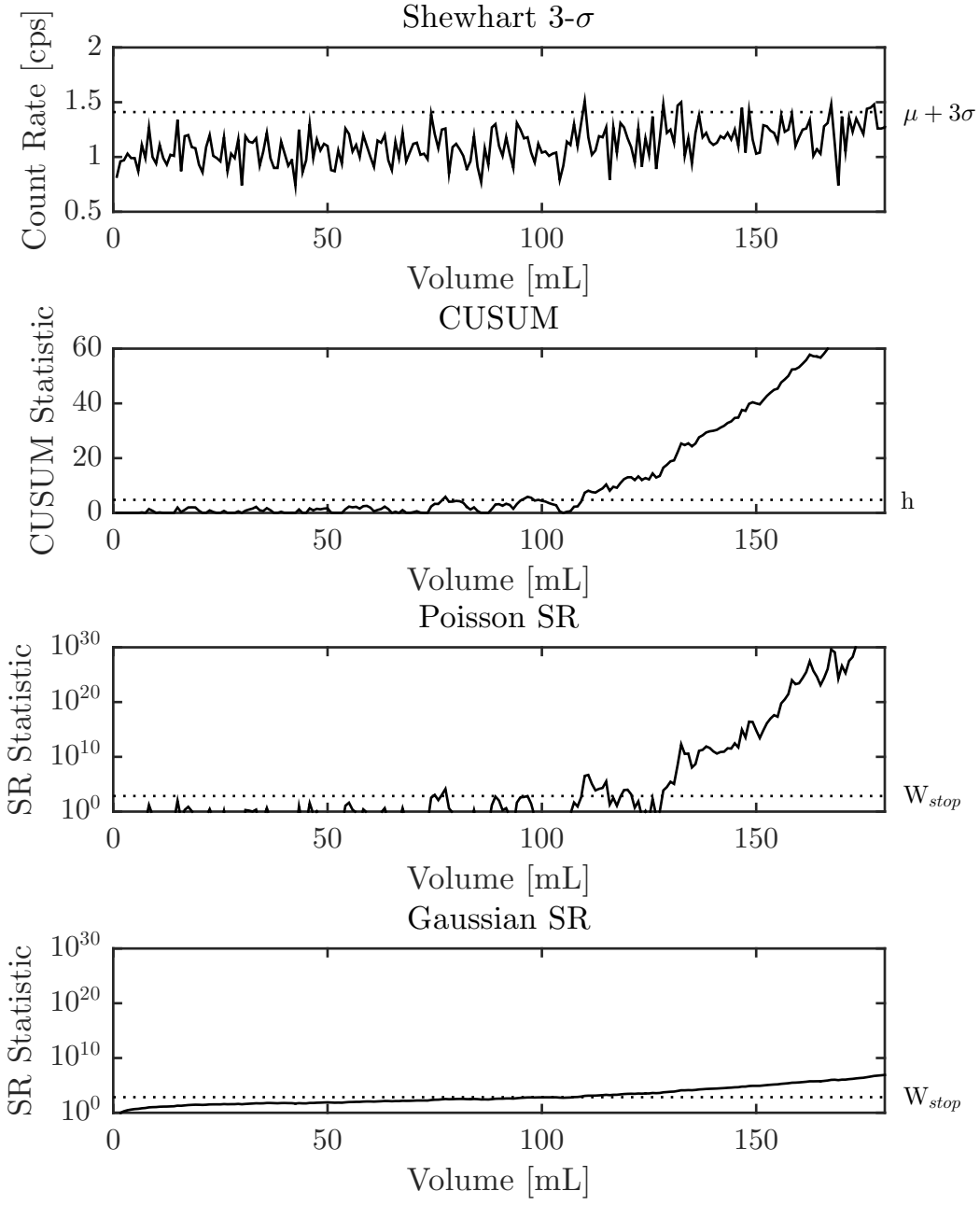

Figure C.11: Shewhart, CUSUM, S-R control charts for 150 mL of 2.53 Bq/L $^{99}TcO_4^-$ preceded by 30 mL of 0.01 M HNO_3

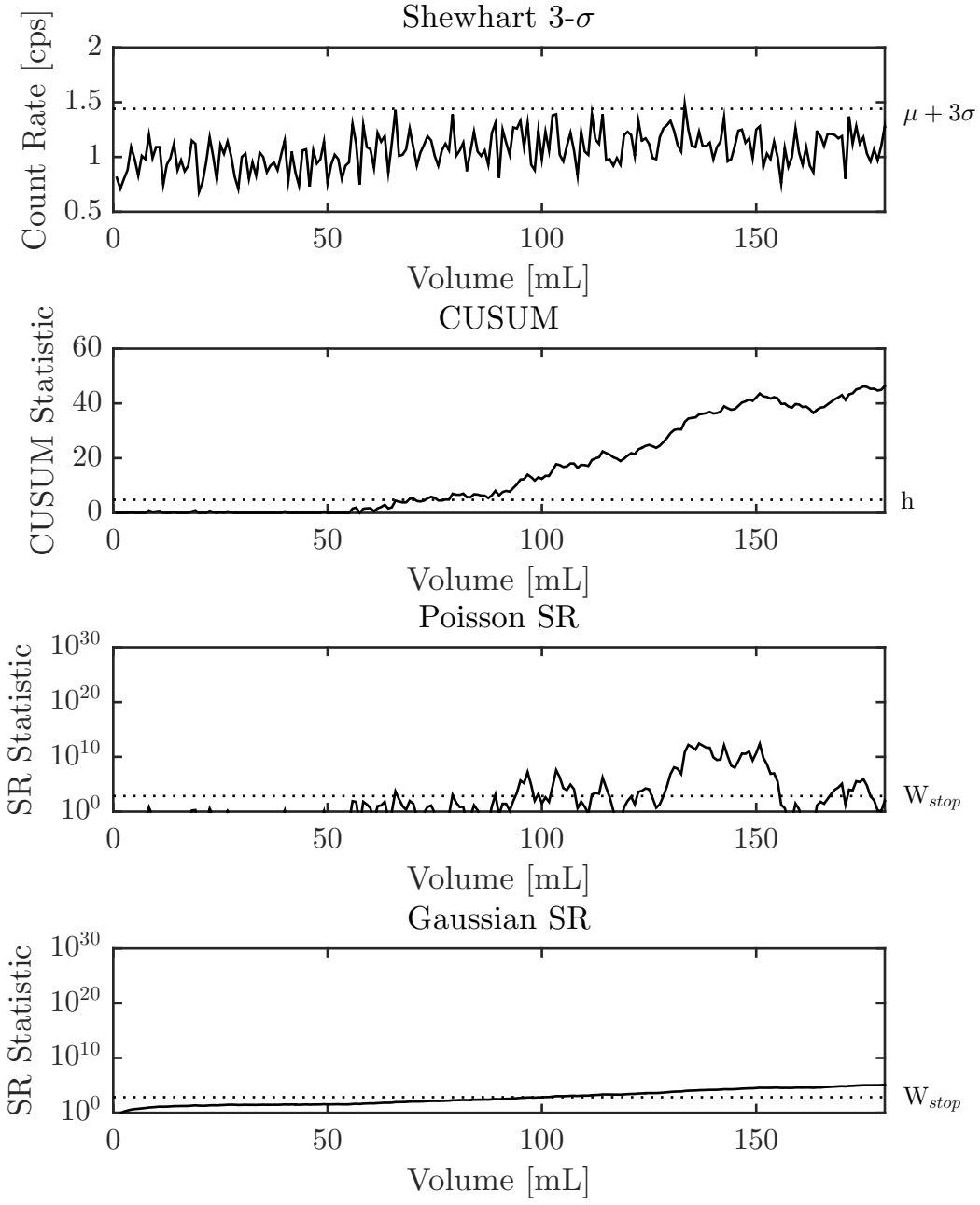

Figure C.12: Shewhart, CUSUM, S-R control charts for 150 mL of 2.5 Bq/L $^{99}TcO_4^-$ preceded by 30 mL of 0.01 M HNO_3

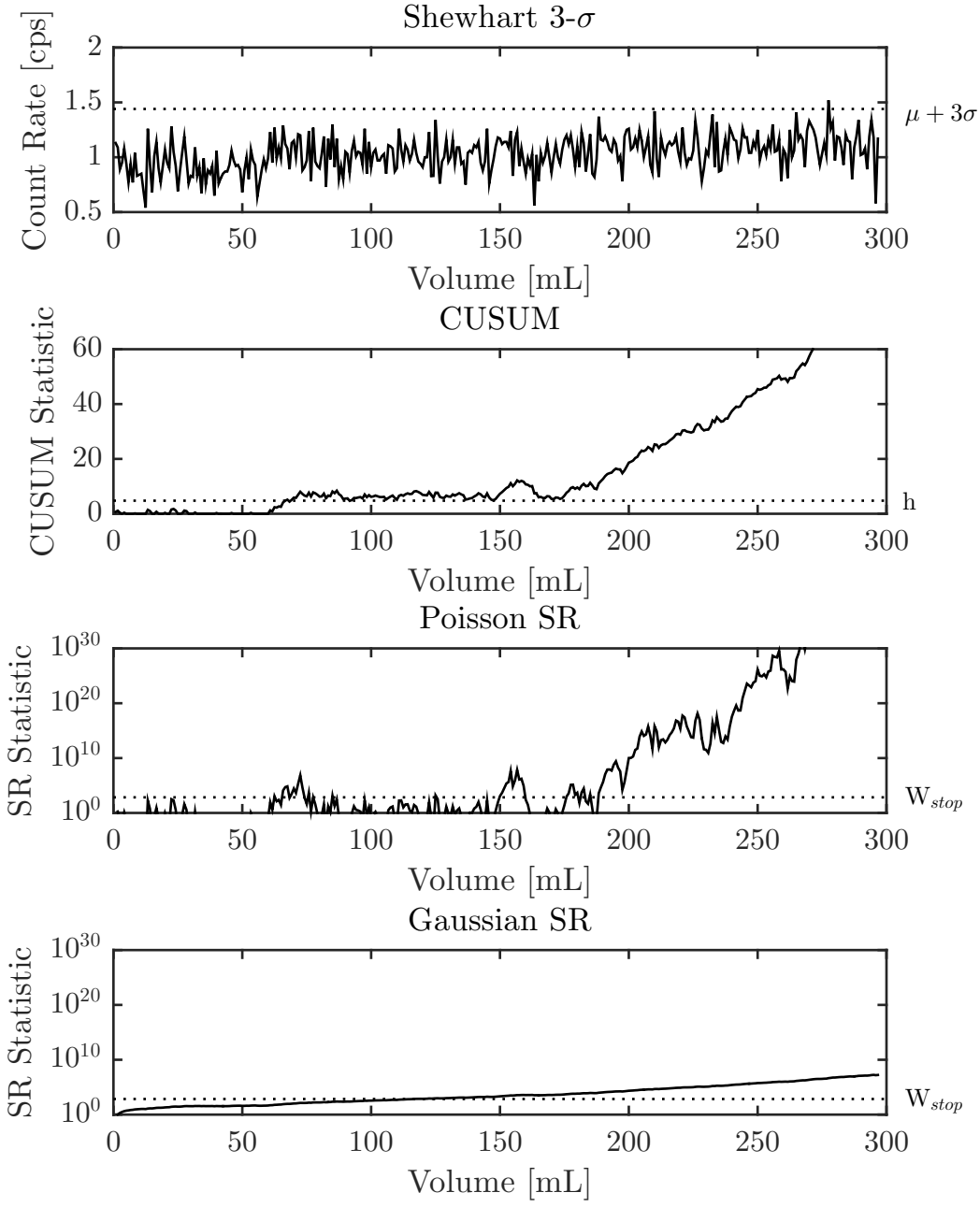

Figure C.13: Shewhart, CUSUM, S-R control charts for 270 mL of 1.5 Bq/L $^{99}TcO_4^-$ preceded by 30 mL of 0.01 M HNO_3

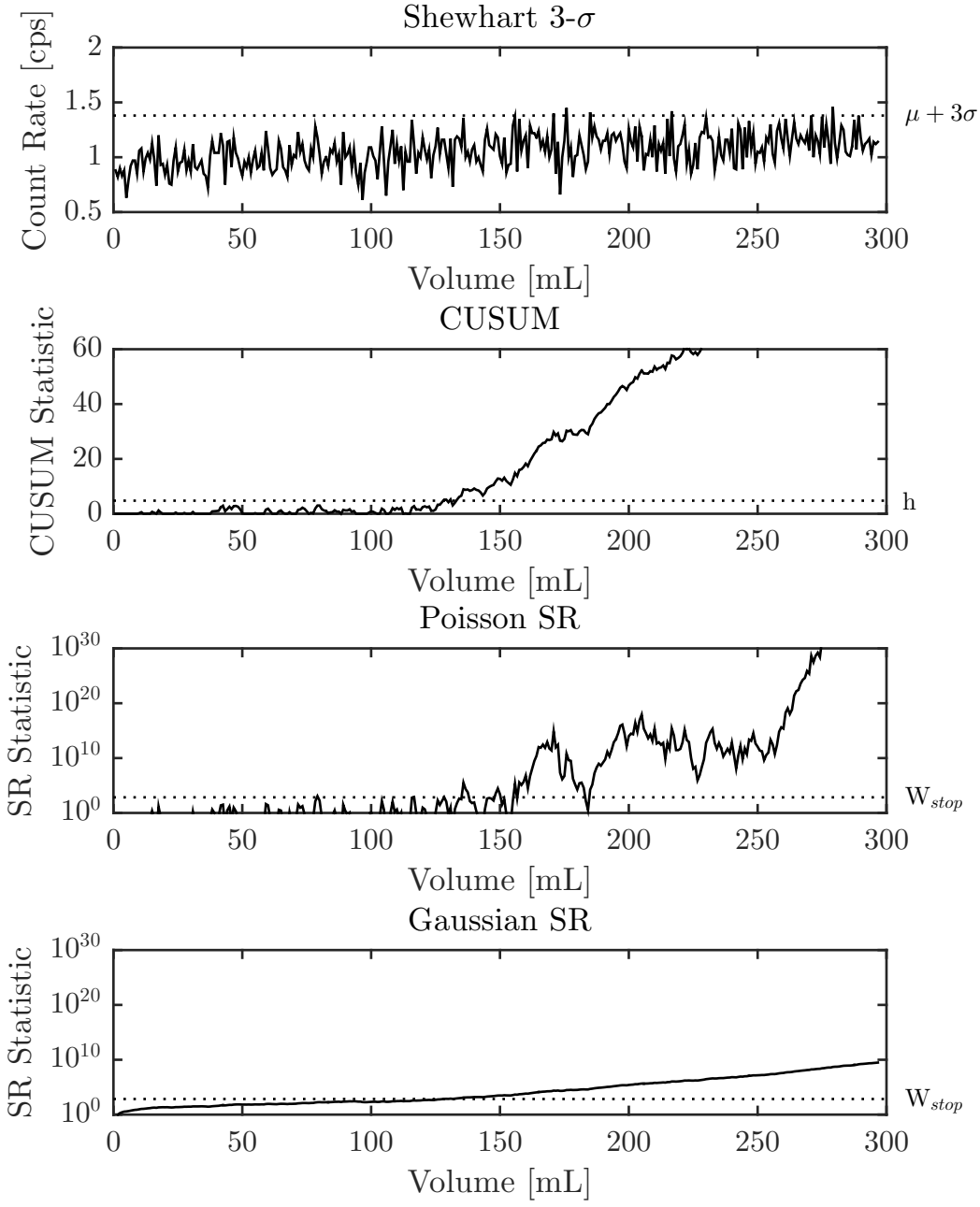

Figure C.14: Shewhart, CUSUM, S-R control charts for 270 mL of 1.05 Bq/L $^{99}TcO_4^-$ preceded by 30 mL of 0.01 M HNO_3

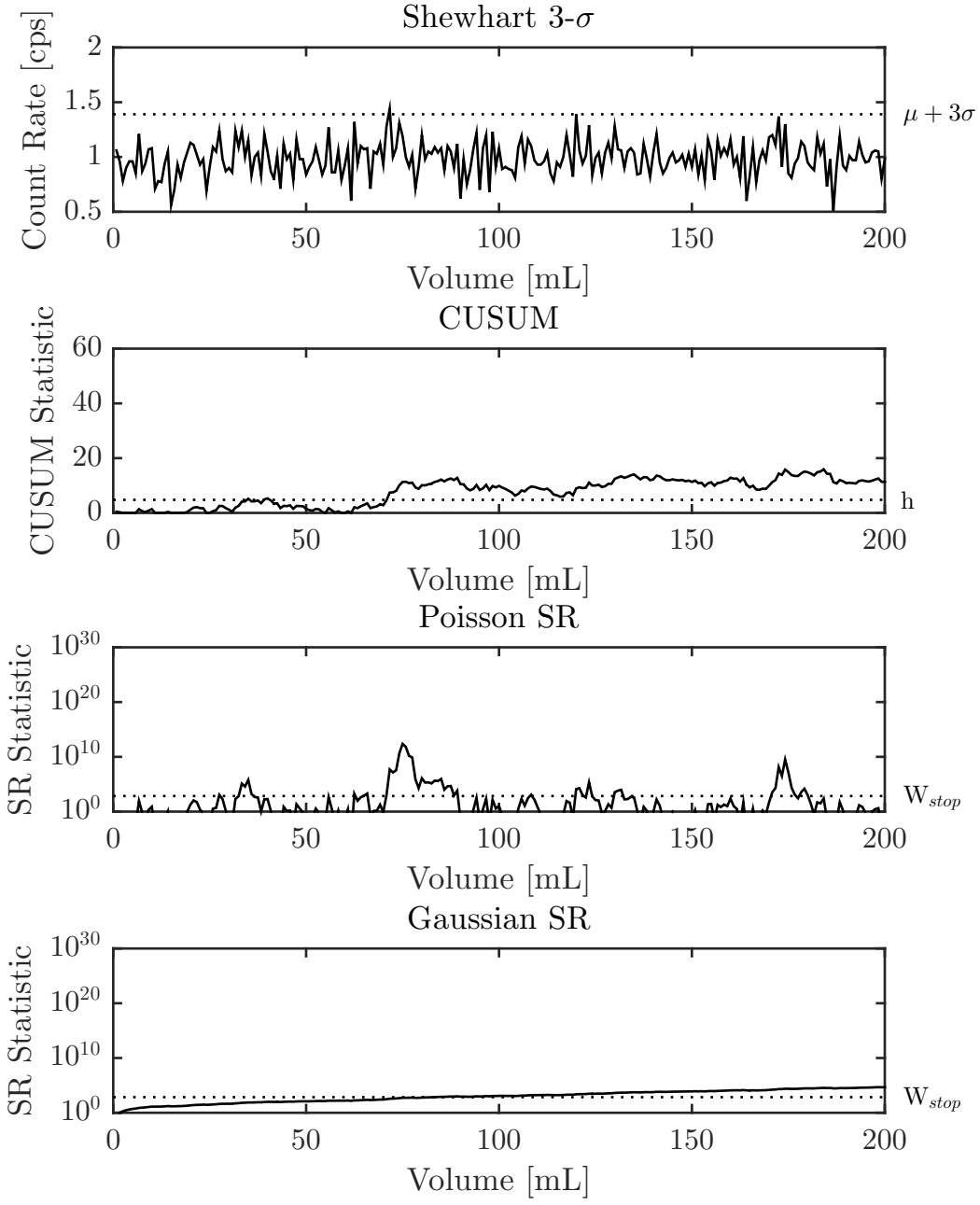

Figure C.15: Shewhart, CUSUM, S-R control charts for 170 mL of 1 Bq/L $^{99}TcO_4^-$ preceded by 30 mL of 0.01 M HNO_3

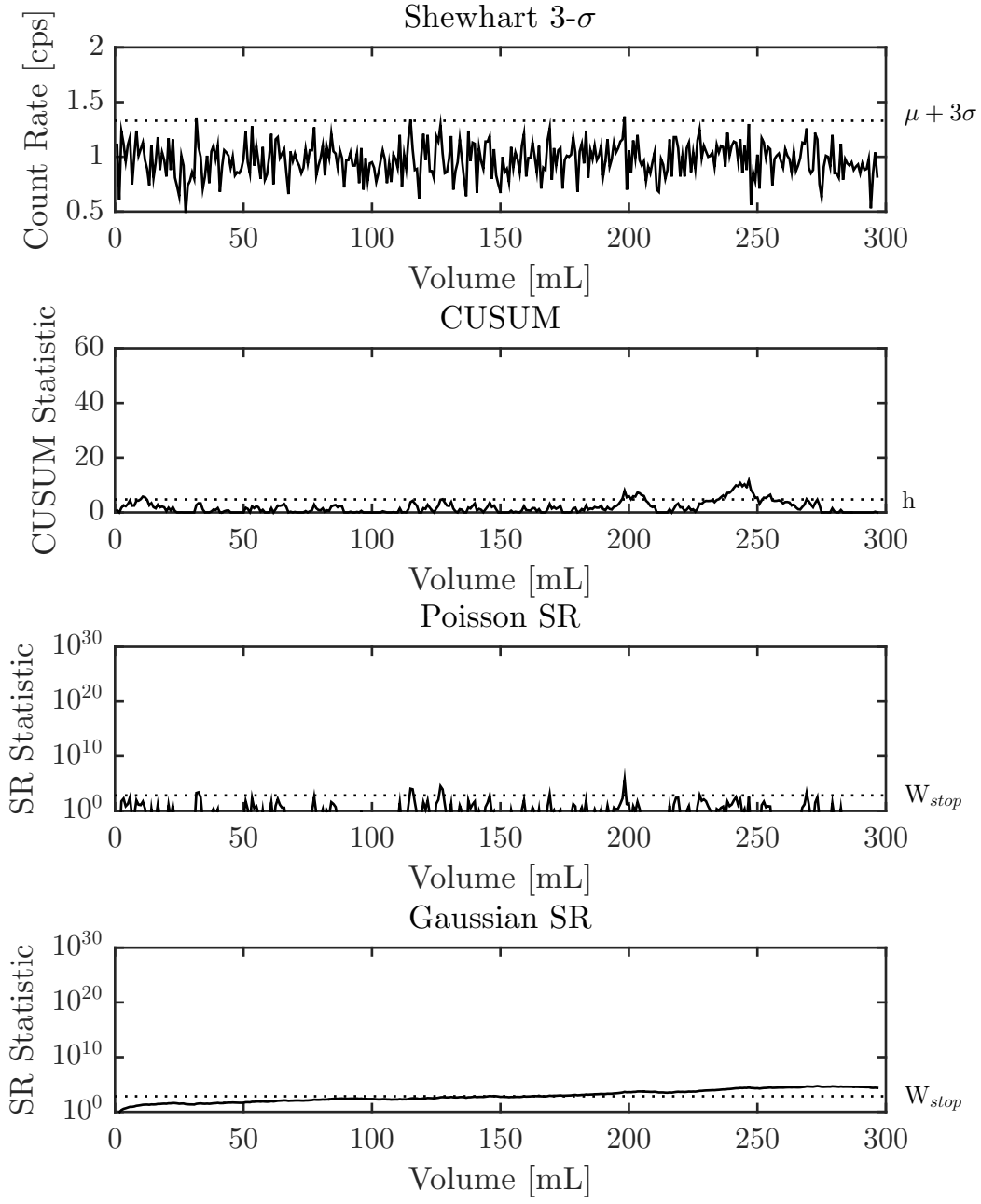

Figure C.16: Shewhart, CUSUM, S-R control charts for 270 mL of 0.5 Bq/L $^{99}TcO_4^-$ preceded by 30 mL of 0.01 M HNO_3

Appendix D Activity to Exceed Control Limit

Table D.1: Activity to exceed control limit for Shewhart 3σ, CUSUM, Poisson SR, and Gaussian SR methods

Activity Conc. (Bq/L)	Activity (Bq)			
	Shewhart 3-σ	CUSUM	Poisson SR	Gaussian SR
5.08	0.31	0.17	0.16	0.16
5.03	0.14	0.19	0.12	0.23
4.97	0.42	0.16	0.15	0.22
2.54	0.14	0.14	0.039	0.15
2.50	0.14	0.16	0.035	0.15
2.49	0.12	0.17	0.089	0.16
1.53	0.17	0.11	0.055	0.092
1.51	0.22	0.12	0.070	0.12
1.49	0.15	0.072	0.016	0.088
1.02	0.13	0.058	0.041	0.068
1.00	0.18	0.13	0.067	0.067
0.997	0.18	0.091	0.085	0.091
0.513	0.091	0.091	0.020	0.074
0.500	0.053	0.057	0.019	0.056
0.497	0.16	0.09	0.0054	0.042
0.110	0.035	0.008	0.0073	0.031
0.103	N/A	N/A	0.019	0.036
0.0986	0.036	0.018	0.0031	0.018

References

Ayaz, B., DeVol, T. A., (2003) "Application of MnO_2 coated scintillating and extractive scintillating resins to screening for radioactivity in groundwater," *Nuclear Instruments and Methods in Physics Research A*, 505, 458-461.

Bliznyuk, V. N., Duval, C. E., Apul, O. G., Seliman, A. F., Husson, S. M., DeVol, T. A., (2015) "High porosity scintillating polymer resins for ionizing radiation sensor applications," *Polymer*, 56, 271-279.

Bolstad, W. M., (2007) *Introduction to Bayesian Statistics*, 2nd edition. John Wiley & Sons, Inc., Hoboken, NJ.

Chen, F., Mankarios, G., (2004) "Near-Field Behavior of ^{99}Tc During the Oxidative Alteration of Spent Nuclear Fuel," *Journal of Nuclear Materials*, 278, 225-232.

Clapham, B., Sutherland, A. J., (2000) "Use of a scintillant-containing macroporous resin in both solid phase synthesis and subsequent on-bead scintillation-based analysis," *Tetrahedron Letters*, 41(13), 2257-2260.

DeVol, T. A., Roane, J. E., Williamson, J. M., Duffey, J. M., Harvey, J. T., (2000) "Development of scintillating extraction media for separation and measurement of charged-particle-emitting radionuclides in aqueous solutions," *Radioactivity and Radiochemistry*, 11, 34-46.

DeVol, T. A., Egorov, O. B., Roane, J. E., Paulenova, A., Grate, J. W., (2001) "Extractive scintillating resin for ^{99}Tc quantification in aqueous solutions," *Journal of Radioanalytical and Nuclear Chemistry*, 249(1), 181-189.

DeVol, T. A., Leyba, J. D., Roane, J. E., (2002) "Application of Extractive Scintillator Resins to Quantification of Beta-Emitting Radionuclides in Aqueous Solutions," LSC 2001 Advances in Liquid Scintillation Spectrometry (Conference Record), 415-423.

DeVol, T. A., Gohres, A. A., Williams, C. L., (2009) "Application of Classical Versus Bayesian Statistical Methods to On-line Radiation Monitoring," *Journal of Radioanalytical and Nuclear Chemistry*, 282, 933-938.

Egorov, O. B., Fiskum, S. K., O'Hara, M. J., Grate, J. W., (1999) "Radionuclide Sensors Based on Chemically Selective Scintillating Microspheres: Renewable Column Sensor for Analysis of ^{99}Tc in Water," *Analytical Chemistry*, 71, 5420-5429.

Groer, P. G., Lo, Y., (1996) "Measurement of Airborne ^{218}Po–A Bayesian Approach," *Health Physics*, 71(6), 951-956.

Groer, P. G., (2002) "Exact and Approximate Bayesian Estimation of Net Counting Rates," *Radiation Protection Dosimetry*, 102(3), 265-268.

Hamada, M. S., Wilson, A. G., Reese, C. S., Martz, H. F., (2008) *Bayesian Reliability*. Springer Science + Business Media, LLC, New York, NY.

Hughes, L. D., DeVol, T. A., (2003) "On-line gross alpha radiation monitoring of natural waters with extractive scintillating resins," *Nuclear Instruments and Methods in Physics Research A*, 505, 435-438.

Hughes, L. D., (2006) "Radionuclide Sensors for Monitoring of $^{99}TcO_4^-$ in Aqueous Solutions: Characterization of Detector Configurations and Data Analysis Methods." Dissertation, Clemson University, Department of Environmental Engineering and Science.

Hughes, L. D., DeVol, T. A., (2008) "Evaluation of statistical control charts for on-line radiation monitoring," *Journal of Radioanalytical and Nuclear Chemistry*, 227(1), 227-234.

Kenett, R., Zacks, S., (1998) *Modern Industrial Statistics*. Duxbury Press, Pacific Grove, CA.

Little, R. J. A., (1982) "The Statistical Analysis of Low-Level Radioactivity in the Presence of Background Counts," *Health Physics*, 43(5), 693-703.

Lucas, J. M., (1985) "Counted Data CUSUM's," *Technometrics*, 27(2), 129-144.

Luo, P., Sharp, J. L., DeVol, T. A., (2013) "Bayesian Analysis of Time-Interval Data for Environmental Radiation Monitoring," *Health Physics*, 104(1), 15-25.

Lynch, S. M., (2007) *Introduction to Applied Bayesian Statistics and Estimation for Social Scientists*. Springer Science + Business Media, LLC, New York, NY.

Miller, G., Inkret, W. C., Martz, H. F., (1993) "Bayesian Detection Analysis for Radiation Exposure," *Radiation Protection Dosimetry*, 48(3), 251-256.

Miller, G., Inkret, W. C., Schillaci, M. E., Martz, H. F., Little, T., T., (2000) "Analyzing Bioassay Data Using Bayesian Methods–a Primer," *Health Physics*, 78(6), 598-613.

Miller, G., Inkret, W. C., Little, T. T., Martz, H. F., Schillaci, M. E., (2001) "Bayesian Prior Probability Distributions for Internal Dosimetry," *Radiation Protection Dosimetry*, 94(4), 347-352.

Miller, G., Martz, H. F., Little, T. T., Guilmette, R., (2002) "Using Exact Poisson Likelihood Functions in Bayesian Interpretation of Counting Measurements," *Health Physics*, 83(4), 512-518.

Miller, G., Little, T., Guilmette, R., (2003) "The Application of Bayesian Techniques in the Interpretation of Bioassay Data," *Radiation Protection Dosimetry*, 105(1-4), 333-338.

Miller, G., (2008a) "Analytical Approximation of Exact Poisson-Lognormal Likelihood Functions," *Health Physics*, 94(2), 188-191.

Miller, G., Martz, H., Little, T., Bertelli, L., (2008b) "Bayesian Hypothesis Testing–Use in Interpretation of Measurements," *Health Physics*, 94(3), 248-254.

Montgomery, D.C., (2009) *Introduction to Statistical Quality Control*, 6th edition. John Wiley & Sons, Hoboken, NJ.

Moustakides, G. V., Polunchenko, A. S., Tartakovsky, A. G., (2009) "Numerical comparison of CUSUM and Shiryaev-Roberts procedures for detecting changes in distributions," *Communications in Statistics–Theory and Methods*, 38(16), 3225-3239.

Page, E. S., (1961) "Cumulative Sum Charts," *Technometrics*, 3(1), 1-9.

Pawel, D. J., (2013) "U.S. Environmental Protection Agency radiogenic risk projections: uncertainty analysis," *Health Physics*, 104(1), 26-40.

Pollak, M., Siegmund, D., (1985) "A diffusion process and its applications to detecting a change in the drift of Brownian motion," *Biometrika*, 72(2), 267-280.

Pollak, M., Tartakovsky, A. G., (2008) "Exact Optimality of the Shiryaev-Roberts Procedure for Detecting Changes in Distributions." International Symposium on Information Theory and its Applications, Auckland, New Zealand, 7-10 Dec 2008.

Pourbaix, M., (1966) *Atlas of electrochemical equilibria*, 1st edition. Pergamon Press, Oxford, UK.

Roane, J. E., (2001) "Radionuclide Separation Using Coupled Chromatographic and Scintillation Detection Techniques." Dissertation, Clemson University, Department of Environmental Engineering and Science.

Roane, J. E., DeVol, T. A., (2002) "Simultaneous Separation and Detection of Actinides in Acidic Solution Using Extractive Scintillating Resin," *Analytical Chemistry*, 74, 5629-5634.

Roane, J. E., DeVol, T. A., (2005) "Evaluation of an extractive scintillation medium for the detection of uranium in water," *Journal of Radioanalytical and Nuclear Chemistry*, 263(1), 51-57.

Seliman, A. F., Samadi, A., Husson, S. M., Borai, E. H., DeVol, T. A., (2011) "Preparation of Polymer-Coated, Scintillating Ion-Exchange Resins for Monitoring of ^{99}Tc in Groundwater," *Journal of Analytical Chemistry*, 83, 4759-4766.

Seliman, A. F., Helariutta, K., Wiktorowicz, S. J., Tenhu, H., Harjula, R., (2013) "Stable and selective scintillating anion-exchange sensors for quantification of $^{99}TcO_4^-$ in natural freshwater," *Journal of Environmental Radioactivity*, 126, 156-164.

Seliman, A. F., Bliznyuk, V. N., Husson, S. M., DeVol, T. A., (2015) "Development of polymerizable 2-(1-naphthyl)-5-phenyloxazole scintillators for ionizing radiation detection," *Journal of Materials Chemistry C*.

Strom, D. J., (2011) "Statistics Concepts I Wish I Had Understood When I Began My Career". Savannah River Chapter of the Health Physics Society, Aiken, SC, 15 Apr 2011.

United States Environmental Protection Agency, (2000) "National primary drinking water regulations; radionuclides;final rule," 40 CFR parts 9, 141, 142.

Walpole, R. E., Myers, R. H., Myers, S. L., and Y. Keying, (2012) *Probability and Statistics for Engineers and Scientists*, 9th edition. Pearson Education, Inc. Boston, MA.

Weise, K., Hbel, K., Rose, E., Schlger, M., Schrammel, D., Tschner, M., Michel, R., (2006) "Bayesian Decision Threshold, Detection Limit and Confidence Limits in Ionising-Radiation Measurement," *Radiation Protection Dosimetry*, 121(1), 52-63.